DEPARTMENT OF EARTH SCIENCE

Master thesis

An investigation into the potential of a new quantitative DHI method

---

Tor Naustdal Helgheim

UNIVERSITY OF BERGEN

June, 2018

Abstract

The seismic response of a layer boundary is dependent on a variety of geological factors and is likely to vary significantly along a given reflector. An aspect that seems to be underutilised in the current DHI methods is that the contrast in seismic response across a fluid contact is less likely to vary significantly. Likewise, it appears that amplitude variations at the top reservoir reflector due to the tuning between the top reservoir and the fluid contact and the strength of intra-reservoir reflectors are not fully utilised in the current DHI methods.

This thesis includes modelling the expected variations in amplitude and AVO response across a fluid contact along a given top reservoir reflector, and development and testing of DHI-finding algorithms with data from the Luva and Gullfaks fields. The modelling was based on well logs and included modelling of the tuning effect between the top reservoir reflector and the fluid contact. The algorithms were designed to search along seismic reflectors for the amplitude and AVO response that was expected across a fluid contact based on the modelling.

The result of the testing demonstrates that the algorithms are able to locate the fluid contact in many areas. The results are affected by several elements, and the most significant are the effects of erosion, onlapping layers, tuning, the presence of faults and the quality of the seismic data and interpretation. The AVO results are less consistent than the amplitude results, but in some areas, the results from the AVO algorithm and the amplitude algorithm agree and hence increases the reliability of the results.

Based on the lessons learned while developing the algorithms and the experience gained from testing them at Luva and Gullfaks, it is concluded that the developed methods have the potential to be a valuable addition to the current DHI methods. Further improvements to the methods can be made by including more attributes, extend the methods to work in settings where the reservoir position is unknown and systematically test the methods against real data.

Acknowledgements

This thesis has been written at the geoscience department at the University of Bergen. My main supervisor has been professor Christian Hermanrud. I would like to give him my sincere gratitude for his guidance, enthusiasm and discussions during the time I have been working on this thesis. His feedback has been invaluable.

I would also like to thank Statoil, with the licence partners Wintershall, OMV and ConocoPhillips, for providing me with and allowing me to publish their data.

A lot of gratitude also goes to my fellow geophysics students at the University. These five years would have been a big black hole without you. Thank you for the good times and all the great memories! Also, a big thanks to family and friends for always being supportive and to Mari for warm hugs and encouragement.

A final thank you to Sindre Steen Eikeland for proof-reading parts of my thesis.

Contents

1 Introduction

Most of the large hydrocarbon accumulations, both on the Norwegian continental shelf (NCS) and worldwide, have probably already been discovered. Because of this, exploring for oil and gas has become more challenging for each year. Many new methods and technologies have been developed with the goal of improving exploration success. Traditionally, qualitative seismic interpretation has been the most widely used method for interpreting seismic data and locating prospects. However, in the last few decades, quantitative methods have become a widely used addition to the qualitative interpretation workflow (Avseth et al., 2005).

One such method is direct hydrocarbon indicators (DHI), where DHI's is referred to as: "any feature on seismic data that gives evidence for the presence of hydrocarbons..." Bacon et al. (2012)

In the 60's and 70's, it became clear that seismic reflections contained useful information that previously had not been utilised. This lead to the successful and extensive use of what is known as bright spot technology. A bright spot is an anomalously strong amplitude that could indicate the presence of hydrocarbons. Churlin and Sergeyev (1963) described how one could use bright spots to locate hydrocarbons directly on a seismic section. At the time, automatic gain control (AGC), which is a processing step that aims to enhance weak reflections, was routinely used. The problem was, however, that this obscured the amplitudes of the seismic section and the bright spot did not stand out (Ashcroft, 2011). After this realisation, the full potential of the bright spot was released, and the bright spot is still one of the most important characteristics to look for in seismic data.

Since the realisation that there is a lot of useful information 'hidden' in the seismic data, developing new methods to utilise this information has been heavily researched. Backus and Chen (1975) presented a thorough review of flat spot reflections and also identified that an amplitude shut-off or polarity reversal at the top reservoir reflector often accompanied flat spots. Taner et al. (1979) noted that low-frequency shadows were often present below hydrocarbon reservoirs, which implies that analysis of the frequency content of seismic data could be used as a DHI method. Ostrander (1984) showed that amplitude versus offset (AVO) analysis in many cases could separate between gas related amplitude anomalies and other anomalies.

A significant and parallel development was the advance of rock physics. Essential work on how the pore-fluids affect the elastic rock properties of a porous rock was conducted by Gassmann (1951) and Biot (1956a,b). Since then, rock physics models that describe the effect in seismic properties of parameters such as porosity, permeability, fractures, stress and fluid-saturation have been developed and improved (Dvorkin et al., 2014). Today, rock physics is an essential part of the quantification of reservoir properties.

A standard tool for visualising the expected seismic response of different reservoirs and settings is the use of rock physics templates (RPT), first introduced by Ødegaard and Avseth (2003). Elastic properties of different lithologies, pore fluids and porosities can be modelled using appropriate rock physics models. By cross-plotting the modelled values and superimposing real data, commonly from well logs or seismic inversion, it is frequently observed that the values for caprocks and reservoir rocks with different fluid contents cluster in different regions of the plots. A prediction of the lithology and pore-fluids of the different zone can be made based on how these zones plot relative to the modelled trends. An example of an RPT is shown in figure 1.1, where the acoustic impedance is plotted versus the Vp/Vs ratio.

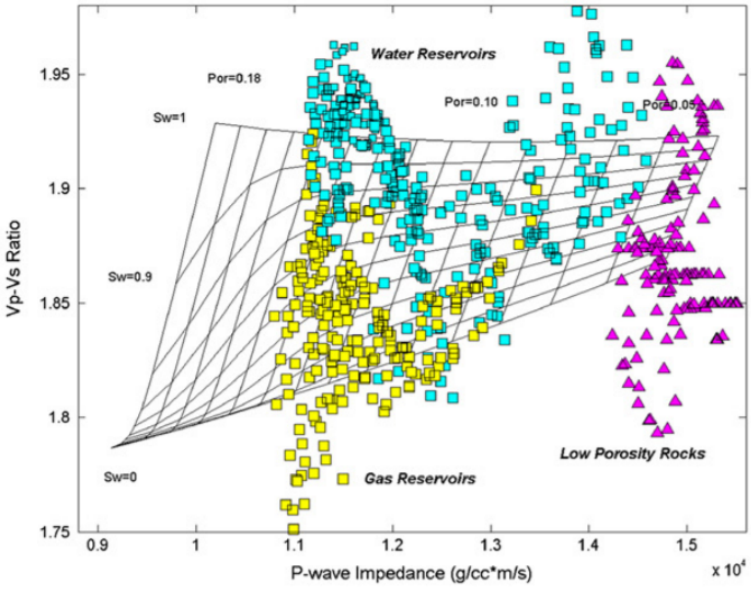

Figure 1.1: An example of an RPT. The black lines indicate the expected values for different fluid saturations and porosities. The coloured dots represent inverted seismic data, where yellow dots are values from a gas reservoir, blue dots are from a water-filled reservoir, and purple dots are from low porosity, non-reservoir rocks. Notice the significant overlap between the different zones. From: Ba et al. (2013).

However, typical of such cross-plots is that there is a significant overlap between the

different lithologies and fluids and that the regions for hydrocarbon-filled and water-filled rocks overlap. Such an overlap is evident in figure 1.1, where some of the data points from the different zones plot in the same area.

Wrobel et al. (2012) have developed a method that simultaneously quantifies several DHI's directly from a seismic volume. Depending on pre-defined criteria, different regions of the seismic data are labelled according to the likelihood that they image hydrocarbon-filled reservoirs. However, because the pore-fluid is only one of many factors that affect the amplitudes, such DHI analysis will not unambiguously reveal the fluid content of the reservoir. The main reason for this is that the elastic properties of different lithologies and pore fluids are often overlapping.

In a given reservoir, amplitude variations related to other factors than a change of pore-fluid are less likely to occur exactly at the fluid contact. The dry rock properties above and below the fluid contact will therefore often be constant, both in the caprock and the reservoir. The contrast in amplitude across the fluid contact will be related to the change of fluids. It appears that this is a fact that is not fully exploited in the current DHI methods. Also, it seems like analysis of amplitude variations associated with the fluid content of the reservoir have not previously been described as DHI methods. To the best of my knowledge, amplitude variations due to tuning between the top reservoir and the fluid contact reflectors and the difference in internal reflectivity above and below a fluid contact in a reservoir, have not systematically been analysed as a DHI before.

This study proposes a workflow for how the expected contrast in amplitude variations and AVO response along a top reservoir reflector, both due to a change in pore-fluid and the tuning effect between reflections from the top reservoir and the fluid contact reflectors, can be utilised in a DHI workflow. The primary focus has been development and implementation of parts of this workflow. This was done by modelling the expected change in acoustic impedance and change in AVO response across a fluid contact using well logs, and creating algorithms to search for responses that are of the expected contrast. The algorithms were tested at Gullfaks and Luva, and the results of these tests were used to sketch a plan for future development of the method. How the methods perform, and different factors affecting the results, will be discussed in chapter 6.

2 Background theory

To successfully utilise DHI's in oil and gas exploration it is important to understand the mechanisms and theory behind them. This chapter aims to give an understanding of the fundamental theory and underlying principles behind the different DHI's and how we can use them to aid in the search for oil and gas.

2.1 Seismic reflection

A standard model for seismic reflections is the simple, but useful, convolutional model. The Earth's subsurface consists of different layers with different properties, and regarding seismic reflections, the most important properties are the bulk density and the seismic velocities of the rocks. There is an important distinction between compressional (P-wave) and shear (S-wave) velocities. These properties are dependent on many factors and will typically be different for different rocks and at different depths. A seismic survey involves sending pressure waves into the Earth, and it is the contrasts in properties, from a layer to the next, that leads to some portion of the energy being reflected back towards the surface. Seismic receivers at the surface measure this reflected energy, and by processing this data, it can be presented as a seismic section or cube.

The portion of the energy being reflected can be quantified by the reflection coefficient and the acoustic impedance of the layers. For normal incident seismic waves, the acoustic impedance (I) is given as the product of the P-wave velocity (V_p) and the density (ρ):

$$I = V_p \, \rho \tag{1}$$

Reflections arise at the boundary between two layers where there is a contrast in acoustic impedance between the layers. The strength of the reflections is determined by the reflection coefficient (RC). For a normally incident seismic wave, that is, a wave that hits the boundary at normal angles, the reflection coefficient is given as the contrast in acoustic impedance between two layers. If I_2 is the acoustic impedance of the deepest layer and I_1

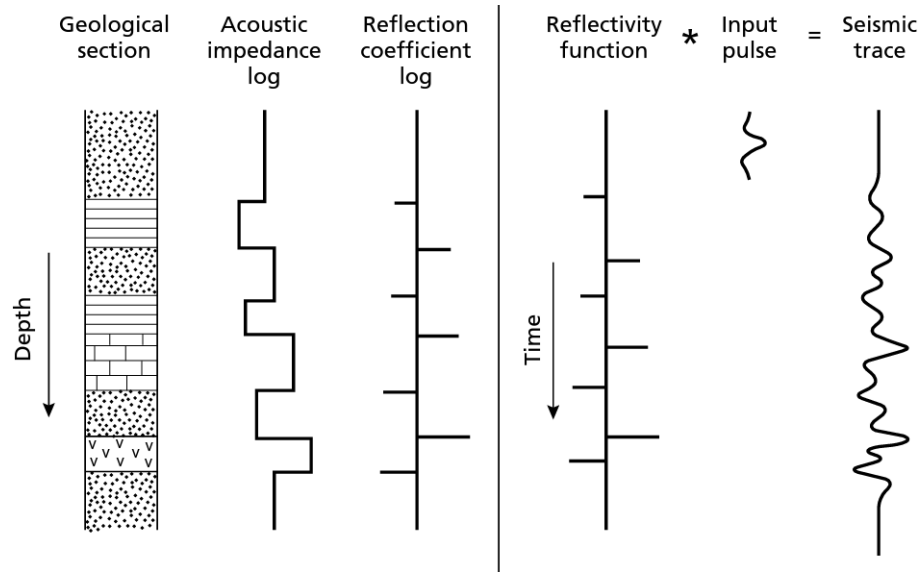

Figure 2.1: Illustration of the convolutional model. Seismic reflections arise at boundaries where there is a contrast in acoustic impedance. Convolving the input pulse with the reflectivity function provides the final seismic trace. From: Kearey et al. (2002).

is the impedance of the shallowest layer, the reflection coefficient is defined as:

$$RC = \frac{I_2 - I_1}{I_2 + I_1} \tag{2}$$

The reflection coefficient is a number between -1 and 1 at the layer boundaries and zero elsewhere. If the density and velocities of the layers are known, it is simple to calculate the acoustic impedance of each layer and the reflection coefficients at the different layer boundaries. A reflection coefficient log can be computed using P-wave velocity and density data from well logs.

The idea behind the convolutional model is that the seismic response is a convolution of the reflection series with the wavelet created by the seismic source. This wavelet is referred to as the seismic pulse, and a simplified shape is shown in figure 2.1. The convolution of the seismic pulse with the reflection coefficient at each interface produces the seismic response at each interface. The final seismic signal is the interference, or sum, between all the individual responses and gives the seismic trace seen on the right side of figure 2.1.

It is important to stress that the convolutional model is only a simplification, as it is

only valid for waves that are reflected at right angles at an interface. The seismic waves recorded at the surface are reflected at different boundaries within a range of different incident angles. Therefore, the reflection coefficient from equation 2 and the convolutional model is only an approximation of reality. For non-normal incident angles, the reflection coefficient is a function of incident angle, density, and P- and S-wave velocity of the rocks at both sides of the interface. How the reflectivity varies with increasing incident angle is a field on its own, and will be discussed more in detail in section 2.5.

As stated in equation 1 and 2, the seismic response is dependent on the density and velocity of the rocks. The bulk modulus of a rock, K, describes how resistant the rock is to compression and the shear modulus, μ, describes how resistant the rock is to shearing. P- and S-wave velocities (V_p and V_s) depends on the bulk and shear elastic moduli, as well as the density of the rock. The exact relations are given in equation 3 and 4.

$$V_p = \sqrt{\frac{K + \frac{4}{3}\mu}{\rho}} \tag{3}$$

$$V_s = \sqrt{\frac{\mu}{\rho}} \tag{4}$$

Various minerals have different elastic properties and densities. Quartz minerals are typically said to have a bulk modulus of 37 GPa. Clay minerals, like kaolinite and illite, are given a wide range of values in the literature. Mavko et al. (2009) report that kaolinite has a bulk modulus of 1.5 GPa. For unconsolidated sands, the main control on the rock's bulk modulus is the bulk modulus of the mineral constituents. For a cemented sandstone, this is no longer a good approximation because a small amount of cement at grain contacts can significantly impact the bulk modulus of the rock (Avseth et al., 2005). The contact cement model (Dvorkin and Nur, 1996) describes the effect of adding small amounts of cementation at grain contacts. The key point is that rocks with different mineral constituents and different amounts of cementation will have different impedance and give rise to reflections in the seismic data. So if a shale overlies a sandstone, the boundary will in most cases represent a contrast in acoustic impedance and can be identified as a reflection in the seismic data.

2.2 Amplitude

The strength, or amplitude, of a reflected seismic wave, is dependent on the contrasts in rock properties. Another important fact is that the fluid content of a porous rock will influence the properties of the rock. Seismic attributes are information contained in the seismic data, and the simplest and most important attribute is amplitude. In this section, amplitude related DHI's will be covered.

2.2.1 Bright spot

Depending on the depositional environment and the constitutive mineral of the rock, some proportion of the rock will consist of open space, commonly known as the pore space. The percentage of the rock that consists of pore space is referred to as porosity. Similarly to how a dry sponge will behave and feel differently to a wet sponge, a water-filled rock will be different from a gas-filled rock. The pore-filling fluid will affect the properties of the rock, and therefore also seismic velocities and the density of the rock.

Natural gas is easier to compress than water or brine, so the bulk modulus of gas is lower than that of brine. If gas replaces brine in the pore space of a rock, the consequence is that the bulk modulus of the entire rock is reduced. So, a gas-filled porous rock has lower bulk modulus than the same rock with brine in the pore space. How large the reduction is, depends on the properties of the gas, the properties of the solid part of the rock and its porosity. At shallow depths, a hydrocarbon-filled sandstone will generally have lower acoustic impedance than a water-filled sandstone, and shales will have higher acoustic impedance than both. This is illustrated in figure 2.2. The contrast in impedance between a shale and a hydrocarbon-filled sandstone will therefore be more significant than the contrast between a shale and a water-filled sandstone. This leads to larger amplitudes at a boundary between a shale and a hydrocarbon-filled sandstone compared to a boundary between a shale and a water-filled sandstone. These anomalously strong amplitudes will often stand out in the seismic data, and this is what is referred to as bright spots. The same effect applies to oil, but since the elastic properties of oil are closer to brine than gas, the effect is less pronounced.

It is, however, important to note other lithological events can cause similar bright spots. Examples include volcanic intrusions, cemented sands, overpressured sands or shales

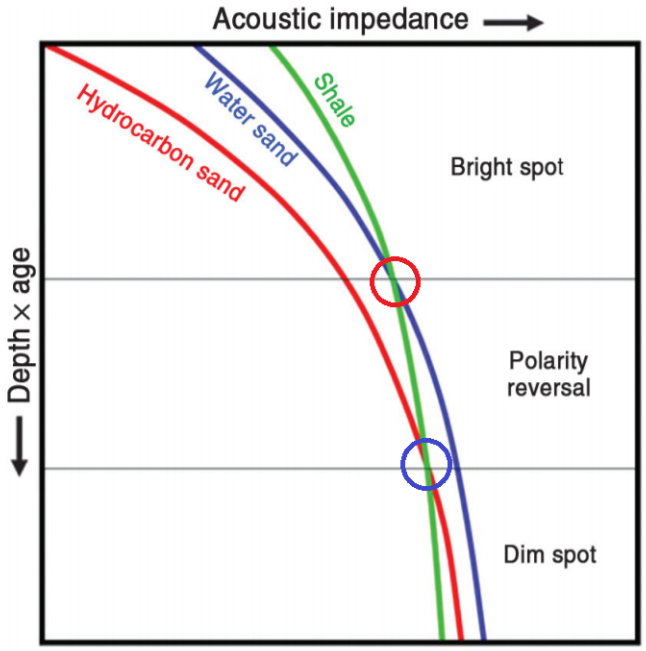

Figure 2.2: Illustration of how the acoustic impedance of different lithologies are expected to vary with depth and age in a single basin. Note that dim spots and polarity reversals typically occur at greater depths then bright spots. From: Brown and Abriel (2014).

and coal beds (Avseth et al., 2005). A bright spot caused by hydrocarbons will represent a decrease in AI, and will therefore be represented as a through in the seismic data. Cemented sands and volcanic intrusions will represent an increase in impedance, and by inspecting the polarity of the data, these can be separated from a bright spot. Therefore, it is essential to know the polarity of the seismic data before analysing potential bright spots.

Another important factor to consider is if the bright amplitudes conform to structure. The hydrocarbons will try to migrate towards the surface, and when they are trapped their lower boundary will be flat. Therefore, the bright amplitudes should follow depth contours in map view, that is, they should conform to the structure (Bacon et al., 2012).

2.2.2 Amplitude shut-off

Another characteristic of the seismic response often associated with bright spots is what is referred to as an amplitude shut-off or a down-dip termination. A shut-off is a decrease in amplitude typically observed along a dipping layer across the point where the pore

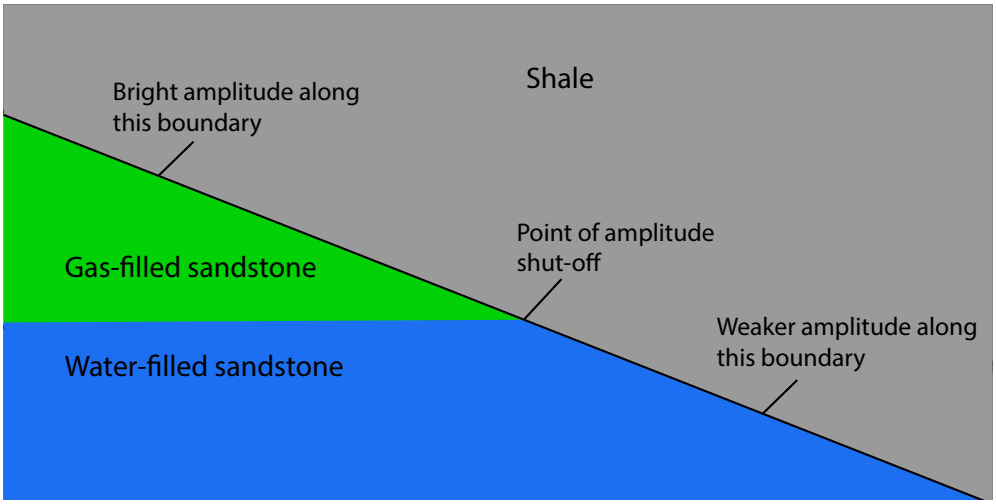

Figure 2.3: Illustration of a geological setting where an amplitude shut-off could occur. A low impedance gas-filled sandstone below a high impedance shale will lead to bright amplitudes in the seismic data. The same sandstone, but with water in the pore space, will have a lower amplitude. The amplitude shut-off, can be seen across the fluid contact.

fluid changes from hydrocarbons to water. A geological setting where a shut-off could occur is illustrated in figure 2.3.

An example of an amplitude shut-off effect can be seen on the synthetic seismic on the bottom left of figure 2.4. There, the blue top reservoir reflector is strong above the gas zone (top middle) and weaker down dip on both sides of the flat spot (in the water zone).

2.2.3 Polarity reversal and dim spot

As discussed, hydrocarbons will in many cases cause anomalously high amplitudes, but this is not always the case. Under certain conditions, the presence of oil or gas can lead to a weakening or a phase reversal of the amplitudes.

As illustrated in figure 2.2, the acoustic impedance of a rock will change with increasing depth and age of the rock. Mechanical and chemical compaction have different effects on sandstones and shales, and they will follow different impedance versus depth curves. Sandstones will typically have a larger increase in acoustic impedance with depth compared to shales, so at some point, there will be a crossover for the impedance between shale and a water-filled sandstone. This crossover can be seen in figure 2.2 (red circle). Below this crossover, water-filled sandstones will have a higher impedance than shales,

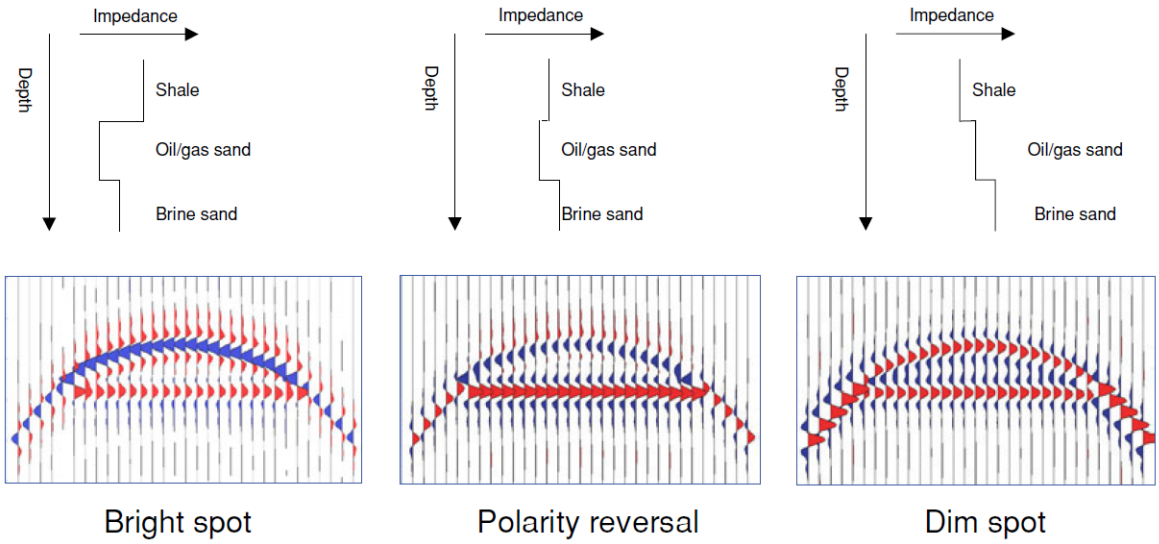

Figure 2.4: Schematic illustration of three significant impedance variations that can be caused by a hydrocarbon accumulation. In the synthetic seismic, the blue colour represents a soft reflection, that is, a decrease in acoustic impedance. From: Bacon et al. (2012).

but shales will still have higher impedance than hydrocarbon-filled sandstones. When this is the case, there will be a change in polarity of the top reservoir reflection at the point where the pore fluid changes from hydrocarbons to water. This effect is shown schematically in the middle of figure 2.4, where the top reservoir reflection changes from a soft (blue) reflection in the hydrocarbon zone to a hard (red) reflection in the water zone. This is a characteristic that can be used as a DHI and it is known as a polarity reversal.

At further increasing depths, the acoustic impedance of sands will continue to increase. At some point, the hydrocarbon filled sandstone will have a larger acoustic impedance than shales. This crossover is marked by the blue circle in figure 2.2. In this regime, a shale overlying a water-filled sandstone represent a larger acoustic impedance than a shale overlying a hydrocarbon-filled sandstones. This result in weaker amplitudes above the hydrocarbon zone than in the brine zone. Such low amplitude zones are another potential hydrocarbon indicator and are referred to as dim spots. This effect is shown schematically on the right side of figure 2.4, where the amplitude in the hydrocarbon zone is weaker than the amplitude in the water zone.

An obvious problem with dim spots is that it is harder to look for weak amplitudes than bright amplitudes. Also, since dim spots usually occur at greater depths where the signal to noise ratio and the resolution tend to decrease, making interpretation harder. Still, Brown and Abriel (2014) claim that dim spots and polarity reversals are underexploited

in the exploration community.

Before trying to interpret the amplitudes and searching for amplitude related DHI's, it is strongly advised to analyse which regime to expect. Is it likely that hydrocarbons will lead to a bright spot, a polarity reversal or a dim spot? If the reservoir rock is soft compared to the caprock, then hydrocarbons will lead to a brightening of the amplitude compared to the same rock filled with brine. On the other hand, a stiff reservoir rock below a shale will have brighter amplitudes when filled with brine then with hydrocarbons. In other words, the properties of the reservoir and the caprock are important when searching for DHI's. This analysis could be based on the likely depositional environment and the age and depth to the rocks (Avseth et al., 2005).

2.2.4 Flat spot

Another DHI that has proven very useful is the flat spot. Oil, gas and water have different densities and will not mix. Gas will therefore float on top of oil and oil will float on top of water. If a porous rock is filled with both hydrocarbons and water, the boundary between them will be flat, with water below the hydrocarbons. Since different fluids have different properties, a change of pore-fluid will lead to a change in acoustic impedance, and under the right conditions, this will be seen as flat reflections in the seismic data. Such flat reflections are therefore used as an indicator of a contact between water and hydrocarbons. In areas where the surrounding geology is dipping, such flat reflections typically stand out and they are to identify hydrocarbons.

Flat spots can also be caused by other boundaries than those between different fluids. A well-known example is the boundary between Opal-A and OPAL-CT, which is a temperature dependent diagenetic event. The transition from OPAL-A to OPAL-CT changes the rock properties and gives rise to a change in impedance, often in a similar way to a fluid-induced flat spot. Dry wells have been drilled on flat spots that are caused by diagenetic events rather than fluids (Avseth et al., 2005). Other possible causes of flat events in seismic data are multiples, paleo-contacts and volcanic sills. Because of this, a flat event in the seismic data is not necessarily strong evidence of hydrocarbons on its own. Simm and Bacon (2014) suggest that if an apparent flat spot is seen, one should also investigate if the reflection has the following characteristics:

- correct polarity
- crosses the reservoir layering
- an AVO response consistent with a fluid contact
- conforms to structure
- is consistent with other DHI's

The better the real data match these expectations, the more confident one can be that the flat spot is caused by a hydrocarbon-water contact.

Another point to be aware of is that fluid contacts might not appear as perfectly flat events in the seismic data. Since seismic data are collected in time and not depth, low velocities in the reservoir or lateral velocity variations in the overburden might cause a seismic event to appear deeper than what it is. Tuning between the fluid contact and strong internal reflectors might cause a modest dip of the fluid contact as well (Brown, 2004).

2.2.5 Geological factors affecting amplitude similarly to a change of pore fluid

According to the convolutional model, the amplitudes are only affected by the reflection coefficients, the seismic wavelet and the interference between reflections. In practice, this is a simplification, and Sheriff (1975) and Henry (2004) have summarised different causes that can affect seismic amplitudes. Tuning, amplitude variations with angle, transmission effects and the processing scheme are identified as some of the most significant factors.

Figure 2.5 shows a geological setting where the amplitude will vary along the top reservoir reflector. Since the amplitude is not dependent on the impedance of the reservoir rock alone, but on the contrast in impedance between the reservoir and the caprock, a change in the caprock will affect the amplitude at the top reservoir boundary as well. In areas with erosion, it is not uncommon to have onlapping layers, and as illustrated in figure 2.5, this can lead to a change in caprock for the reservoir. Exactly how such changes will affect the amplitude is hard to state in general terms, but if such changes are consistent in depth and have the correct polarity, such changes could be confused with those caused by a change of pore-fluid.

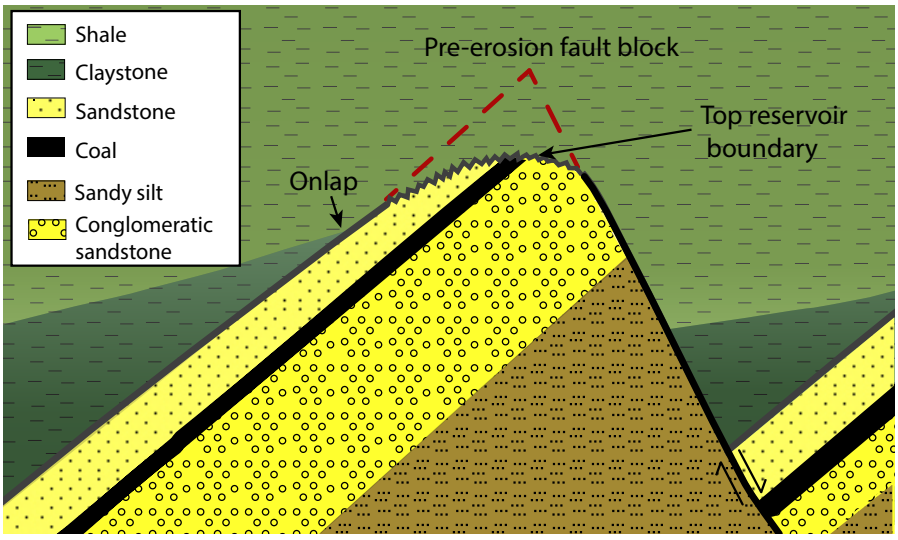

Figure 2.5: An illustration of a geological setting where the top reservoir reflector will have different amplitudes because of internal changes in the reservoir, erosion and changes in the caprock.

No reservoir is completely homogeneous, and the reservoir properties will, at least to some extent, vary both laterally and vertically. There could, for example, be areas with different porosities, shale content and amount of cementation. Sometimes a reservoir consists of different formations, and an example of this is the Gullfaks reservoir, which consist of sandstones of the different formations in the Brent group. If the erosion is extensive enough, the top formation(s) could be completely removed. Since the different formations represent different depositional environments, their properties will vary and so will their acoustic impedance. This setting is illustrated in figure 2.5, where there is a change in the top reservoir formation at the apex of the structure.

Another factor that could affect the amplitude is internal shale or coal layers, which is not uncommon in the North Sea. In figure 2.5, the internal shale layer would be expected to affect the amplitude at the top reservoir.

2.3 Seismic resolution and tuning

A limitation regarding seismic data is the resolution, and as defined by Sheriff (1977), the resolution of seismic data is how close two features in the subsurface can be and still be distinguishable in the seismic data. There is a distinction between horizontal resolution from trace to trace, and vertical resolution in depth or time. A common rule of thumb is that the vertical resolution is about one-quarter of the dominant wavelength of the

seismic wavelet, but the exact resolution will vary according to the complexity of the geology and the noise level in the data. The resolution is not the same as detectability, because even if two reflectors cannot be fully separated, it might still be possible to detect that there is more than one layer. In favourable conditions, that is, low noise and large impedance contrasts, layers down to a thickness of 1/30 of the wavelength can potentially be detected (Simm and Bacon, 2014).

Horizontal or lateral resolution is given by the diameter of the Fresnel zone which is the two-dimensional area of a reflector that contributes to the reflection recorded at the surface (Sheriff, 1977). Waves that are reflected within this area of the reflector will interfere and add to the same reflection event. The diameter of the Fresnel zone, F_d, is given by (Simm and Bacon, 2014):

$$F_d = \sqrt{\left(z + \frac{\lambda}{4}\right)^2 - z^2}$$

where z is depth and λ is the wavelength of the seismic wave.

The effect of interference, constructively or destructively, between two separated reflectors, is known as the tuning effect. For a thin layer, the reflection from the top and base will interfere and affect the amplitude. If the top and base reflections have opposite polarity, then there will be maximum constructive interference if the bed thickness is equal to one-quarter wavelength. This thickness, Z, is referred to as the maximum tuning thickness and is given by:

$$Z = \frac{\lambda}{4}$$

For two reflectors with opposite polarity, the maximum tuning effect depends on the size of the sidelobes of the wavelet and the relative reflection strength of the two reflectors. A good rule of thumb is that the increase in amplitude due to tuning would rarely exceed 40 % (Brown, 2011).

For two reflectors of the same polarity, the situation is different. The maximum tuning effect then occurs when there is interference between the two main lobes. Therefore, the tuning will increase the reflectors converge. Since the constructive interference is

between the main lobe of the two reflections, it is likely that this interference will be more significant than the interference between two reflections of different polarity.

2.4 Optical stacking

While looking for amplitude variations caused by a change in pore-fluid, all other variations can be considered noise. A method that could remove unwanted noise and enhance amplitude effects related to fluid contacts is optical stacking, which is to stack adjacent seismic lines. By doing this, events that are constant in depth will be enhanced while the effect of amplitude variations that are not consistent in depth will be reduced or removed. Since fluid contacts are usually flat, changes in amplitude related to fluid contacts and amplitude shut-offs would be enhanced after optical stacking.

2.5 Amplitude versus offset

2.5.1 AVO theory

Equation 2 gives the reflection coefficient for a normally incident seismic wave, and as previously mentioned, this is a simplification. Since a full stack seismic section typically contains angles from 0-30 degrees, it is important to know how the reflections, or amplitudes, changes with angle (or offset). This variation is the basis for what is known as amplitude versus angle (AVA) or amplitude versus offset (AVO) analysis.

The fundamental theory behind AVO analysis is the Zoeppritz equations, which are a set of equations formulated by Karl Zoeppritz in the early 20th century (Zoeppritz, 1919). These equations give the reflection and transmission coefficients at an interface as a function of the incident angle, the P- and S-wave velocities and the density at both sides of the boundary. The equations are complex and offer little intuitive meaning, and they will not be stated explicitly here.

A few centuries after Zoeppritz published his equations, effort was put into simplifying them. Both Richards and Frasier (1976) and Aki and Richards (1980) wrote the P-P reflection coefficient, $R_{pp}(\theta)$, as a convenient three-term equation. This form contains one term with V_p, one with ρ and the final term containing V_s. The Aki and Richards (1980)

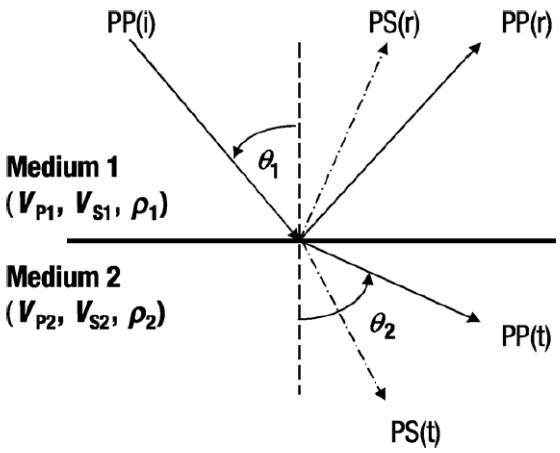

Figure 2.6: Illustration of how an incident P-wave will split into four converted waves at an interface. PP(i) is the incident P-wave, PP(r) and PS(r) are the reflected P- and S-wave while PP(t) and PS(t) are the transmitted P- and S-wave. From: Avseth et al. (2005).

equation, as formulated by Avseth et al. (2005) is given by:

$$R_{pp}(\theta) = a\frac{\Delta V_p}{V_p} + b\frac{\Delta \rho}{\rho} + c\frac{\Delta V_s}{V_s} \tag{5}$$

where the coefficients are defined by:

$$a = \frac{1}{2cos^2\theta},\ b = 0.5 - \left[2\left(\frac{V_p}{V_s}\right)^2 sin^2\theta\right],\ c = -4\left(\frac{V_s}{V_p}\right)^2 sin^2\theta$$

Here, and in the following, V_p, V_s, rho and θ represent the average of the properties across an interface. That is, the average of the values in the top and bottom layer, or medium 1 and 2, as illustrated in figure 2.6. ΔV_p, ΔV_s and $\Delta\rho$ represent the contrast across the layer boundary, that is, the value in medium 2 subtracted from the value in medium 1. A sketch of an incident P-wave on a layer boundary with its reflected and transmitted waves are illustrated in figure 2.6. It is the relative strength of these waves that are described by the Zoeppritz equations.

The Aki and Richards equation (eq. 5) is based on the work done by Bortfeld (1961). His approach was to assume that the change in properties across layer boundaries is small. Therefore, the change in velocities and density across the boundary has to be small for

the approximation to be valid. Shuey (1985) made further simplification to the Aki and Richards equation and presented the P-P reflection coefficient in the following form:

$$R_{pp}(\theta) = R_0 + G\, sin^2(\theta) + F\left(tan^2\theta - sin^2\theta\right) \tag{6}$$

The coefficients R_0, G and F, are defined as:

$$\begin{aligned} R_0 &= \frac{1}{2}\left(\frac{\Delta V_p}{V_p} + \frac{\Delta\rho}{\rho}\right) \\ G &= \frac{1}{2}\frac{\Delta V_p}{V_p} - 2\frac{{V_s}^2}{{V_p}^2}\left(\frac{\Delta\rho}{\rho} + 2\frac{\Delta V_s}{V_s}\right) \\ F &= \frac{1}{2}\frac{\Delta V_p}{V_p} \end{aligned} \tag{7}$$

The advantage of equation 6 is that each term represents the reflection coefficient at different incident angles. The first term, R_0, is an approximation of the reflection coefficient at normal incidence ($\theta = 0$). The second term, G, often termed the AVO gradient, gives the reflection coefficient at intermediate angles ($0 < \theta < 30$), and the final term, F, gives the reflection coefficient at large angles ($\theta > 30$).

A seismic survey will have a limited range of angles, and by assuming that there are no reflections with incident angle larger than 30 degrees, the last term in equation 6 can be omitted. The equation then reads:

$$R_{pp}(\theta) = R_0 + G\, sin^2\theta \tag{8}$$

The coefficients, R_0 and G, are known as the AVO intercept and gradient, respectively. Equation 8 is linear in terms of $sin^2\theta$, and this is a relation that is utilised in AVO inversion.

Wiggins et al. (1986) made further approximations by setting the V_p/V_s ratio to 2. The

AVO gradient can then be written as:

$$G = R_p - 2R_s \tag{9}$$

where R_p and R_s are the normal incidence P- and S-wave reflection coefficients, approximated by:

$$\begin{aligned} R_P &= \frac{1}{2}\left(\frac{\Delta V_p}{V_p} + \frac{\Delta \rho}{\rho}\right) \\ R_S &= \frac{1}{2}\left(\frac{\Delta V_s}{V_s} + \frac{\Delta \rho}{\rho}\right) \end{aligned} \tag{10}$$

2.5.2 AVO in practice

The next step is to investigate how AVO can be beneficial in oil and gas exploration. The AVO response is dependent on P- and S-wave velocities as well as the density of the rocks. These parameters will be different in a gas-filled sandstone compared to other lithologies. A gas induced bright spot will therefore have a different AVO response than a bright spot caused by other lithological effects or a water-filled sandstone. This effect was first demonstrated by Ostrander (1984). The basic idea is that by analysing the AVO response of a potential prospect, one should, in theory, be able to separate a bright spot caused by gas sands and bright spots from other causes (Gelfand et al., 1986).

2.5.3 AVO classes

Rutherford and Williams (1989) defined three different classes based on how the amplitude changes with offset for different gas-filled sandstones. Castagna and Swan (1997) added the fourth class. The different classes have the following characteristics (Castagna, 1993):

- Class 1: the reflection coefficient (RC) is positive at zero offset and decreases with increasing offset

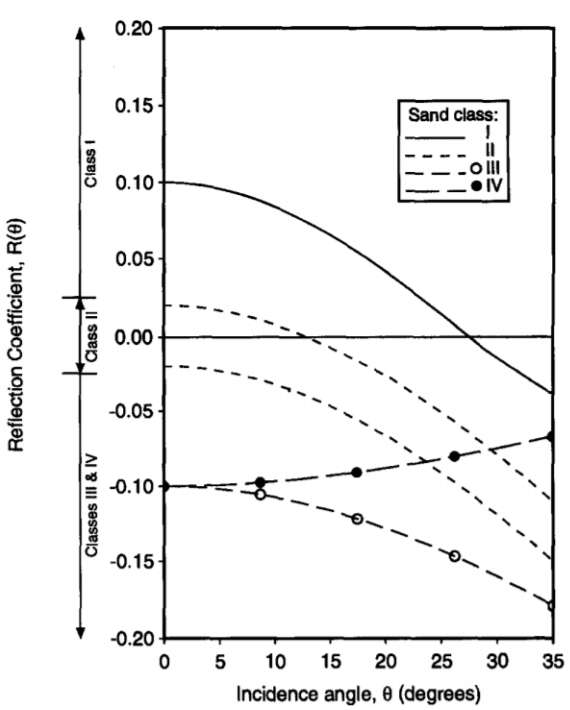

Figure 2.7: Based on how the amplitude or reflection coefficient varies with angle for a gas-filled sandstone, four different AVO classes are defined. From: Castagna et al. (1998).

  - This is the case when a sandstone has a large impedance contrast with the overlying unit

- Class 2: the reflection coefficient is near zero at zero-offset and decreases with increasing angle
  - this is the case when a sandstone has a similar impedance to the overlying unit (dim spot)
  - if the RC is positive at zero-offset, a polarity reversal will occur
- Class 3: reflection coefficient is negative at zero-offset and increasingly negative with increasing offset
  - this is the case when a sandstone has a lower impedance than the overlying unit
  - will be seen as a bright spot in the full stack seismic data
- Class 4: same as class 3, but the reflection coefficient increases (towards zero) for increasing angles

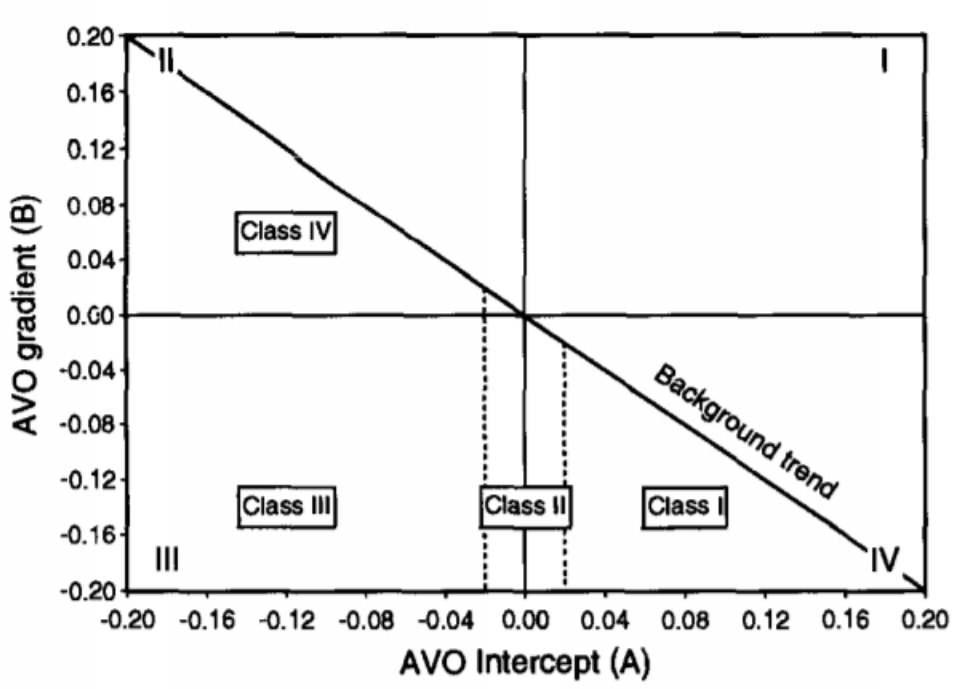

Figure 2.8: A typical cross-plot of gradient versus intercept with the four AVO classes marked. The background trend indicates where shales and water-filled sandstones should plot. From: Castagna et al. (1998).

A plot of the AVO classes and how their reflection coefficient varies with angle is illustrated in figure 2.7. An important part of AVO analysis is to estimate the intercept and gradient of a reflector. There are, at least, two ways to evaluate the AVO trend of a prospect. The first method is to locate a reflector of interest in the full stack section and then inspect the pre-stack gathers at the trace of interest, for example at the top of a prospect. By obtaining the least-squares solution to the amplitude variation at a given event, the AVO intercept and gradient can be estimated (Avseth et al., 2005). A typical intercept versus gradient plot is illustrated in figure 2.8. The second method is to use partial stacks or angles stacks. Pre-stack data contains a lot of data and is expensive to store, and therefore it is common to obtain partial stacks instead. Partial stacks contain a certain range of angles from a CMP gather. Typically, one would obtain a near stack, containing small angles, a mid stack, containing intermediate angles and a far stack containing the largest angles from the gather. Then, by extracting the amplitude in each partial stack and plotting against the angle, it is possible to approximate the AVO gradient and intercept. This technique is illustrated in figure 2.9.

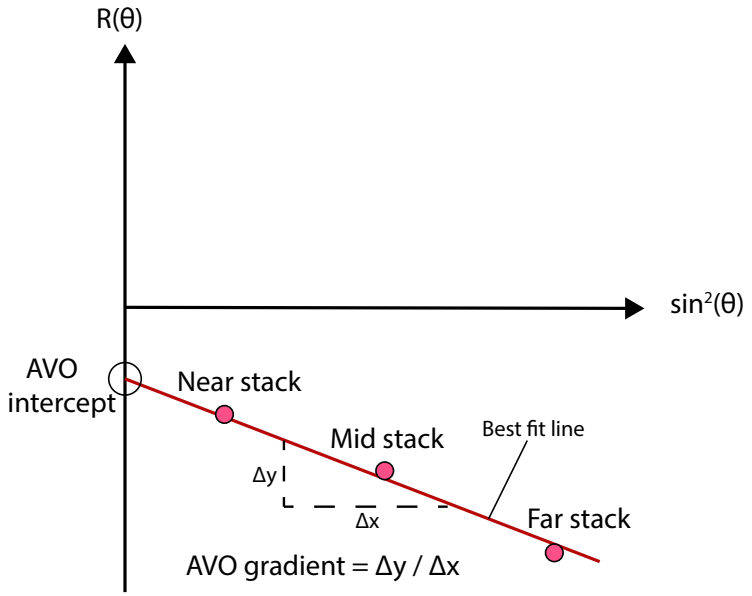

Figure 2.9: Illustration of how to estimate AVO gradient and intercept using partial stacks. By picking a reflector of interest, the amplitude is picked in the different cubes and plotted against $sin^2\theta$, where θ is the mean of the angle range contained in each partial stack. By fitting a straight line to the amplitudes, both AVO gradient and intercept can be estimated.

2.5.4 Fluid factor

There exist several different ways of evaluating and quantifying the AVO response of a prospect. One approach is to calculate what is known as the fluid factor, first developed by Smith and Gidlow (1987).

The empirical V_p/V_s relationship developed by Castagna et al. (1985), is known as the mudrock line and is stated in equation 11.

$$V_p = 1.36 + 1.16V_s \tag{11}$$

By following the approach of Avseth et al. (2005), the following relationship is obtained by deriving equation 11:

$$\frac{\Delta V_p}{V_p} = 1.16\,\frac{V_s}{V_p}\frac{\Delta V_s}{V_s} \tag{12}$$

Since the Mudrock line is only valid in water-filled siliciclastic rocks, a fluid factor, or a residual, ΔF, can be defined as:

$$\Delta F = \frac{\Delta V_p}{V_p} - 1.16\,\frac{V_s}{V_p}\frac{\Delta V_s}{V_s} \tag{13}$$

The fluid factor will be close to zero in water-filled siliciclastic rocks, while in hydrocarbon-filled siliciclastic rock, due to a decrease in Vp/Vs ratio, the fluid factor will be negative.

According to Castagna and Smith (1994), the following characteristics are highly desirable for a hydrocarbon indicator:

- The value in non-hydrocarbon zones should be constant and near zero
- The value should be negative for shale over gas-sands and more negative than the value for shale over brine-sands

The fluid factor satisfies both characteristics and should therefore be suitable as a hydrocarbon indicator.

The fluid factor can also be defined in terms of the AVO intercept and gradient. Gardner's relation (Gardner et al., 1974) is an empirical equation that relates the density of a rock with the P-wave velocity of the rock. In differentiated form, it is given as:

$$\frac{\Delta\rho}{\rho} = \frac{1}{4}\frac{\Delta V_p}{V_p} \tag{14}$$

Combining equation 14 with the equations for R_P and R_S, given in equation 10, and by assuming $Vp/Vs = 2$, we end up with the following relationship between the fluid factor and the intercept and gradient:

$$\Delta F = 1.252R_0 + 0.58G \tag{15}$$

A limitation of using the fluid factor as a hydrocarbon identifier is several lithologies do not follow the mudrock line and that could lead to negative fluid factors. Examples

includes igneous and carbonate rocks (Avseth et al., 2005).

2.6 Rock physics modelling

As explained in section 2.1 seismic reflections are a result of changes in elastic properties in the subsurface. The role of rock physics is to provide a link between the seismic properties and the underlying geological properties (Avseth et al., 2005). Therefore, rock physics is an essential tool for analysing amplitudes and interpreting seismic data. There exists a wide range of rock physics models that each focuses on a different aspect of geology. Examples include models for predicting seismic properties for different compaction trends, for saturation effects, for different lithologies and cementation effects.

2.6.1 Fluid effects

The ultimate goal of exploration is to locate oil or gas. It is therefore vital to know how different pore fluids affects the seismic response. Gassmann (1951) developed a relation describing how the bulk modulus of a porous rock changes with different fluids. By using Gassmann's equation, it is possible to calculate the effective bulk modulus of a saturated rock, K_{sat}. If the rock has porosity ϕ, dry rock bulk modulus K_{dry}, mineral bulk modulus K_0 and is saturated with a fluid with bulk modulus K_{fl}, then Gassmann's equation is, as formulated by Smith et al. (2003):

$$K_{sat} = K_{dry} + \frac{\left(1 - \frac{K_{dry}}{K_0}\right)^2}{\frac{\phi}{K_{fl}} + \frac{1-\phi}{K_0} - \frac{K_{dry}}{K_0^2}} \tag{16}$$

The dry rock bulk modulus is the effective bulk modulus of a porous rock with empty (or air-filled) pores, and the mineral bulk modulus is the bulk modulus of the solid part of the rock (pore space excluded).

An equally important fact is that the shear modulus of the rock is not affected by the pore fluid. The simple reason for this is that all fluids have shear modulus equal to zero. The result is that the dry rock shear modulus is equal to the shear modulus of a rock saturated

with any fluid, as stated in equation 17.

$$\mu_{sat} = \mu_{dry} \tag{17}$$

The assumption and limitation governing Gassmann's equation are important to be aware of before applying it. The following conditions need to be met for the equation to be valid (Adam et al., 2006; Mavko et al., 2009; Gelius and Johansen, 2012):

- the rock is porous, homogeneous and isotropic and filled with only one fluid
- the pore fluid is homogeneously distributed within the pores
- all pores are connected
- the system is closed, that is, no fluid flow out of the system
- the fluids have time to reach equilibrium pressure between pores, which is typically true for seismic frequencies or lower
- no chemical interactions between rock frame and pore fluid

Usually, some of these conditions are broken. A rock will typically consist of more than one mineral and will in most often have at least a small amount of anisotropy. Brown and Korringa (1975) published an anisotropic form, but its complicated nature and the lack of necessary information about the anisotropy renders it not applicable in most cases. Any anisotropy is in practice often ignored (Avseth et al., 2005). A rock will likely consist of several minerals, and a standard approach to calculating the effective properties of the minerals is to use a mixing model. The effective moduli are calculated using upper and lower bounds (see section 2.6.2) and taking their average. Similarly, a pore system containing several fluids can be approximated by the effective properties of the fluids. For a system containing a proportion of gas, V_g, and a proportion of brine, V_b, the effective bulk modulus of the mixed fluid, K_{fl}, can be approximated by the effective bulk modulus of the fluid (Avseth et al., 2005):

$$\frac{1}{K_{fl}} = \frac{V_g}{K_g} + \frac{V_b}{K_b} \tag{18}$$

where K_g and K_b are the bulk moduli of gas and brine. The density of the effective fluid is defined by:

$$\rho_{fl} = \rho_g V_g + \rho_{br} V_{br} \tag{19}$$

ρ_g and ρ_b are the density of gas and brine. These equations can be extended to an infinite number of different fluids.

2.6.2 Effective elastic properties

Before applying Gassmann's equation, we need to estimate the input parameters. In case a rock consists of several minerals, the effective mineral bulk modulus, which is the bulk modulus of the solid part of the rock (pore space excluded), can be estimated by upper and lower bounds. The simplest models are the Voigt (1910) and the Reuss (1929) upper and lower bounds. For simplicity, it is often assumed that the mineralogy is a mix between clay and quartz, but the bounds can be extended to an infinite amount of different mineralogies. If a rock consists of N different minerals where V_i and M_i are the volume fraction and elastic modulus of mineral i, then the effective elastic modulus of the mixture can be computed. The Voigt bound, M_V, is the highest possible modulus of the mixture while the Reuss bound, M_R, is the softest possible mixture. The equations are defined as (Avseth et al., 2005):

$$M_V = \sum_{i=1}^{N} V_i M_i \tag{20}$$

$$\frac{1}{M_R} = \sum_{i=1}^{N} \frac{V_i}{M_i} \tag{21}$$

The elastic modulus, M, can represent bulk, shear or other elastic moduli. There exist other and more complicated mixing models. The Hashin–Shtrikman upper and lower bounds (Hashin and Shtrikman, 1963) are often used since they provide a more narrow bound between the upper and lower bounds.

The bulk modulus and density of the pore-filling fluid also need to be estimated. Both are dependent on pressure and temperature and can be estimated using the equations of Batzle and Wang (1992). If several fluids are present, effective moduli and density can be computed using equation 18 and 19.

Another important property is the dry rock bulk modulus. If well logs are available, the V_p, V_s and ρ values, corresponding to a porous rock filled with a specific fluid, can be used to calculate K_{sat} and μ_{sat} by rearranging equation 3 and 4. Then, by solving Gassmann's equation for K_{dry} the dry rock bulk modulus of the given rock can be calculated. If well logs are not available, there exist theoretical rock physics models that can provide an estimate of the dry rock bulk modulus. Commonly used models include Hertz-Mindlin theory (Mindlin, 1949), differential effective medium theory (Norris et al., 1985) and the contact-cement model by Dvorkin and Nur (1993).

Once all necessary properties have been estimated, Gassmann's equation allows one to compute the bulk modulus of the rock with different fluids and for different porosities. The new K_{sat} can be used to estimate seismic velocities and predict the change in seismic response that accompanies a change in pore fluid.

2.6.3 Patchy saturation

One of the assumptions of Gassmann's equation is that the pore-fluid is homogeneously distributed, but this is not always the case. An alternative is that the fluid could be arranged in patches, where a fully saturated patch could be surrounded by partially saturated or dry patches (Dvorkin and Nur, 1998). According to Knight et al. (1998), the manner in which the fluid is distributed can have a significant impact on the P-wave velocity for different saturations.

In cases where Gassmann's equation does not achieve results that match the observed values, it might be worth investigating if the fluid distribution is inhomogeneous. Dvorkin and Nur (1998) propose a workflow that could aid in such investigations. Using well log data to invert for the dry-rock Poisson's ratio, both under the assumption that the saturation is patchy and that it is homogeneous, they claim that the saturation pattern can be determined based on which methods provides the most realistic values.

Seismic cube	Field	Domain	Polarity	Phase	Partial stacks
AVO_ST11MZ07	Gullfaks	Time	Normal	Zero-phase	Near, far
BPN9601STRZ15	Aasta Hansteen	Time	Normal	Zero-phase	Near, mid, far

Table 1: Information about the two seismic cubes used in this study. The data have been provided by Equinor ASA and licence partners.

3 Data and workflow

This chapter provides an overview of the seismic data used, the workflow of this study as well as the modelling procedures.

3.1 Datasets

To develop and test the algorithms and methods that have been created in this study, two seismic cubes are used. The first one is a seismic dataset which covers the Aasta Hansteen field in the Norwegian Sea, consisting of the Snefrid, Haklang and Luva prospects. The second dataset is a seismic cube covering most of the Gullfaks field in the North Sea. For each field both full stack cubes and partial stacks of different angle ranges are available. Further details about the seismic data are summarised in table 1, and the location and coverage of the cubes are shown in figure 3.1. Equinor ASA and license partners provided the seismic cubes. In addition to the seismic data, a variety of well data have been used. Well data have been either been provided by Equinor ASA or downloaded from the Discos database.

In both the seismic cubes, an increase in acoustic impedance is represented by a peak (positive amplitude, red colour).

3.2 Software

Petrel™, which is a trademark of Schlumberger Technology Corporation, has been used to visualise, inspect and store seismic and well data. The main result of this study is the algorithms and methods that have been created, and they are developed in MATLAB™ (trademark of The MathWorks, Inc.). The MATLAB Support Package for Petrel, which

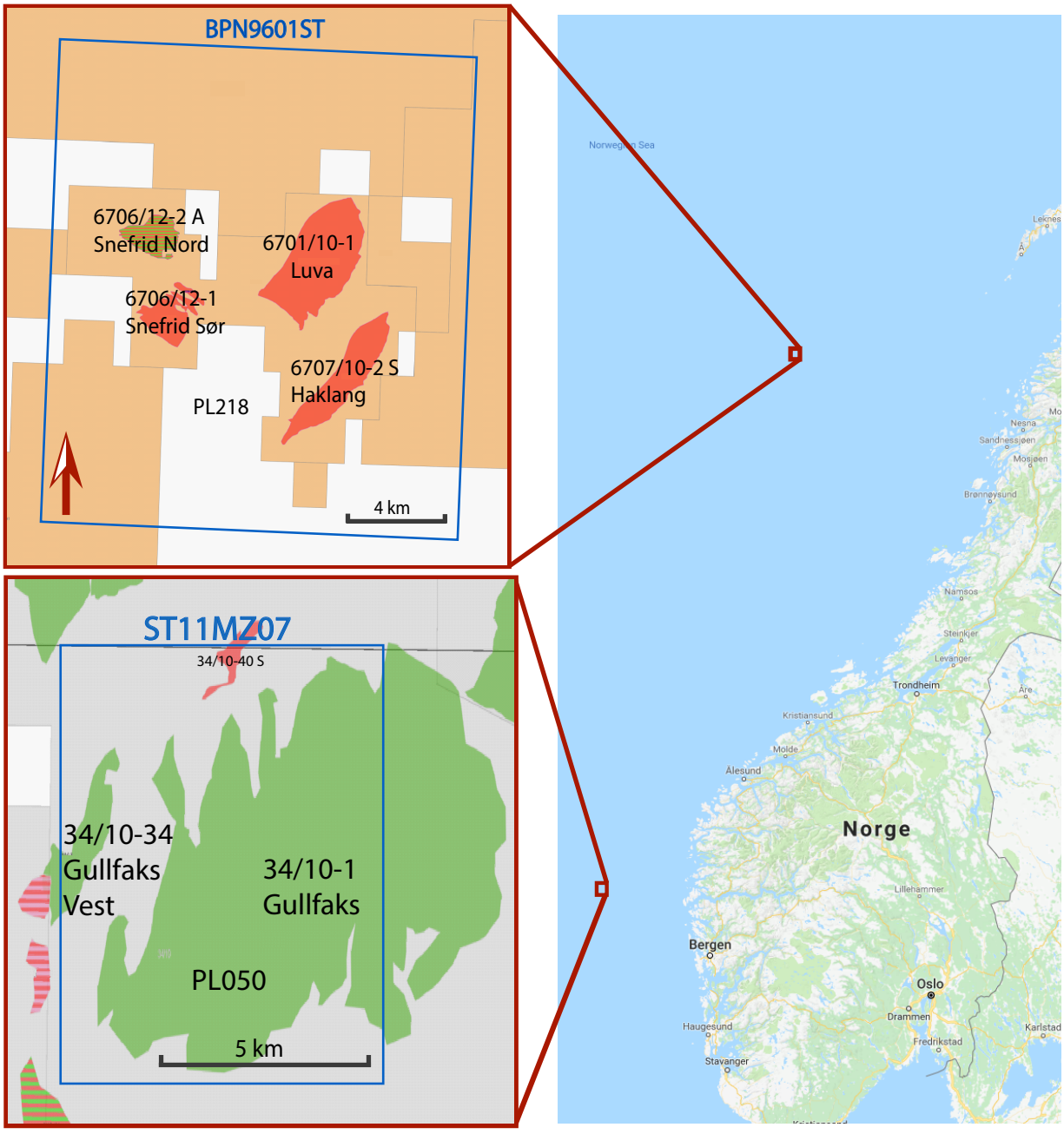

Figure 3.1: The coverage of the seismic cubes at Gullfaks (BPN9601STRZ15, top left) and Luva (AVO_ST11MZ07, bottom left) and their geographic location.

allows for simple transferring of data between MATLAB and Petrel has also been used.

3.3 Workflow

Figure 3.2 shows the complete workflow of this study. The broad idea is to quantify the expected values of different seismic attributes and DHI's, both in a hydrocarbon-filled and brine-filled reservoir, and use these values as input into the algorithms. The algorithms will search along an interpreted reflector for the expected contrasts with the goal of locating possible fluid contacts.

At first, the methods are tested at the Luva and Gullfaks datasets. Since the position of the fluid contact at Luva and Gullfaks is known, the result of the algorithms can be analysed in terms of how accurately the position of the fluid contact is predicted. The effect of different factors, parameters and methods are tested to optimise the algorithms.

The entire workflow is not completed in this study; the focus has been to develop algorithms related to the changes in amplitude (including tuning effects) and AVO at the top reservoir. The algorithms have been designed to search along the top reservoir at Luva and Gullfaks. Based on the experience from the testing at Luva and Gullfaks, it will be determined if it is worthwhile to complete the rest of the workflow, and specifically, if it is possible to develop the algorithms to work in an exploration setting. Possible future developments are addressed in chapter 8.

3.4 Modelling

As seen in figure 3.2, the two DHI's included in this study are amplitude shut-off (see section 2.2.2) and AVO (see section 2.5). Before the algorithms for fluid contact prediction in the seismic data can be developed, the expected values of these attributes are modelled. The idea is to model the expected value of the seismic attributes both in the hydrocarbon and brine zone. The modelling procedures were first performed for the Luva dataset, and the following sections will explain the details. For the modelling, the minimum input needed is well logs from the relevant field, at least containing a sonic log and a density log.

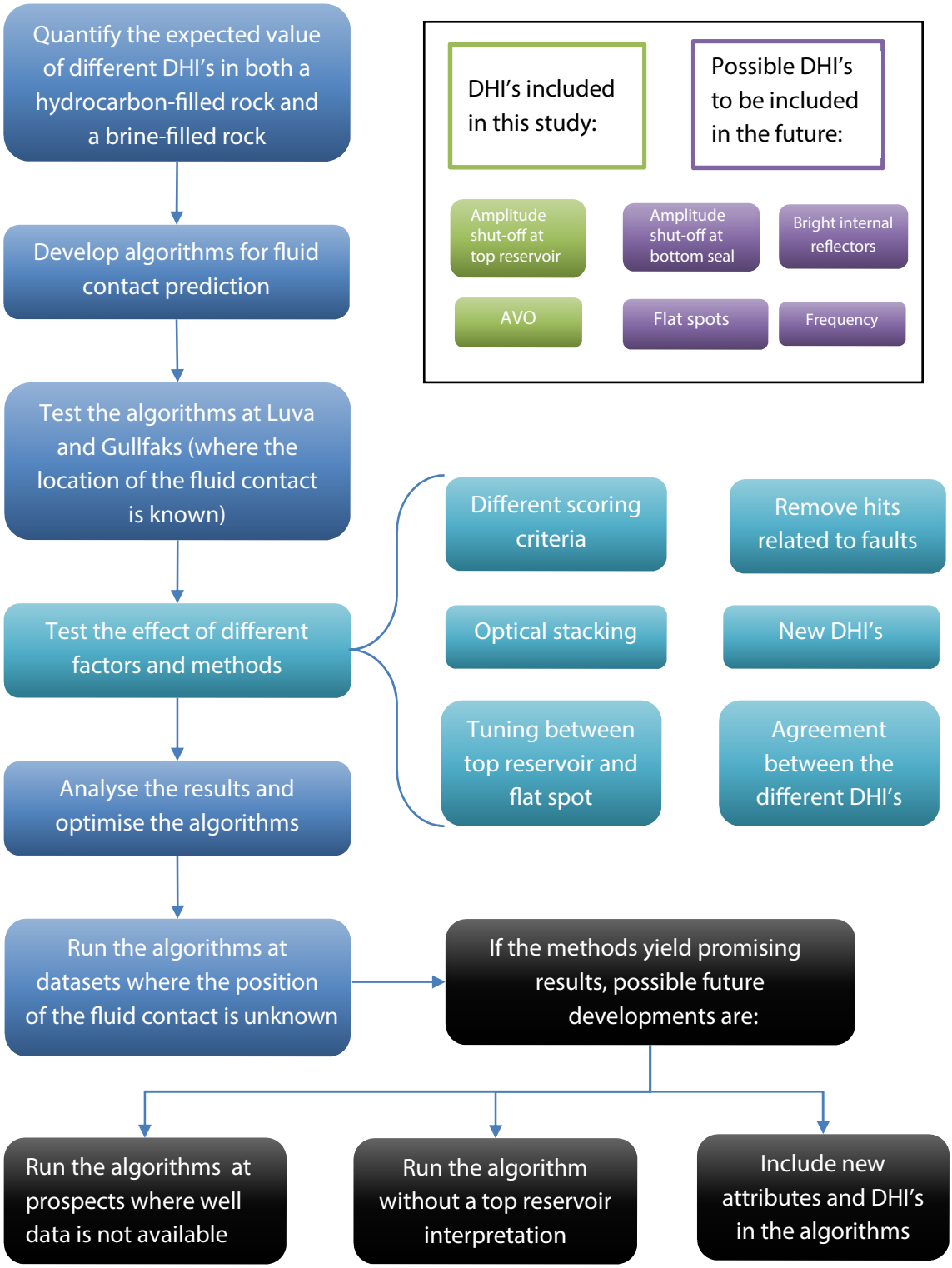

Figure 3.2: Flowchart showing the workflow and the main ideas of this study.

All the modelling routines are solved by creating scripts in MATLAB or by using scripts that are available in SeisLab package, which is available for free download at mathworks.com.

3.4.1 Amplitude modelling

The first step is to model the amplitude at the top reservoir reflector. At Luva, this is done by using data from well 6707/10-1, which penetrates the top reservoir. By creating a synthetic trace from the well logs and performing fluid substitution, the response at the top reservoir, both in the gas zone (in-situ) and in the water zone, can be modelled.

Before calculating the reflection coefficients, a few other steps need to be completed. The necessary inputs to the Zoeppritz equations are sonic (P- and S-wave) and density logs. If a shear wave sonic log is not available, the S-wave velocities were estimated using the P-wave log and Castagnas well known empirical relationship (Castagna et al., 1985). This relationship is often referred to as the mudrock line and is stated in equation 11. This relation is valid in water-filled siliciclastic rocks but will not be accurate in hydrocarbon-filled rocks. If the well penetrates a hydrocarbon filled zone, fluid substitution must be performed before applying the mudrock line. Since S-wave velocities are not available, Gassmann's equation is not applicable. Therefore, the substitution was performed using the approximate Gassmann's equation proposed by Mavko et al. (1995).

To be able to compare the data from the well logs, which are in depth, with the seismic data, which are in time, a time-depth relationship is computed. The process of calculating this relationship is called a well-tie. By defining a velocity in the water layer and the overburden (above the first log point) and then integrating the sonic log, a time-depth relationship is obtained. The focus was to obtain a good match in the reservoir zone, and some trial and error regarding the overburden velocity were necessary to get a good match.

Well logs are sampled with a higher frequency than seismic data and are therefore able to resolve features on a smaller scale. Well logs are typically on a scale of tens of centimetres while seismic data are on a scale of tens of meters. Before creating the synthetic traces, the well logs are therefore up-scaled so that they are on a similar scale as the seismic data. This is done by sub-dividing the well logs into blocks of 2 metre length, where each block is assigned the average of the values in the given block.

After performing the upscaling and the well-tie, the P-wave, S-wave and density logs are used to calculate the reflection coefficient along the well path. This calculation is done using the full Zoeppritz equations for the appropriate angle range. For the Luva dataset, the amplitude is modelled to match the full stack seismic cube, which contains angles in the 0-38 degrees range. The result from the Zoeppritz equations are the calculated reflection coefficients along the well path for a given angle. The reflectivity series is convolved with the seismic wavelet to obtain the synthetic trace. The seismic wavelet can be estimated by extracting a wavelet from the seismic data using the Wavelet toolbox in Petrel or a simple Ricker wavelet with an appropriate central frequency can be used. By stacking the synthetic traces for all the angles, the final synthetic trace is obtained. This trace should match the traces near the well path in the full stack seismic cube. If there is a poor match between the seismic and the synthetic trace, the well-tie is modified or a bulk shift in time is applied.

A comparison between the real and synthetic traces from Luva is displayed in figure 3.3. There is a good match between synthetic and real seismic, especially at the top reservoir, which is the negative (blue) reflector at -3315 ms. At the flat spot (gas-water contact), which is the red (positive) reflector at -3420 ms, the reflector from the synthetic trace is slightly shallower than in the real seismic data. Inaccurate velocities from the well logs could lead to an imprecise well-tie, and hence, somewhat mispositioned reflectors.

Since well 6707/10-1 penetrates the gas zone, the top reservoir reflection represents the response in the gas zone. A fluid substitution therefore had to be done to estimate the expected response in the brine zone. The fluid substitution is performed using Gassmann's equation (eq. 16) and the methods explained in section 2.6. An overview of fluid and rock properties used in the fluid substitution at Luva are listed in table 2. The fluid properties are calculated using the equations of Batzle and Wang (1992), and the mineral moduli are found in Mavko et al. (2009).

Knowledge of the rocks' lithologies and porosities is needed to perform the fluid substitution. Shale volume is estimated using the gamma ray log. First, upper and lower cut-off values, corresponding to shales and clean sands, are determined from inspecting the gamma ray log. Then, by interpolating linearly between the upper and lower cut-off values, the shale volume along the well path is approximated. Porosity can be estimated using the density log and the following relationship:

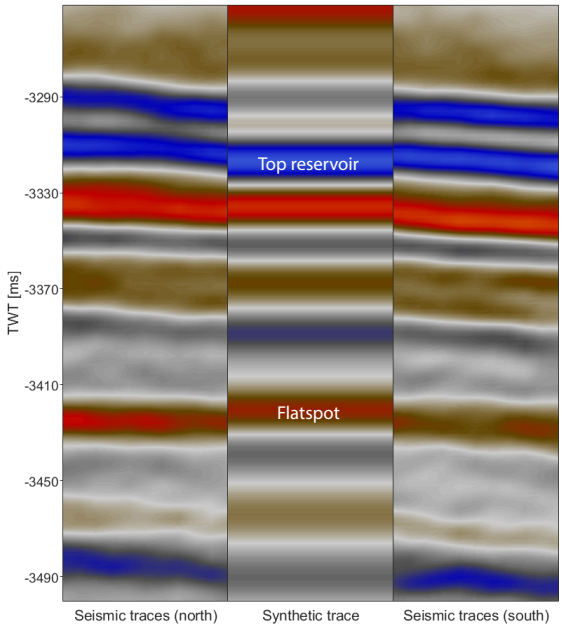

Figure 3.3: The scaled synthetic trace along with the nearby seismic traces. The synthetic traces was generated using well logs from well 6707/10-1 and a Ricker wavelet with a peak frequency of 20 Hz.

$$\phi = \frac{\rho_m - \rho_b}{\rho_m - \rho_{fl}}$$

where ρ_m is the matrix density, ρ_b is the formation bulk density (from the density log), and ρ_{fl} is the density of the pore-filling fluid.

As explained in section 2.6, K_{dry} is calculated using the well logs. Then, by inputting K_m, K_{dry} and K_{brine} into Gassmann's equation, the bulk modulus in case the reservoir is brine-filled is estimated. The effective density in the water zone, p_{eff}, is estimated according to the following equation:

	bulk modulus [GPa]	shear modulus [GPa]	density [g/ccm]
Gas (in-situ)	0.074	0	0.179
Brine	2.97	0	1.04
Quartz	36.6	44	2.65
Clay	20.9	10.9	2.58

Table 2: The properties used in the fluid substitution at Luva. Rock properties are from Mavko et al. (2009), and fluid properties are calculated, at appropriate reservoir conditions, using the equations of Batzle and Wang (1992).

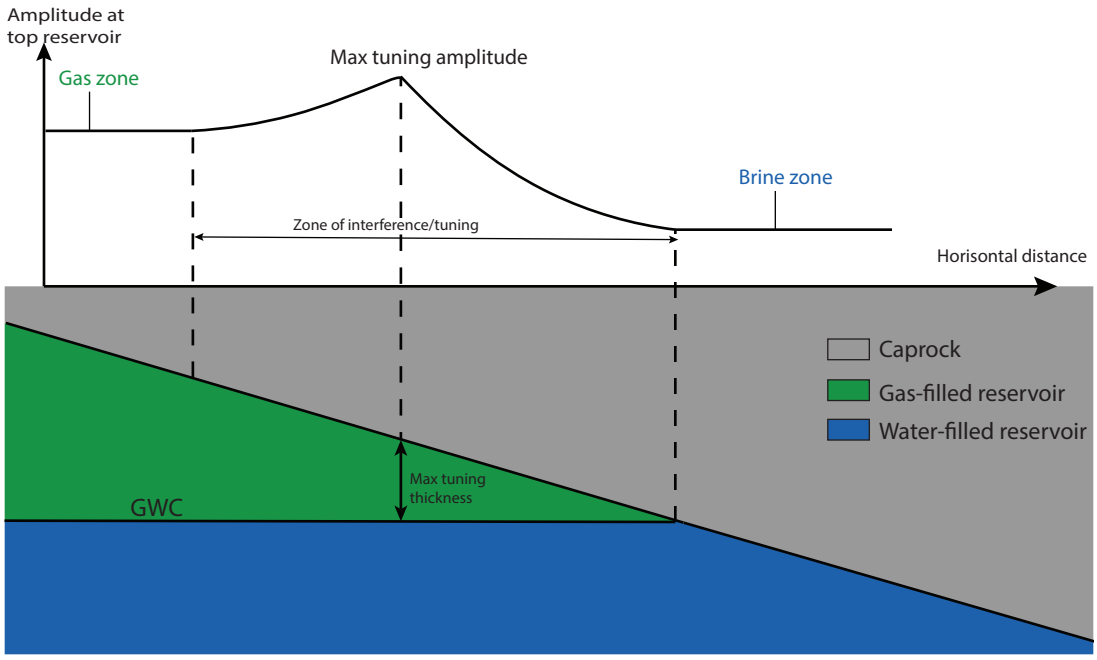

Figure 3.4: Schematic illustration of how the tuning effect could affect the amplitude at the top reservoir reflector above a fluid contact. In this case, it is assumed that the rock properties, apart from the change of pore-fluid, are constant.

$$\rho_{eff} = \rho_{res} + \phi \left(\rho_{brine} - \rho_{gas} \right)$$

Where ρ_{res} are the densities from well logs taken in the reservoir (gas zone), ϕ is the reservoir porosity and ρ_{brine} and ρ_{gas} are the densities from table 2.

By using the new bulk modulus and density (shear modulus stays the same, in accordance with Gassmann's theory) the new P- and S-wave velocities are calculated. Another synthetic trace is generated, this time using the fluid substituted well logs, and the result is a synthetic trace representing the top reservoir response in the brine case.

The synthetic traces at the well location, that is, the synthetic trace generated from well logs (gas case) and the synthetic trace generated from after fluid substitution (brine case), are scaled to match the amplitude at the top reservoir from the real seismic trace.

3.4.2 Tuning effect

In a geological setting with a dipping top reservoir and flat a gas-water contact, as illustrated in figure 3.4, a tuning effect between the top reservoir and the flat spot reflectors is expected. The effect of tuning at the top reservoir depends on the size of the sidelobes of the wavelet and the polarity and strength of both reflectors (see section 2.3). The situation illustrated in figure 3.4 is similar to the setting at Luva. Therefore, to model how the amplitude changes down dip along the top reservoir reflector at Luva, this tuning effect is included in the modelling.

A simple two-layer model is created to model the tuning effect. By picking values in the caprock and the reservoir from the well logs, the reflections from the top reservoir and the fluid contact are replicated. The maximum tuning effect is calculated by convolving a wavelet with the calculated reflection coefficients at the top reservoir and the flat spot.

The final result of the amplitude modelling is the following values:

- the expected amplitude at the top reservoir in the gas zone
- the expected amplitude at the top reservoir in the gas zone when there is maximum tuning between the top reservoir and flat spot
- the expected amplitude at the top reservoir reflection in the brine zone

These amplitudes should correspond to the different sets of amplitudes illustrated at the top of figure 3.4. These amplitudes will be used as input into the amplitude search algorithm, which will be explained in chapter 4.

3.4.3 AVO modelling

The next attribute to investigate is the AVO response. According to Avseth et al. (2005), the first step of any AVO analysis should be a feasibility study. Will there be a clear AVO response, and if so, what kind of response? To answer this, the AVO response is modelled using well data.

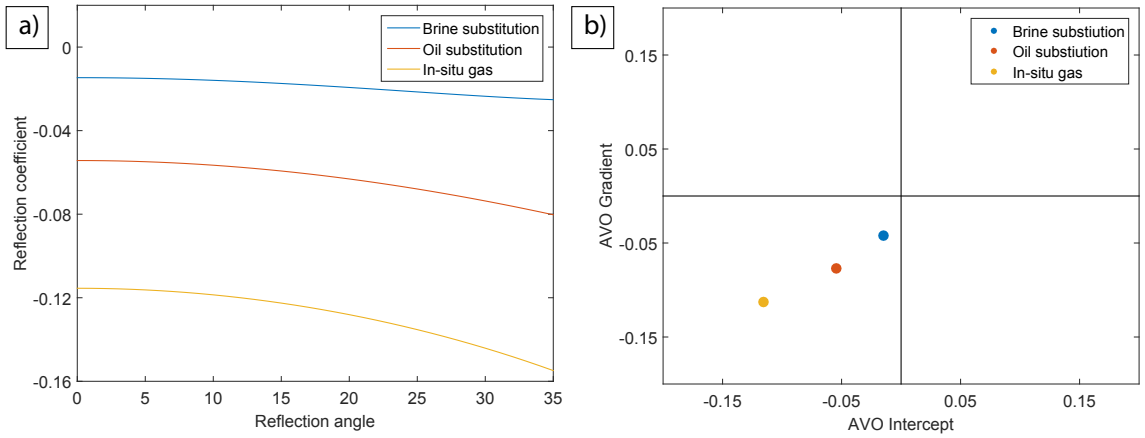

Figure 3.5: (a) Reflection coefficient versus angle for the three different two-layer models (see table 3). (b) The calculated intercept and gradient values for each of the three cases.

P- and S-wave velocities and density values are picked from the well logs, both in the caprock and in the gas zone. Using Gassmann's equation, the gas is substituted with brine and oil to calculate the Vp, Vs and ρ values in the brine and oil case. These values are listed in table 3, and the amplitude versus angle variation along the top reservoir are calculated using the Zoeppritz equations. The caprock is kept constant while the reservoir is modelled with the different fluids. The result can be seen in figure 3.5 (a), where the reflection coefficient versus angle is plotted for the different fluid cases.

The values from table 3 are also used as input into Shuey's two-term approximation of the Zoeppritz equation, and the AVO gradient and intercept are calculated directly from equation 7. The values in the gas-, oil- and brine-zone are plotted in an intercept versus gradient plot in figure 3.5 (b). The gas zone exhibits a class 3 AVO response, with strong negative amplitudes at zero offset and increasingly negative amplitudes with increasing angle. Brine plots in the same quadrant, but the response is weaker than in the gas zone. The oil case is included as a control, and as expected, the oil zone plots between the gas zone and the brine zone.

	Caprock	**Reservoir: in-situ gas**	**Oil substitution**	**Brine substitution**
Vp [ms]	2811	2612	2769	2938
Vs [ms]	1340	1551	1502	1487
ρ $[kg/m^3]$	2447	2088	2273	2227

Table 3: Values used in a two-layer model to calculate the expected AVO response. Values in the gas case are extracted from the well logs, and oil and brine values are obtained by performing fluid substitution of the well logs.

Different AVO parameters can be derived from the gradient and intercept values. The fluid factor, as explained in section 2.5.4, can be used to discriminate between gas/oil and brine in many cases (Smith and Sutherland, 1996). By using the calculated gradient and intercept values, the fluid factor in each zone is calculated using equation 15. The result indicates that the fluid factor should be notably stronger (more negative) than the fluid factor in the brine zone. So, the final product of the AVO modelling is the expected fluid factor value at the top reservoir reflector, both above the gas zone and brine zone. The expected fluid factor values at Luva are listed in table 4, and will be used as input in the AVO search algorithm, which will be explained in chapter 4.

	Gas zone	Oil zone	Brine zone
Fluid factor	-0,21	-0,11	-0,04

Table 4: Modelled fluid factor at Luva for the different pore-fluids.

3.5 Sources of error

The selected workflows introduce a set of uncertainties. Most notably is the accuracy of the modelling, and this will have a direct impact on the results. If the well tie, the attribute modelling or the fluid substitution is inaccurate or based on wrong assumptions, the algorithms will search for values that do not correspond to the real case.

All models are based on simplifications and in many cases that is adequate. If the simplifications are too far from the real case, the results will not reflect reality, and this would be a bad thing. An important part of the modelling is the fluid substitution, and all the inputs into Gassmann's equation are based on assumptions and estimates.

There are some uncertainties regarding the input parameters to Gassmann's equation. The bulk modulus of the dry rock, the matrix and the pore-fluid, the porosity, the lithology and the water saturation are all estimated before applying Gassmann's equation. Any error in these estimations will propagate to errors in the calculated saturated bulk modulus. A good idea is to check that the calculated values are consistent. Brine or oil substituted for gas should lead to an increase in density and a decrease in S-wave velocity (Smith et al., 2003), and if this is not the case, there is likely something wrong.

As explained in section 2.6, the results from Gassmann's equation depends on how the fluids are distributed in the pore space. The elastic properties of a reservoir will be dif-

ferent if the fluids are distributed in a patchy manner than if they are homogeneously distributed. The latter is a common assumption. Smith et al. (2003), investigated the effect of patchy saturation on the estimation of P-wave velocity from Gassmann's equation. The findings from this study are that the effect of patchy saturation is most significant in high porosity at low gas saturation. At gas saturations between 0-30 %, the maximum difference in P-wave velocity estimation is around 5%.

It is well documented that both tuning (Avseth et al., 2005; Bakke and Ursin, 1998) and anisotropy (Wright, 1984; Kim et al., 1993) have an impact on the AVO response. Since neither of these effects is included in the AVO modelling, this could affect the accuracy of the modelled values.

Since the methods are based on programming, and there are many thousand lines of codes involved, small errors or inaccuracies in the code could have an impact on the results. It has therefore been of importance to do thorough testing and analyse the results with a critical eye. For the modelling part, evaluating the results to see if they comply with the theory and what is expected, have been important. An example is the results of the AVO modelling, where the model indicates a stronger AVO response in the gas zone than in the brine zone, with the oil response in between.

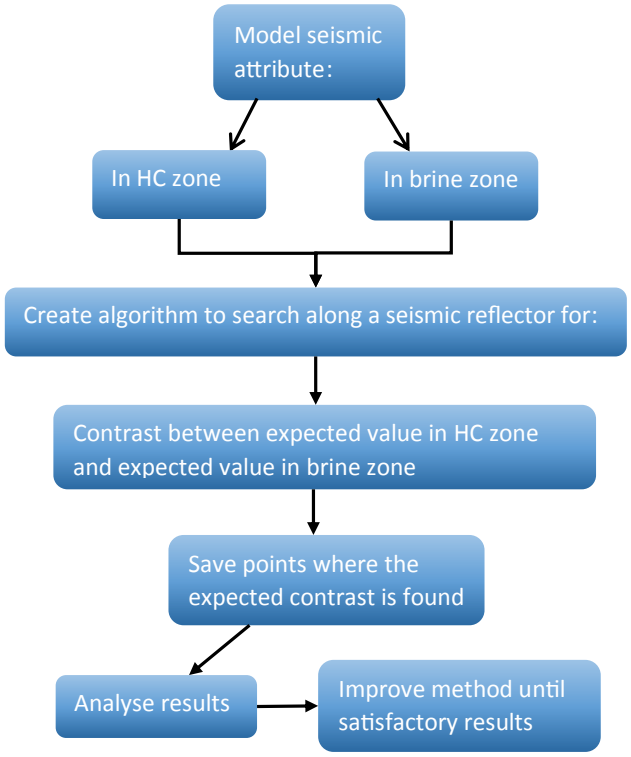

Figure 4.1: Flowchart of the simplified workflow that was followed to develop the algorithms.

4 The algorithms

The main result of this thesis is the algorithms that have been created. The flowchart in figure 4.1 illustrates the workflow that was followed in the process of developing the algorithms. The main idea is to develop algorithms to search along a given seismic reflector for a change in response that is consistent with a change of pore-fluid from hydrocarbons to brine. Two different search algorithms are created, one searching for the change in amplitude and one searching for the change in AVO response.

4.1 Amplitude search

The flowchart in figure 4.2, sketches the basic idea behind the amplitude search algorithm. The top three boxes in the flowcharts represent the necessary input data, which in this case is a seismic cube, an interpretation of the top reservoir and the values from the amplitude modelling. The amplitude modelling, as explained in the previous chapter,

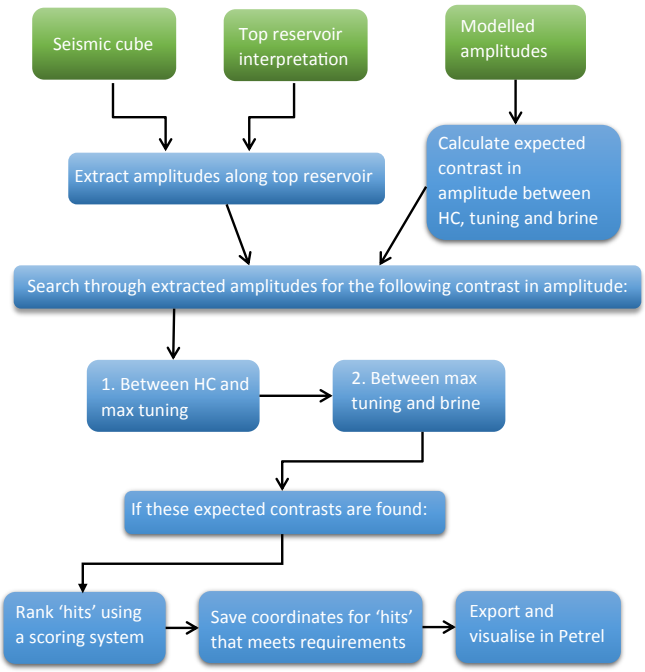

Figure 4.2: Flowchart illustrating the workflow of the amplitude search algorithm.

resulted in three amplitude values, one corresponding to the amplitude in the gas zone, one corresponding to the amplitude at maximum tuning and one corresponding to the amplitude in the brine zone.

In the following subsections, details for the main parts of the amplitude search algorithm will be provided.

4.1.1 Amplitude extraction

A top reservoir interpretation is required input, as this is what makes it possible to extract the relevant amplitude values from the seismic cube.

The seismic cube and the top reservoir surface is imported into MATLAB using the MATLAB plugin for Petrel. The top reservoir surface and the seismic data consists of discrete points. The seismic data is a large matrix, consisting of seismic traces that typically are sampled every 2 or 4 ms in the vertical direction and every 12,5 meters in the cross line and inline direction. Therefore, before extracting the amplitudes along the top reservoir reflector, the points at the top reservoir surface needs to be matched with a sample from a seismic trace in the cube. First, the seismic data is sorted into crosslines and inlines, and

Modelled amplitude values at Luva		
In gas zone	At max tuning	In brine zone
-2097	-2980	-1348

Table 5: The result of the amplitude modelling at Luva. The values represent the amplitude variation expected in the different zones along the top reservoir reflector.

then, by calculating the distance between each point on the top reservoir and the seismic samples, the closest sample is picked and saved.

Since every point on the top reservoir surface is matched with an amplitude sample from the seismic, the amplitude along the top reservoir is saved. But an important aspect regarding the amplitude extraction is that the accuracy is dependent on the quality of the interpretation. If the interpretation is inaccurate, the extracted amplitudes will not reflect the actual amplitudes at the top reservoir. Therefore, a small window of amplitudes around the matched sample is extracted, and the strongest amplitudes are picked. This reduces the issue with an inaccurate interpretation to a certain degree. If the mismatch is significant, the extraction will be inaccurate either way.

At Gullfaks, the interpretation is inaccurate at the apex of the rotated fault blocks. Since this is the most important area, parts of the interpretation were redone to make sure the correct amplitudes were picked. At Luva, where the top reservoir reflector is clear and easy to follow, this was not an issue.

4.1.2 Searching for the expected change in amplitude

The next step is to develop an algorithm that searches along the extracted amplitudes looking for the modelled change in amplitude across the fluid contact. In table 5, the expected amplitude in the different zones at Luva are listed. One option is to search for points on the reflector that has the exact amplitudes in each zone. For Luva, that would mean looking for amplitudes of -2097 to locate points in the gas zone, amplitudes of -2980 to locate the maximum tuning amplitudes, and amplitudes of -1348 to locate points in the brine zone. Instead, the algorithm searches for the contrast in amplitude between the different zones. This is based on the assumption that the contrast will be less affected by lateral changes than the exact values in each zone. Lateral variations in the reservoir or caprock can lead to significant variations in amplitude at the top reservoir reflector. It is believed that the contrast between the hydrocarbon and brine zone will be

less affected by such changes. If there are large variations in the area surrounding the fluid contact, this assumption is violated, and the method is less likely to work.

At Luva, the expected contrast in amplitude between the gas zone and the amplitude at max tuning is a decrease of about 900. The expected contrast between the max tuning amplitude and the amplitude in the brine zone is an increase of approximately 1600. Therefore, two traces with amplitude of -3500 and -1900 or -2400 and -800 would both have the correct contrast between the max tuning and brine amplitudes.

The amplitude algorithm has been in continuous development since the beginning. By analysing the results and doing small modifications, the algorithm has been improved step by step. The current version of the amplitude algorithm does the following:

1. starting at trace number 1 at line number 1, the algorithm calculates the contrast between the extracted amplitude at trace 1 and the extracted amplitude at the n following traces (n depends on the dip of the reservoir and the expected distance between max tuning and the onset of tuning)
2. of the n traces, look for those that have the correct contrast with trace 1, that is, the contrast in amplitude from the HC zone to maximum tuning
3. if the correct contrast is found, the location of the two points are saved
4. since the maximum tuning amplitude should be the strongest amplitude, only points that are located at a local minimum will be accepted
5. the algorithm loops through all the traces at the line and saves all pairs of points that have the expected change in amplitude between the HC zone and the max tuning amplitude are saved
6. the algorithm will then calculate the contrast between all the located max tuning points and the next n traces
7. if the algorithm has located the expected contrast from the HC zone to max tuning between trace 100 and trace 200, then it will calculate the contrast from trace 200 and forward (n number of traces)
8. it then repeats the same procedure looking for the expected contrast, only this time it will search for the expected contrast between the maximum tuning and brine zone amplitudes

9. if, for example, the algorithm then locates the expected max tuning to brine contrast between trace 200 and trace 320, the location of the points at trace 100, 200 and 320 are saved, and these points together constitute a hit
10. finish the procedure at line 1 and do the same for rest of the lines in the cube
11. export all the brine points, as they should be located at, or close to the fluid contact, and visualise them in Petrel

Because the seismic data is in discrete values, it cannot be expected to find the exact contrast between the different zones. A window of uncertainty needs to be added to the expected contrasts. Test runs at Luva and Gullfaks will be used to determine an appropriate uncertainty.

Figure 4.3, illustrate an example of how the extracted amplitude along a given seismic line could vary. From the point A1, which in this example is located in the HC zone, several points are within the expected contrast to the maximum tuning. The contrast is marked with the green dotted lines, and the brightest amplitude within this window is accepted, and in figure 4.3, this is the point marked as A2. The expected contrast between the max tuning point A2 and the brine point is marked as contrast window 2. In this example, many points lie within the accepted contrast window, and it is necessary to determine a way of deciding which of these points should be accepted as the brine point. The brine point should correspond to the first point in the brine zone, which means it should be located at the fluid contact. Ultimately, it is the location of the brine point that determines the algorithm's prediction of the fluid contact. Which of the points within the contrast window to pick is therefore of major significance.

4.1.3 Scoring system

A simple scoring system was developed to rank all potential brine points, that is, all the points that are within the expected contrast window. The scoring system aims to determine which of the potential brine points to accept, and the ranking is done according to the following conditions:

- 1 point if the difference in TWT between max tuning and brine is within a wide range of expected difference in TWT

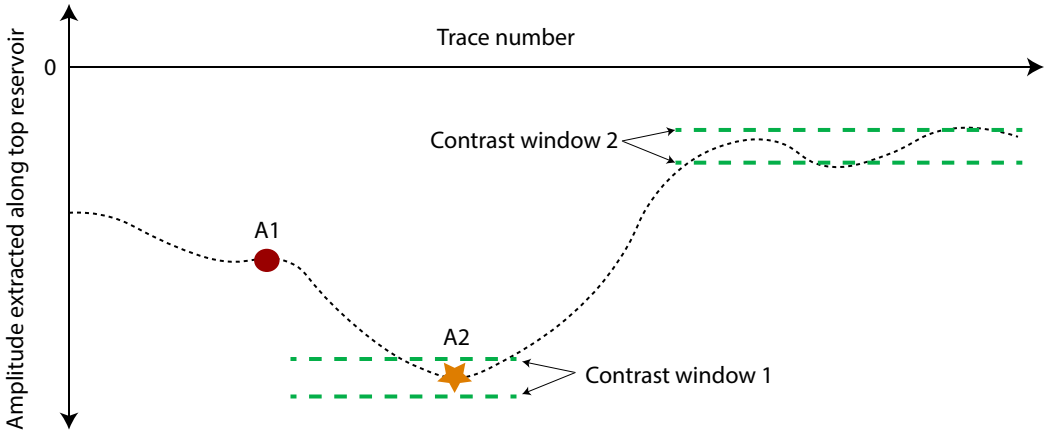

Figure 4.3: An example of how the amplitude might vary along a top reservoir on a given seismic line. The dotted green lines indicate how several points can lie within the accepted contrast window.

- 1 point if the difference in TWT between max tuning and brine is within a narrow range of expected difference in TWT
- 1 point if the brine point is at or close to the end of a shut-off, that is, where the increase in amplitude significantly slows down or flattens out
- 1 point if the HC point is located updip compared to the max tuning point
- 1 point if the max tuning point is located updip compared to the brine point

The tuning effect between the top reservoir and the fluid contact is dependent on the difference in TWT between the two reflectors. By estimating the frequency of the wavelet, the expected maximum tuning thickness in TWT can be calculated. By analysing the frequency spectrum of the wavelet, a narrow range of frequencies around the peak frequency is picked. A corresponding range in TWT is calculated based on these frequencies, and this represents the first condition in the scoring system. In many cases, the frequency spectrum does not have a clearly defined peak frequency but instead has a wider range of high energy frequencies. Therefore, a wider range of frequencies are picked as well. The corresponding range in TWT is calculated, and this is the wider range referred to in the second point in the scoring system.

The reasoning behind these requirements is that if the max tuning and brine points are located at significantly different TWT, there will not be any tuning effects between them. If the max tuning to brine contrast is located, but the difference in TWT between the two

points is 100 ms, it is unlikely that this change in amplitude is caused by a change of pore fluid. For a Ricker wavelet, the peak frequency would have to be less than 4 Hz for the maximum tuning thickness to be 100 ms, which is unrealistically low.

The third criterion is that the brine point is located at or close to the end of a shut-off. In figure 4.3, that would mean the first few points within the contrast window. These points are located at the end of an increase in amplitude. The points to the right are within the same contrast, but since they are further away from the shut-off, they are less likely to represent the first point in the brine zone.

The two final criteria are that the brine point should be located down dip relative to the max tuning point and that the maximum tuning point should be located down dip relative to the HC point. Since oil and gas always are always located updip compared to brine, it can be argued that these two points should be absolute requirements. The problem is that for structures with a hydrocarbon column that is below the maximum tuning thickness, the entire amplitude variation from the HC zone, through the tuning zone and down to the brine zone will not be present. At Gullfaks, many of the segments have a column that is close to the tuning thickness. In these cases, there will no amplitudes corresponding to the HC zone, and by requiring that the HC point is located updip compared to the max tuning point, many of the hits at Gullfaks will be removed. Therefore, to be able to assess points that are not perfect, but still could be caused by hydrocarbons, this requirement is included in the scoring system instead.

Each point that is within the given contrast range will thus be rewarded with zero to five points. This way, which of the points is most likely to be at the fluid contact can be decided. Another point is that we can set a cut-off value, that is, a minimum amount of points required, for any hit to be accepted. If we set the cut-off at three points, then all hits that are rewarded less than three points will not be accepted. If there are more than one point above the cut-off, the middle point will be saved. If we require that all the five requirements are met, only the most ideal hits will be accepted. One could say that the higher the score of a hit, the more it resembles the theoretical expectation. The effect of different cut-off values will be looked at and discussed in chapter 5 and 6.

4.1.4 Optical stacking

As described in chapter 2.4, a method that is commonly used to enhance fluid contacts is optical stacking. By stacking adjacent lines together, trends that are consistent in depth (or time) will be enhanced, while changes that are not consistent in depth will be attenuated/cancelled. By stacking x number of lines together, and then extracting the amplitudes from the stacked line, it is possible that amplitude variations related to the fluid contact would become more evident and noise would be less of an issue. The effect of optical stacking will be demonstrated in chapter 5.

4.1.5 Hits related to faults

A fault cutting through a reflector will affect its reflectivity. So, if a fault cuts through the top reservoir reflector, this will change the amplitude locally. Typically, the amplitude will be reduced in strength in the fault zone. Therefore, it is possible that a fault could lead to a decrease in amplitude similar to the decrease in amplitude caused by a change of pore fluid.

A script was created to deal with potential hits related to faults. First, the dip of the reservoir is calculated over the entire field. Then, by deciding a maximum dip, all hits that are located in areas with dips above this cut-off value will be removed. The appropriate cut-off angle will vary from field to field.

Since the dip is based on the top reservoir surface, the quality of the interpretation will affect how well this method works. If the interpretation is rough in the fault zones, the actual dip of the faults will not be captured. Smoothing the surface will reduce the dip in fault zones as well. Both issues could reduce the efficiency of this method, and it is still possible that some of the hits that are accepted will be related to a decrease in amplitude caused by a fault.

4.2 AVO search

The idea for the AVO algorithm is similar to that of the amplitude algorithm. First, as explained in chapter 3, the expected value of the fluid factor is calculated, both in the

brine zone and in the HC zone. This information is then used as input into a new AVO search algorithm, which will search for the calculated contrast in fluid factor between the gas zone and the brine zone.

By doing this, we get a second opinion on the result of the amplitude search. In the ideal case, the AVO anomaly and the amplitude anomaly would predict the fluid contact at the same depth and in the same areas. The confidence that the hits are caused by a fluid contact would then increase.

4.2.1 Calculating AVO gradient and intercept

The partial stacked seismic cubes are utilised to analyse the AVO response. At Luva near, mid and far stack seismic cubes are available. The angles contained in the near, mid and far cubes are 0-18 degrees, 16-28 degrees and 26-38 degrees, respectively. These partial stacks are used to calculate the AVO intercept and gradient from the seismic data. As mentioned in chapter 2.5.4, the fluid factor is a linear combination of the intercept and the gradient values and are known to be able to discriminate between gas zones and brine zones. Therefore, the calculated fluid factor is utilised to locate the fluid contact.

Before calculating the AVO attributes, the amplitudes in the seismic cubes are scaled. By matching the reflectivities calculated from the well logs with the reflectivities from the seismic data, a scaling factor is decided. The amplitudes in the seismic are scaled according to this scaling factor, prior to the AVO inversion. By doing this, we can compare the modelled values of the AVO attributes directly with those calculated from the seismic data.

In our case, there are at least two possible ways to calculate the AVO gradient and intercept values along the top reservoir reflector. The first one is to calculate the intercept and gradient cubes, that means, for each amplitude sample in the near and far cubes, the intercept and gradient values are calculated and stored in separate gradient and intercept cubes. The fluid factor cube is computed directly from the gradient and intercept cubes using the relationship of equation 15. Then, using the amplitude extraction algorithm, the fluid factor is extracted along the top reservoir interpretation in the same ways the amplitudes were.

The second method is similar; only it is done in a different order. By using the amplitude

extraction algorithm, the amplitudes along the top reservoir are extracted from each of the partial stacks. Then, using these extracted amplitudes, the intercept, gradient and fluid factor values are calculated.

Both methods use the method explained in section 2.5.3. The advantage of the first method is that seismic sections of the fluid factor can be visualised. The second method only provides a graph of how the fluid factor varies along the top reservoir. The advantage of the second method is that it will likely be more accurate in areas where the top reservoir reflector is not positioned exactly at the same location in both cubes.

4.2.2 The AVO search algorithm

The amplitude search algorithm is used as a template when developing the AVO algorithm. Since the methods are similar, many of the scripts can be re-used with some modifications. An important distinction between the methods is that the AVO response is calculated only in the hydrocarbon zone and in the brine zone, no tuning effects are calculated.

In the AVO search, there are only two values and one contrast to search for, and that is the contrast in fluid factor value from the HC zone to the brine zone. By adding a +/- 10% to the modelled contrast, a window of accepted contrasts is calculated. The expected contrast is used as input in the AVO algorithm, which does the following:

- first, locate all local minima in fluid factor along the given line
- for each minimum, calculate the contrast from the minimum and for the following n traces
- search for points that are within the expected fluid factor contrast window
- if the contrast is found, check if the brine point is located down dip relative to the HC point
- save the location of all hits and export to Petrel

As for the amplitude algorithm, the AVO algorithm was developed by running tests on the Luva and Gullfaks datasets. The effect of optical stacking on the seismic before run-

ning the AVO algorithm is also investigated. The result of the final version of the algorithm, with and without optical stacking, will be presented in the next chapter, and the results will be compared to those of the amplitude search algorithm.

5 Test results

As explained in the previous chapter, the methods and workflows were initially developed and tested on the Luva dataset. Luva was chosen due to the uncomplicated geology and the clarity of both the top reservoir and the flat spot. The Gullfaks dataset was then used to test further, modify and develop the algorithms.

In this chapter, we will present the results of running the algorithms at Luva and Gullfaks. How well the algorithms perform, uncertainties and possible reasons for inaccuracies will be described. The chapter is divided into sections, relating to the different fields and methods.

5.1 Luva

The Luva structure is a gas field that is part of the larger Aasta Hansteen field in the Norwegian Sea. The discovery of the gas field was made in 1997 when BP drilled exploration well 6707/10-1. A gas column was found in an Upper Cretaceous sandstone reservoir (Nise formation) in a tilted fault block (Carstens, 2007). The top reservoir is a bright and dipping reflector, and there is an obvious flat spot, which makes it easy to analyse the accuracy of the results.

5.1.1 Amplitude

The result of running the amplitude algorithm at Luva is displayed in figure 5.1, where the hits are displayed on a map of the top reservoir surface. The map is based on a seismic interpretation by Equinor, which they were kind enough to provide for this study. As seen on the map in figure 5.1, the Luva structure is bounded by a large fault to the northwest. The reservoir is dipping towards the east, with several faults cutting through the reservoir. The faults mostly have a strike angle in the same direction as the dip of the reservoir. Based on an interpretation of the flat spot, the gas-water contact (GWC) is drawn on the map in figure 5.1. Across the Luva structure, the fluid contact varies in TWT from about -3400 ms to -3450 ms.

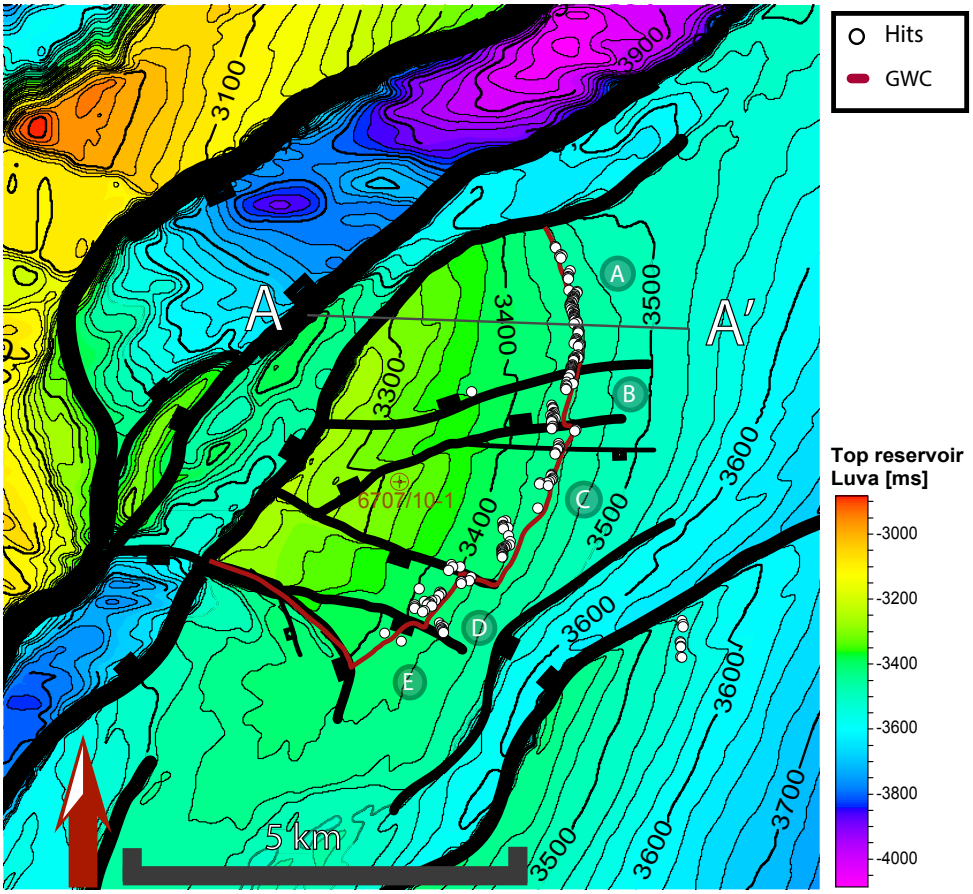

Figure 5.1: Top reservoir map of the Luva structure. In this case, a minimum score of 4 is required for a hit to be approved. The structure is divided into five parts based on the major faults. These segments are marked A-E. The few hits in the south-east belong to the Haklang prospect, and there are no more hits as lines further south have not been analysed.

As mentioned in the previous chapter, the algorithm can search either in the crossline or inline direction. At Luva, the crosslines are oriented in the same direction as the dip of the reservoir (E-W), and the search is therefore done along the crosslines.

One major factor affecting the results of the amplitude algorithm is the minimum score required. As explained in section 4.1.3, the minimum score can be set from zero to five. In figure 5.1, the results, or hits, from the algorithm run with a minimum score of four are presented. These hits have met at least four of the five requirements defined in the scoring system.

The Luva reservoir is divided into five different segments, marked on the map with A-E. In segment A, the hits are located close to the GWC. The hits cover most of the section, apart from the northernmost part. So, the algorithm is able to locate the fluid contact quite

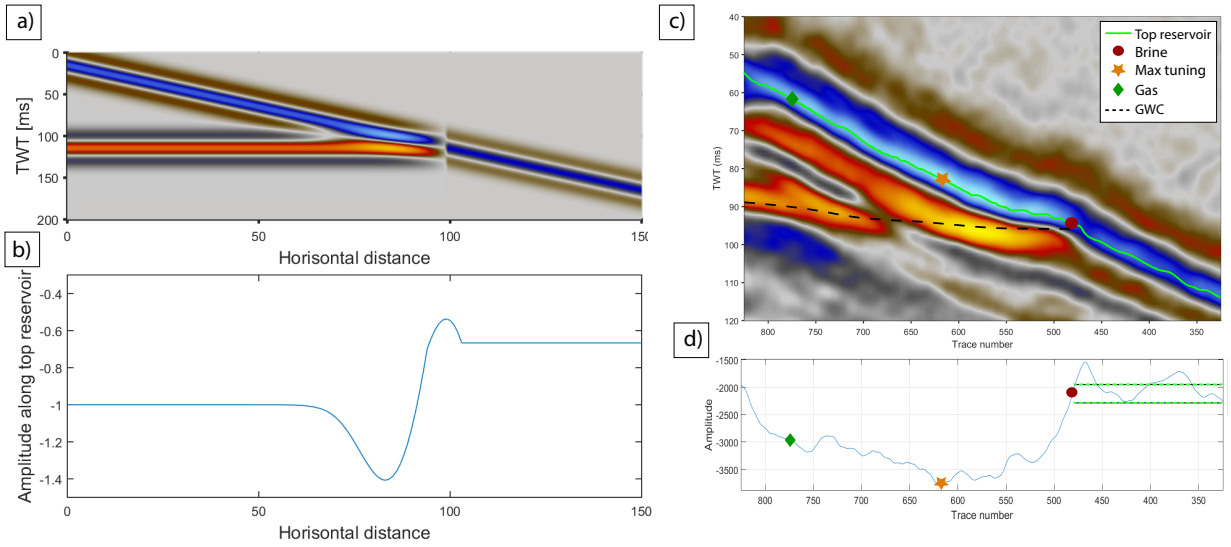

Figure 5.2: (a) Synthetic seismic section from a simple model of a dipping reservoir and a fluid contact. (b) The amplitude extracted along the top reservoir (the blue dipping reflector) in (a). (c) A seismic line at Luva, with the top reservoir interpretation. (d) The extracted amplitude along the top reservoir in (c).

accurately in segment A. Most of the points in this segment receive the full five points as well, which supports this view. The likely reason for the missing hits in the northern part of the segment is that the GWC is too close to the large fault to the north-west.

In segment B, the hits do not match the GWC as well as in segment A. The location of most hits is slightly shallower than the interpreted GWC with a maximum discrepancy of about 10-15 ms. Faults bound this segment both to the north and to the south. In this case, however, the faults do not have an impact on the amplitude along the top reservoir reflector. However, there appears to be a small discontinuity in the amplitudes and an increase in the dip of the top reservoir exactly at the fluid contact. This effect is seen in segment B, but also in parts of segment A and C. A possible cause for this effect is the destructive interference between the top reservoir and the flat spot. By creating a simple model of a dipping reservoir and a flat spot, a similar effect is replicated. This model is shown in figure 5.2 along with a seismic section from segment B. The destructive interference between the top reservoir and flat spot reflectors could lead to a more significant shut-off than what one would expect. If this is the case, it is likely that it has an affects on the algorithm's prediction of the fluid contact. If this is a common effect is hard to say without inspecting other settings.

The hits in segment C are less consistent than in segment A as well. There are gaps

between the hits, and the hits have a larger spread in TWT. The brine amplitude appears to be constant, but the maximum tuning amplitudes vary locally. The result is that the contrast between the maximum tuning amplitude and the brine amplitude varies locally. This variation in contrast affects the location of the hits. The maximum tuning amplitude can vary with values up to about 300 at adjacent lines. Where the max tuning amplitude is at its weakest, the contrast at the shut-off is in some areas too low to be within the accepted window. These large variations in max tuning amplitude are the reason for some areas missing hits in segment C. The variable amount of tuning could be due to local variations in geology, for instance, changes in porosity.

In segment D, there are hits at most lines, but they have an even more significant variation in TWT than the hits in segment C. The maximum spread in TWT in this segment is approximately 25 ms. Some of the inaccuracies are related to amplitude variations caused by the faults bounding the segment. Many of the crosslines in segment D cross one of the faults, and this is the most likely reason for the inaccuracies.

In segment E, there are only a few hits, and again, the lack of hits are related to the large faults which cause discontinuities in the amplitude.

It is the discontinuities in the top reservoir amplitudes due to faults that are the major problem at Luva. Because of these discontinuities, the expected amplitude variation is not present at all lines. Instead, the gas zone amplitudes might be on one side of the fault and the maximum tuning and brine zone amplitudes on the other side. The algorithm is not equipped to deal with such cases, and the result is either no hits or inaccurate hits in these cases.

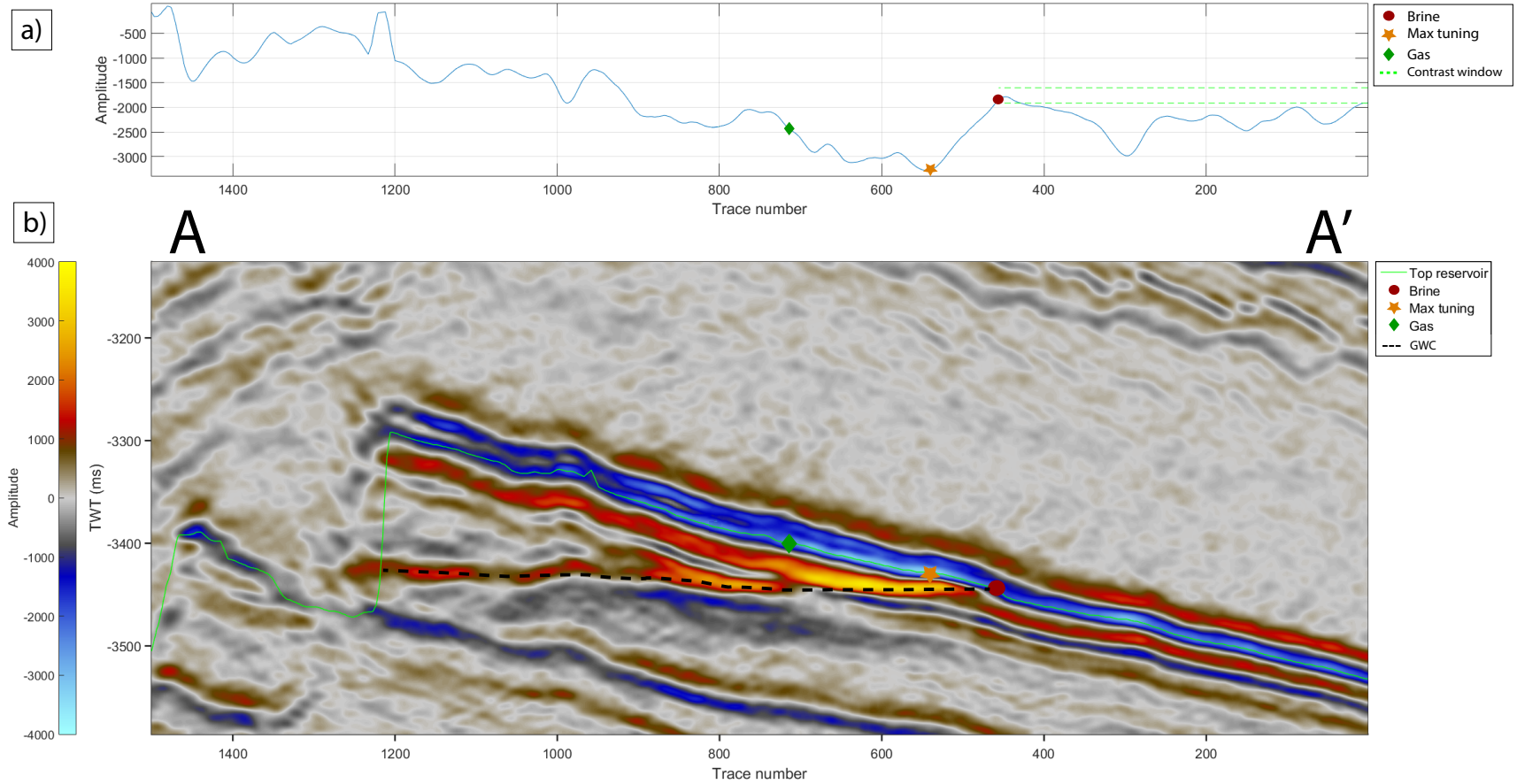

Figure 5.3: (b) A seismic section across the Luva structure. (a) The amplitude extracted from the top reservoir along the seismic section in (b).

The seismic section A-A', whose location can be seen in figure 5.1, is displayed in figure 5.3 (b). In (a), the extracted amplitude along the top reservoir is plotted. The green diamond, orange star and red circle represent what the algorithm suggests to be the HC point, maximum tuning point and brine point/fluid contact, respectively. This means that the algorithm has found the expected contrast from HC to maximum tuning between the green diamond and the yellow star and the expected contrast from max tuning to the brine zone between the yellow star and the red circle. The red point should be the first point in the brine zone and is therefore expected to be located at, or very close to, the fluid contact. The hit in this figure is located at the GWC.

All hits are classified based on the scoring system explained in section 4.1.3. The hit displayed in figure 5.3 receives the maximum score of 5:

- 2 points since the difference in TWT between max tuning and brine zone is within both the narrow, and therefore also the wide, range of expected difference in TWT
- 1 point since the HC point is located updip relative to the max tuning point
- 1 point since the max tuning point is located updip relative to the brine point
- 1 point since the brine point is located at (or close to) the end of a large increase in amplitude

So, according to the scoring system, this is an ideal hit.

5.1.2 The effect of optical stacking

In chapter 2.4, optical stacking was mentioned as a possible way of reducing noise and enhancing the amplitude variations related to fluid contacts. The amplitudes are extracted after the stacking (in this case, ten lines is stacked), and the algorithm is run at the stacked amplitudes. The result of the stacked search is displayed in figure 5.4. This time, a minimum score of 3 is required for a hit to be approved. In segment A and B, the difference between the two is insignificant. The hits are, for both the stacked and unstacked lines, similar to the hits in figure 5.1. In the segment C, there are some differences between the stacked and unstacked hits. The location of the stacked hits are more consistent than the unstacked hits; they do not have the same spread in TWT as the hits from the unstacked

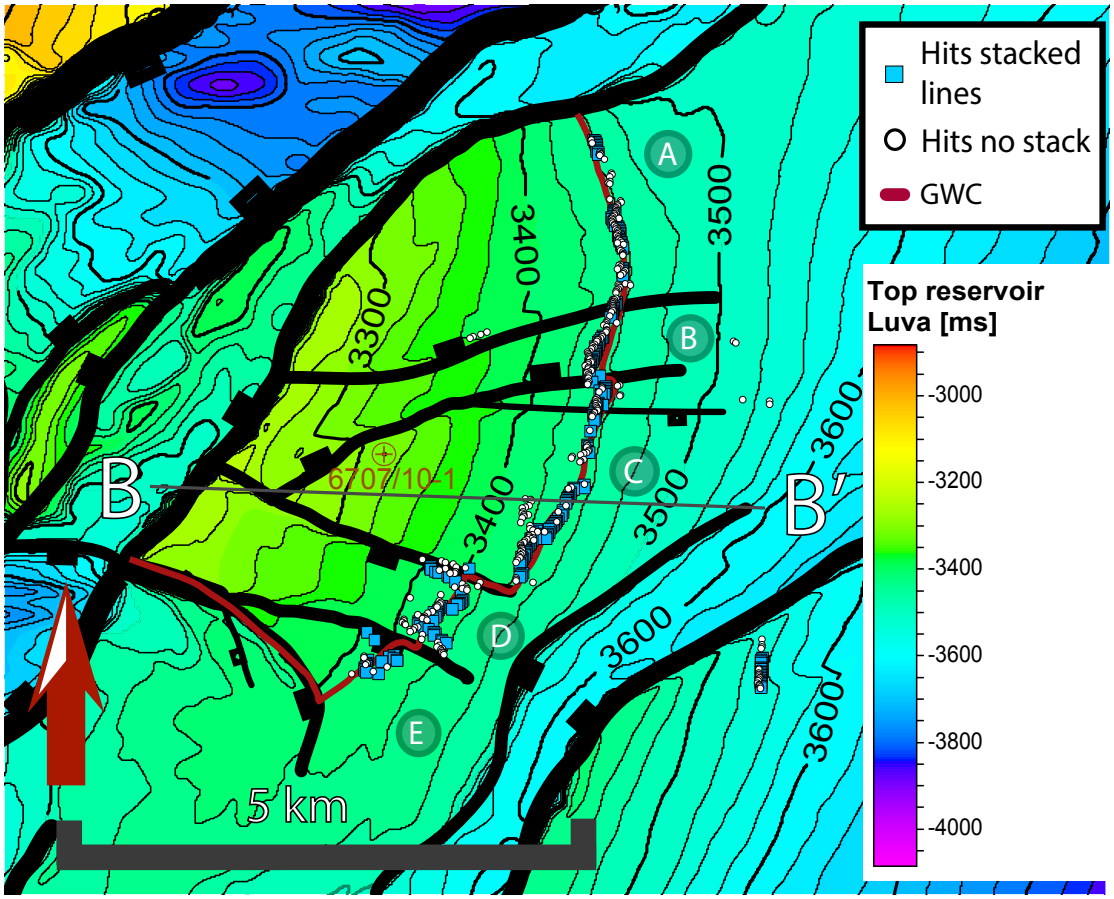

Figure 5.4: Top reservoir map of the Luva structure. The white dots represent the amplitude algorithm run on lines that have not been stacked before the search and the blue rectangles represent hits from lines that have been stacked before the search. The minimum score required is set to 3.

lines. So, in this segment, it appears that the stacking of the lines improves the accuracy of the algorithm. In segment D and E, the hits are quite unreliable, similarly to those in figure 5.1, and again, this is probably due to the faults. Although there are more hits on the stacked lines than the unstacked lines in segment E, they are inconsistent and likely affected by the fault. The stacked lines do not improve the result in any significant way.

The seismic section from B-B' is displayed in figure 5.5, and the location of the line is marked in figure 5.4. From the amplitude curve in (a), we observe that there is a constant decrease in amplitude as we move down dip from trace number 1400. This variation is similar to that observed in the seismic section A-A' in figure 5.3. The largest amplitude is located at around trace 800 and has an amplitude value of around -3800, and this point is suggested to be the point of maximum tuning by the algorithm. From this point and further down dip, the amplitude abruptly increases (towards zero). At the end of this increase, the algorithm has located a point suggested to be the start of the brine zone, and

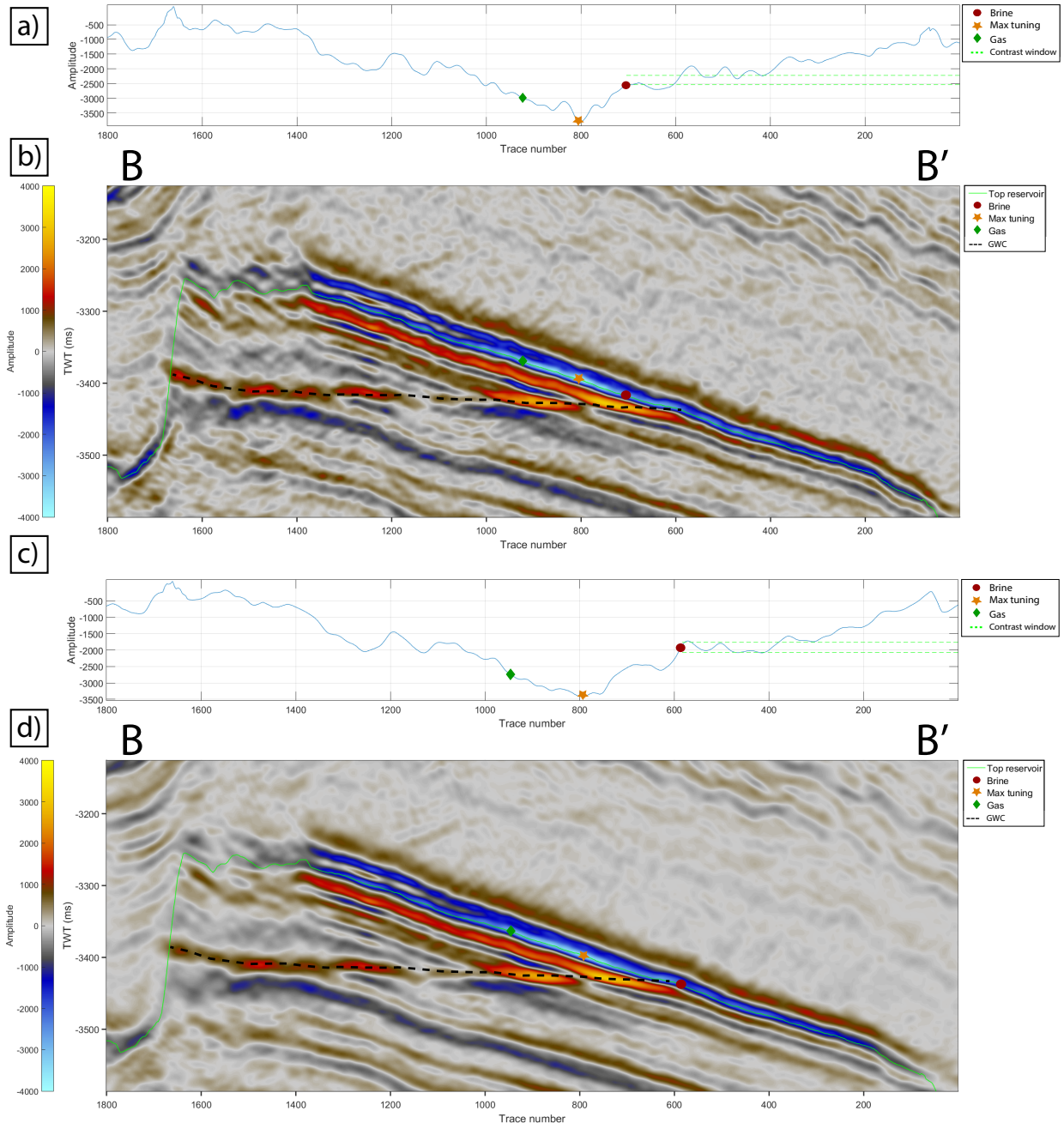

Figure 5.5: (b) The seismic section from B-B′ at Luva with the top reservoir interpretation. (a) The extracted amplitude along the top reservoir from the seismic section in (b). (c) and (d) show the same plots, but for the stacked line. Notice the reduction in noise in the stacked compared to the unstacked section.

it should therefore be located at the fluid contact.

In (c) and (d) the same plots are shown for the stacked seismic section. The shape of the amplitude curve in (c) is very similar to that in (a) and the maximum tuning amplitude has about the same location, but the amplitude is slightly less bright in the stacked section. This leads to the location of the brine point in (a) not being within the accepted contrast range in (c). Therefore, the algorithm locates the brine point in (c) further down dip than in (a). By looking at the interpreted GWC, it appears that the position of the brine point in (d) is more accurate than in (b).

Both of these hits receive 3 of the 5 points. The hit from the unstacked line loses one point because the TWT between the max tuning point and the brine point is not within the narrow range and one point because there is a larger contrast further down dip (around trace 580). The hit on the stacked section loses two points because the TWT is outside both the narrow and wide range in TWT, but the brine point is located at the end of the shut-off (no further increase in amplitude after the brine point). Even though the difference between the amplitudes in the stacked and unstacked case is small, the difference in the result is significant. The hit from the unstacked line is located at -3418 ms while the hit from the stacked line is located at -3436 ms. That is a difference of 18 ms, which is significant.

The fact that only a few hits at Gullfaks receive more than three points indicates that many of the hits do not represent the ideal situation. As already mentioned, there are many complicating factors at Gullfaks that could be causing this. The most important factors are the following:

1. There is extensive erosion of the top reservoir, especially in the eastern parts
2. There is onlap at the top reservoir in many segments
3. Large and small faults are found in all segments
4. The top reservoir reflector is weak and hard to interpret in the southern part of the seismic cube
5. Low data quality affects the amplitude extraction and the accuracy of the algorithm
6. The seismic was shot after production start, which leads to a reduction of the height of the oil column and likely residual saturation in some parts

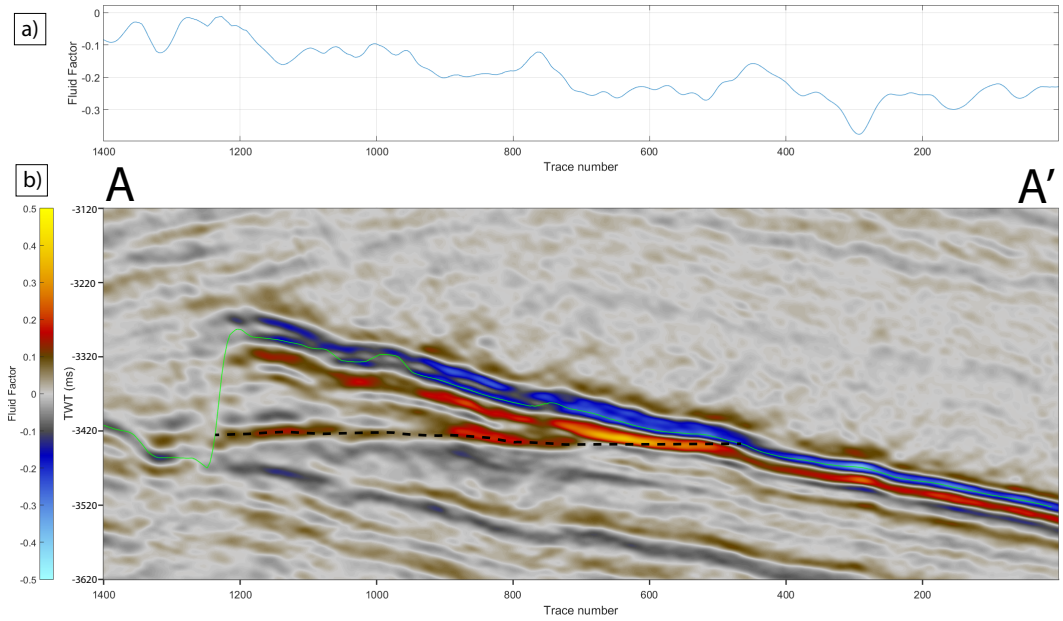

Figure 5.6: (b) a fluid factor section along A-A' at Luva. (a) The extracted fluid factor along the top reservoir reflector.

7. The height of the oil column is below maximum tuning thickness in many areas

The importance of these factors will be further analysed in chapter 6.

5.1.3 AVO

As illustrated in figure 3.5, we expect a class III AVO response in the gas zone. The intercept and gradient values in the brine case plot in the same quadrant in (b), but the gradient and intercept values are close to zero. The modelled fluid factor is therefore significantly more negative in the gas zone than in the brine zone. The modelled fluid factor in the different zones are listed in table 4.

In Figure 5.6 (b) the fluid factor section along A-A' (see figure 5.1) is displayed with the extracted fluid factor along the top reservoir in (a). From the plot in (a), we observe that the fluid factor is, as expected, negative in the gas zone, with a value around -0.20. At the GWC, around trace 480, there is a slight increase in fluid factor, towards zero. The contrast is around 0.1, which is less than the expected contrast of about 0.17. Further down dip the fluid factor decreases again, and it is generally more negative in the brine zone than in the gas zone. According to the modelling, the fluid factor should be close to zero in the

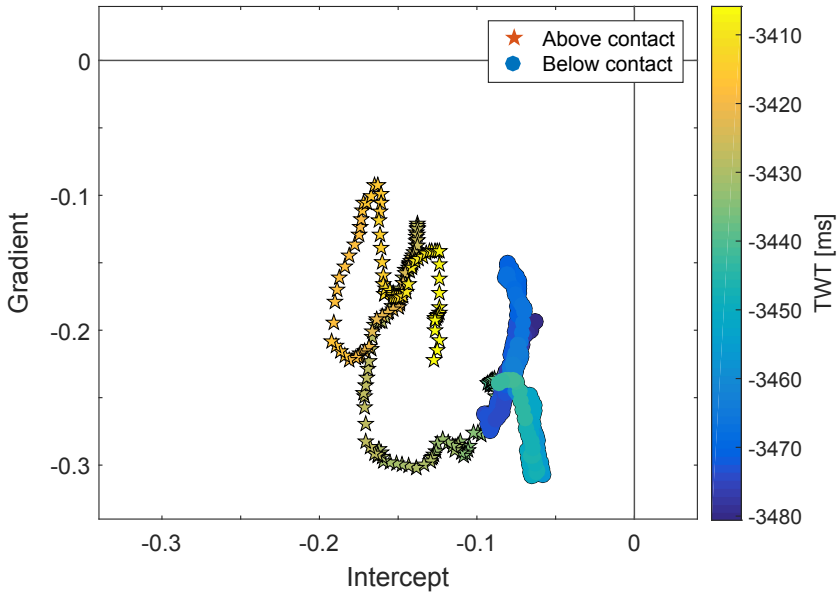

Figure 5.7: Intercept vs gradient values extracted along the top reservoir from the seismic line A-A'. The stars represent the traces above the GWC and the circles represent the traces below the GWC. The colours represent the TWT to the top reservoir.

brine zone.

A plot of the intercept versus gradient values is displayed in figure 5.7. The stars represent the 200 traces above the GWC, and the circles represent the 200 traces below the GWC for the seismic section in figure 5.6. It is again clear that the trend is not as expected from the modelling, and it is the gradient value that is not consistent with the modelling. The gradient in the brine zone is similar, or slightly more negative than the gradient in the gas zone, and by inspecting the amplitudes in the partially stacked cubes, we observe that the amplitudes are brighter in the far stack than in the near stack. This brightening is more pronounced in the brine zone than in the gas zone. This visual observation is further evidence for the fact that the gradient is larger in the brine zone than in the gas zone.

For the line A-A', it is evident that the AVO anomaly we expected is not present in the seismic data. We observe the same trend at the entire Luva structure. Inevitably, running the AVO algorithm and looking for the modelled contrast in fluid factor at Luva returns no significant results.

Several different methods, in addition to the fluid factor, were tested in the search for an anomaly at Luva. Different combinations of the near (N) and far (F) cubes were analysed, and examples include F-N, F+N, F*N and (F-N)*F. None of these indicated an anomaly

across the fluid contact.

Since there is a mismatch between modelled and actual response, there must be something causing this. Some potential reasons will be discussed in chapter 6.

5.2 Gullfaks

The Gullfaks field is located in the North Sea (see figure 3.1) and was discovered by Equinor in 1978 when they drilled the first exploration well at the structure. Well 34/10-1 encountered a 162 m oil column in Brent sandstones. The reservoir quality was excellent, and production from the field started in 1986. Gullfaks consists of large rotated fault blocks in the western part and a horst complex in the eastern part (Fossen and Hesthammer, 1998), and is located in a more geologically complex area than Luva. Therefore Gullfaks was deemed an appropriate place for further testing and development of the algorithms.

An important thing to note regarding the Gullfaks seismic data is that they were acquired in 1996. Since production at Gullfaks started in 1986, the seismic data do not represent the initial conditions at the field. Between 1986 and 1996, 129 production and injection wells were drilled. Peak production was reached in 1994 and by 1996 about 200 of the 380 mill. Sm3 recoverable oil had been produced. Because of this, the original oil-water contact (OWC) at 1947 m MSL will in many areas not reflect the fluid position at the time the seismic was shot.

5.2.1 Amplitude

The expected amplitudes in the oil zone, at maximum tuning and in the water zone has been modelled, and the amplitude values are listed in table 6. The result of running the

Modelled amplitude values at Gullfaks

In oil zone	At max tuning	In brine zone
-1,94	-2,58	-1,27

Table 6: The results of the amplitude modelling at Gullfaks. These values are used as input to the amplitude search algorithm.

amplitude search algorithm on the Gullfaks seismic cube is displayed in figure 5.8. The hits with a minimum requirement of 3 points are displayed as white circles and hits with a minimum requirement of 5 are plotted as red squares.

The algorithm was run both on stacked and unstacked lines, and it was clear from analysing the results that optical stacking improved the results. Therefore, all the results in this section are obtained by running the algorithm on the amplitudes from the stacked lines.

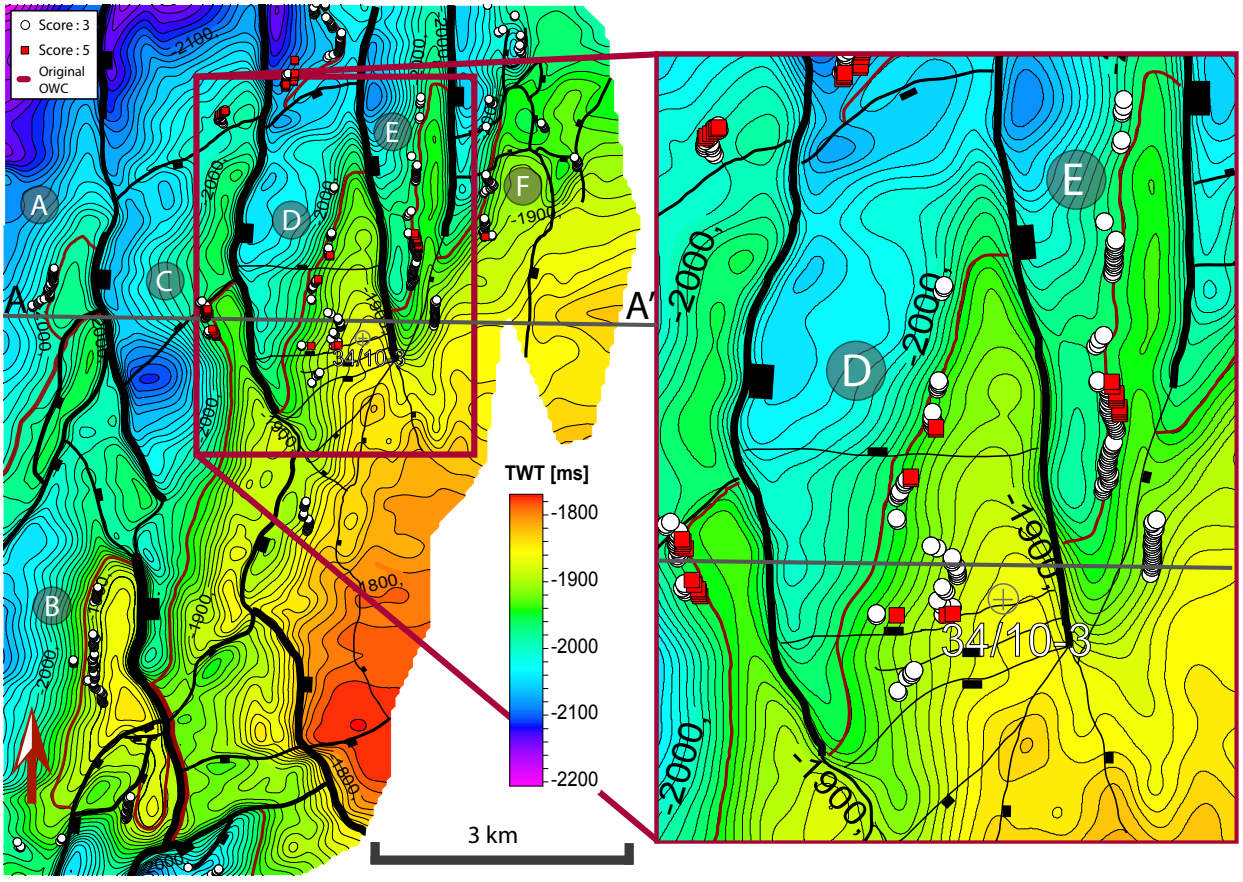

Figure 5.8: Top reservoir map at Gullfaks, with the main faults, original OWC and hits with a minimum score of 3 and 5 are plotted. The field is divided into segments A-F by the major faults.

We divide the Gullfaks field into different segments based on the major faults, and the segments, named A-F, are marked in figure 5.8.

In the northern part of segment A, there is a small structure where the hits are located close to the OWC. These hits do not cover the entire structure, and a few of the hits are located about 10 ms deeper than the OWC. The oil column in this structure is less than 20 ms, which is likely to be below the maximum tuning thickness and is a possible reason

for why there are only a few hits in this structure. There had been no production wells in this structure by 1996, and none of the hits in this segment receive the full five points.

Further south in segment A, just below the line A-A', there is an elongated structure that is separated from the northern part with a fault. There are no hits in this structure, likely due to dim amplitudes. Several production and injection wells have been drilled in this structure prior to 1996, so it is likely that there is complete or partial water flooding, which would explain the lack of hits in this structure. In figure 5.9, the seismic section A-A' is displayed together with the extracted amplitudes along the top reservoir reflector. The orientation of the line is marked on the map in figure 5.8. The two structures in segment A can both be seen in the section. We observe that there is a bright amplitude in the westernmost part, but the contrast is not large enough for the algorithm to accept it. Both these structures are part of Gullfaks vest, which had an initial contact (1988 m MSL) that was deeper than the contact at the main Gullfaks field (1947 m MSL).

In segment B, most hits lie close to, or shallower than the OWC. In the northern part, where most of the hits are located, the hits cover a large part of the structure. There has been production in this segment since 1995, and this could explain why most hits are located shallower than the original OWC. Further south in the same segment, some points deviate from the OWC. In this area, and generally in the southern part of the cube, the signal-to-noise ratio is low, and the top reservoir reflector is hard to follow. These factors lead to an inaccurate interpretation which again affects the amplitude extraction and the results of the algorithm. As in segment A, none of the hits in segment B receive the full five points.

In segment C, there are a few hits at a small closure in the northern part. Equinor has classified this as a prospect, but the fluid content in this structure is unknown. Most of the points in this structure receive five points, which increases the likelihood that hydrocarbon is the cause of these hits. Further south in segment C, some hits locate close to the OWC, but they only cover a small portion of the structure. These hits also receive the full five points. Several production wells have been drilled in this area prior to 1996, but there is probably oil left in different parts of the structure. Partial drainage together with low seismic quality and lots of smaller faults, especially in the southern parts, is the likely explanation for the lack of hits. The hits in segment C can be seen in more detail on the zoomed area on the right side of figure 5.8.

In the northernmost part of segment D, some hits are located close to the GWC, and a

few of these hits receive five points. This structure is gas-filled, and one would expect the amplitudes in the gas zone to be higher than in the oil zone, but the amplitudes in this area are comparable to that of the other segments. In the structure further south, the hits are located close to the OWC, and north of the first E-W bounding faults, there are a few hits, but they are far apart, and some are slightly deeper than the OWC. This structure was undrained in 1996, so the original OWC should still be accurate. There are discontinuities in the top reservoir reflector in this area, which explains why some hits are missing. The reason for the discontinuity could be that erosion has removed parts of the Tarbert formation. At the apex of the fault block, there is a transition from the Tarbert formation to the Ness formation, and since the Ness formation has different properties, this leads to a change in amplitude.

The area south of the mentioned E-W bounding fault in segment D has been in production prior to 1996, and this could explain why the hits have a large spread in TWT. Production well 34/10-B-27 is located close to exploration well 34/10-3, and production from this well is probably the reason why these are shallower than in the adjacent areas.

In segment E, there are a few hits in the northern part, and they are located slightly deeper than the OWC. A possible reason for the deep hits is that the column height in this area is below the max tuning thickness and the amplitudes are therefore not as bright as expected. Further south, the column height increases, which improves the accuracy of the algorithm. The hits follow the OWC reasonably well, but there are only a few hits that receive five points. There had been no production in this area before 1996. The southernmost hits in segment E are far from the original OWC. In figure 5.9, we observe that the deepest part of the top reservoir is shallower than the original OWC. It is likely that production has moved the OWC shallower and that this is the contact located by the algorithm.

In the final segment, segment F, many of the hits are inconsistent. Only a few of the hits are located close to the OWC, and many are located close to a fault. There had been production in this segment before 1996, and production effects and the fact that the small faults in the segment affect the amplitude leads to several hits that are not consistent with the OWC. The eastern part of segment F is in an area where the top reservoir is flat, and therefore there will not be a shut-off in this area.

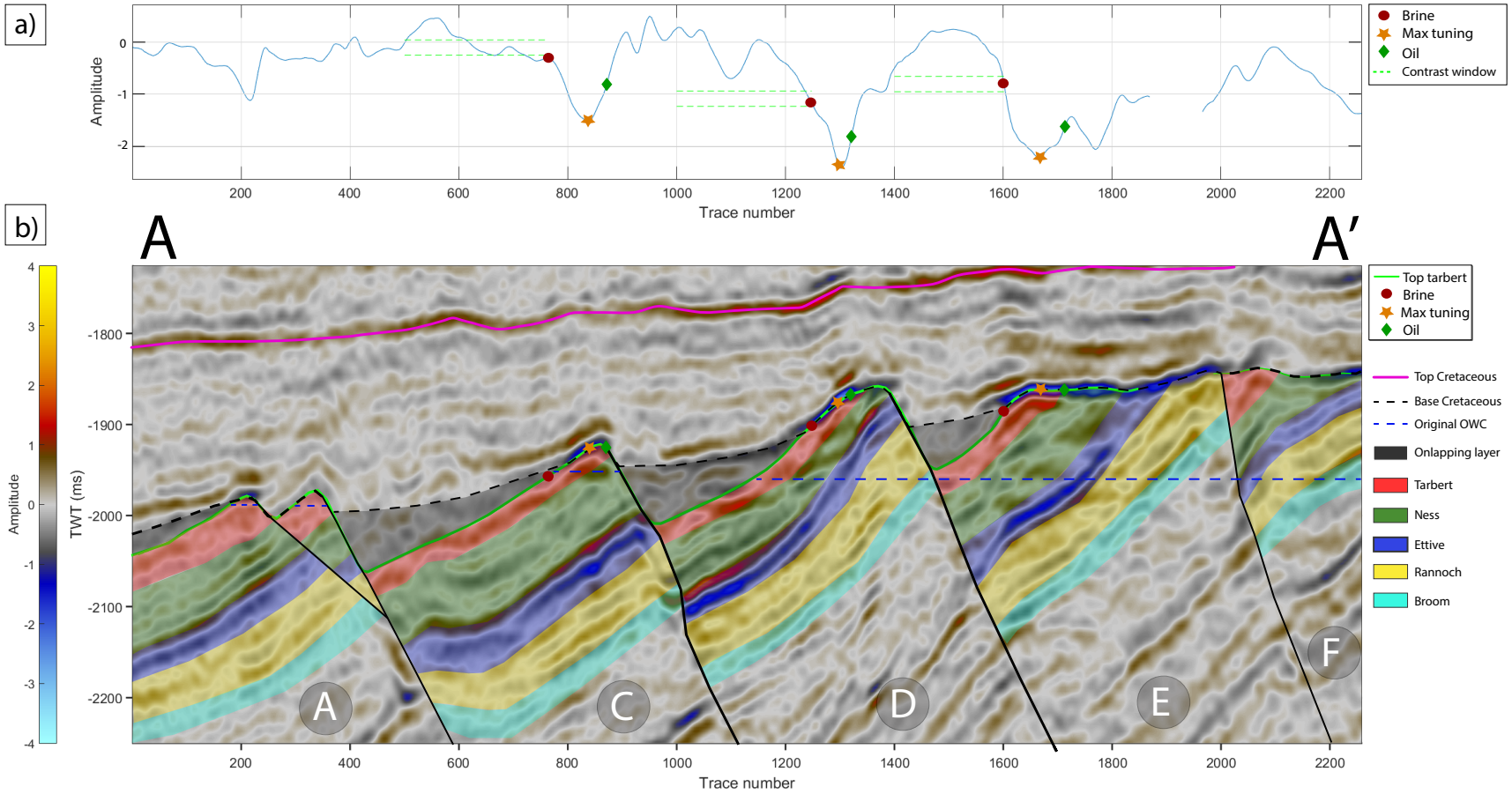

Figure 5.9: (a) The extracted amplitude along the top reservoir from the seismic section in (b), which is displayed with the interpreted layers and the result from the amplitude search algorithm. The onlapping layer is the Heather formation of upper Jurassic age. The segments are the same as in figure 5.8.

By inspecting the amplitude behaviour in figure 5.9, we observe that there are some differences between the amplitude variations in the different segments. In segment C, the brightest amplitudes are at the apex of the structure. The following contrast is within the accepted window, and the algorithm locates a potential brine point. There is also a possible flat spot, located at the original OWC. Out of the possible 5 points, this hit receives a score of 3 points. It loses 1 point because the difference in TWT between max tuning and brine is larger than the narrowest window, and it loses 1 point because the HC point is not located updip compared to the max tuning point. In theory, the HC points should always be located updip compared to both max tuning and the brine points. If we remove all hits that do not fulfil this requirement, many hits at Gullfaks are removed. The reason for this is that in many areas the oil-column is not significant enough to capture the entire amplitude variation from the HC zone, through the max tuning and down to the brine zone along the top reservoir.

In segment D, the maximum amplitude is even brighter than in segment C, and the following increase in amplitude is more significant in segment D than in C. In segment C, the brine point is located at the end of the shut-off, that is, the amplitude increase does not continue after the brine point. In segment D, this is not the case. Instead, the amplitude continues to increase towards zero after the brine points. In other words, the expected contrast is smaller than the maximum contrast in this segment, and the hit loses 1 point because of this, and it loses another point because the TWT difference is only within the wider range. The location of this hit is significantly shallower than the original OWC, and this is likely because of production.

In segment E, the situation is similar to that of segment D. There is a bright amplitude followed by a large contrast. The algorithm locates the brine point in the middle of this contrast, so the amplitude continues to increase after the brine point. There has been significant production in this segment as well, so it is hard to say how accurate the prediction from the algorithm is.

5.2.2 AVO

The result from the AVO modelling at Gullfaks are displayed in figure 5.10. A class 3 AVO response is expected, similar to the modelled response at Luva. The difference is that the intercept and gradient values are close to zero. The reservoir at Gullfaks is oil-

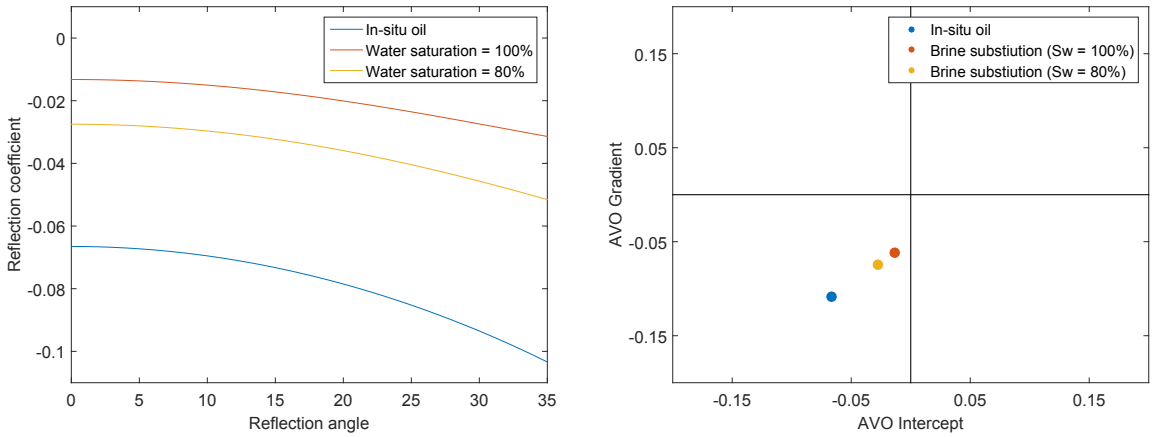

Figure 5.10: The results from the AVO modelling at Gullfaks. The response is modelled in the in-situ oil zone and in with 80% and 100% water saturation. (a) The reflection coefficient versus angle, computed using the exact Zoeppritz equations. (b) The modelled gradient versus intercept plot.

saturated, and Luva is a gas field, so this is as one would expect. It is a well-known fact that gas typically produces a stronger AVO response than oil. Since the seismic data at Gullfaks was acquired after production start, a residual oil saturation of 20% (80% water saturation) is included in the modelling. The calculated fluid factors are listed in table 7.

As discussed in section 4.2.1, there are two different ways to calculate the AVO attributes along the top reservoir. Both methods achieve noisy results, with inconsistent hits spread across large portions of the field. The trend from both methods are similar, but creating the fluid factor cube before extracting the fluid factor along the top reservoir achieves more consistent results. Therefore, all the AVO results presented in this chapter are obtained using this method.

The random variation in the fluid factor is in many areas larger than the contrast we are searching for, and hence, the algorithm locates the correct contrast in fluid factor in areas where we do not expect an AVO response. Optical stacking is a technique that could reduce the variations in the fluid factor that are caused by noise in the data. In this case, the lines, both in the near and far stack, are stacked prior to the AVO inversion. In figure 5.11, the difference between running the AVO search at the stacked and unstacked lines

	Oil zone	Sw = 80%	Sw = 100%
Fluid factor	-0,15	-0,08	-0,05

Table 7: Modelled fluid factor for different pore-fluids at Gullfaks.

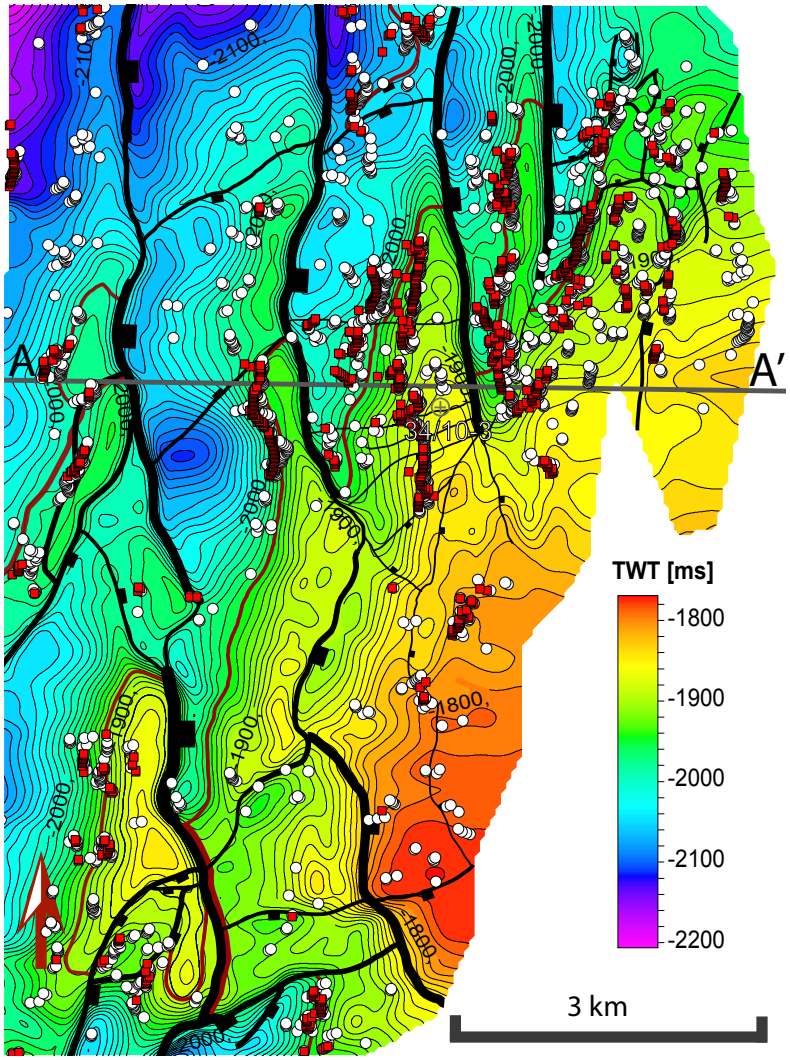

Figure 5.11: Top reservoir map at Gullfaks with the AVO search results, with and without optical stacking.

are displayed. We observe that optical stacking significantly reduces the issues with noise. The hits from the unstacked lines are noisy and much less consistent than the hits from the stacked lines.

In figure 5.12, the results from the amplitude search are compared with the results from the AVO search. The AVO results are the same as the results from the stacked lines in figure 5.11.

In segment A, there are some hits in the northernmost part. There are no amplitude hits here, and the location of the OWC in this structure is 100 ms shallower than these hits. It is therefore unlikely that the AVO hits are related to hydrocarbons. By further inspection

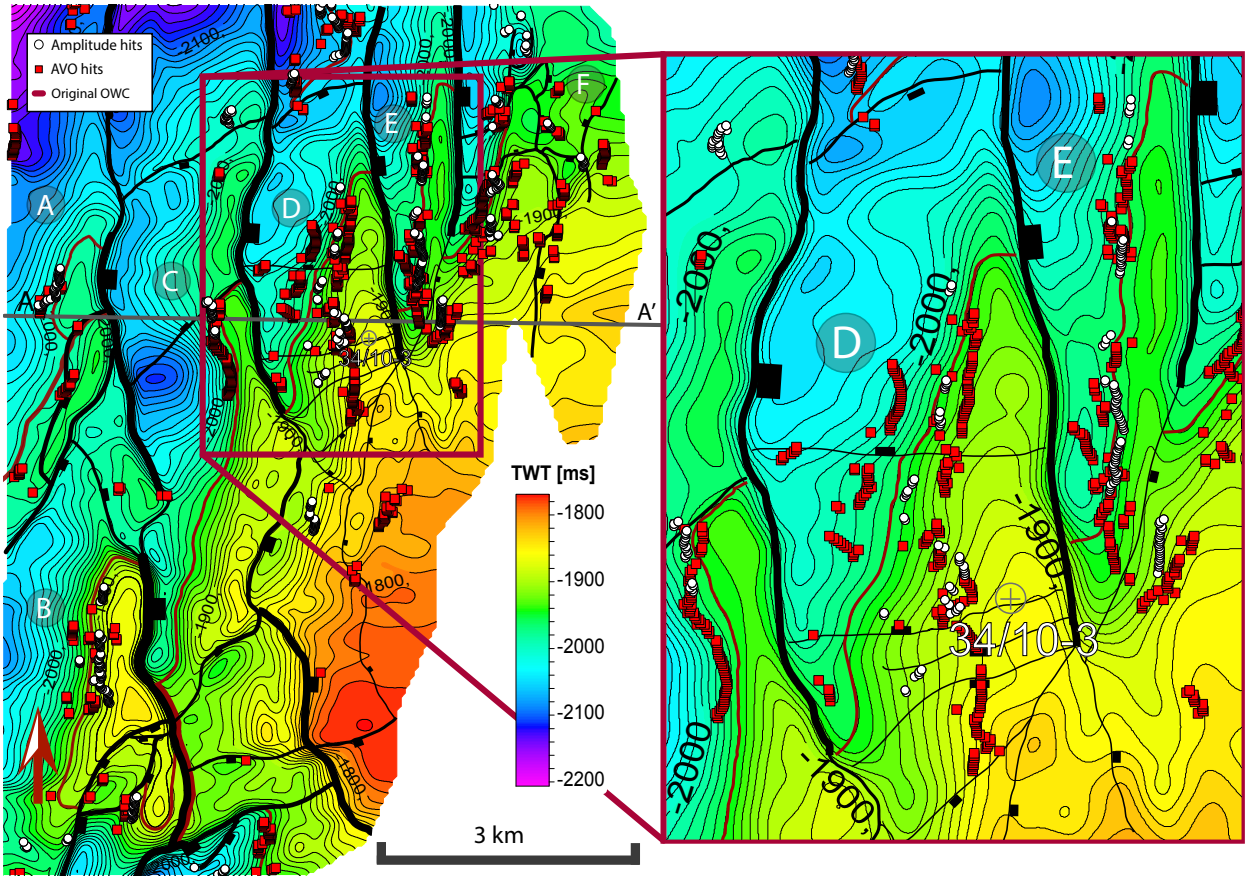

Figure 5.12: Top reservoir map at Gullfaks with a comparison of the hits from the AVO search and the hits from the amplitude search algorithm.

of the fluid factor sections, it appears that inaccuracies in the top reservoir interpretation lead to an inaccurate extraction of the fluid factor. By improving the interpretation in this area, these AVO hits would be removed.

Further south, just north of the line from A-A', the AVO hits and the amplitude hits are consistent, but the fluid factor section, together with the hits along the line from A-A' is displayed in figure 5.13. In the structure south of line A-A', the AVO algorithm locates a contrast in the fluid factor where there are no amplitude hits. In section 5.2.1 it was stated that this structure was likely to be partially or completely drained. It is a possibility that a partial oil saturation could lead to an AVO response that is strong enough to be picked up, but this has not been analysed in detail. Another option is that some of the hits are related to noise in the data.

In segment B, the AVO hits and the amplitude hits are located in the same vicinity, but the AVO hits are less consistent than the amplitude hits. At some lines, there are three closely

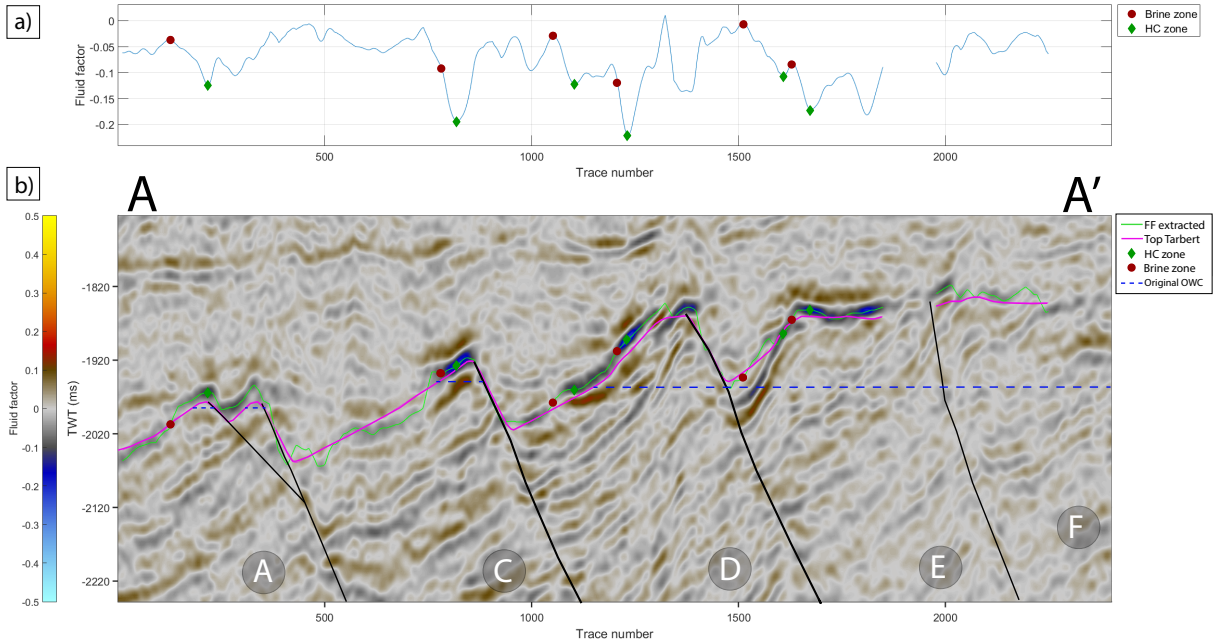

Figure 5.13: (a) The extracted fluid factor from the fluid factor section in (b). Note that the extraction algorithm is allowed to deviate significantly from the interpretation to locate the strongest fluid factor.

spaced AVO hits. This is unlikely a reasonable result as it points to three contacts in the same structure. By inspecting the fluid factor section in the area, it is clear that there are large local variations in the fluid factor. These inconsistencies in the fluid factor lead to several contrasts that are within the expected contrast window. A likely cause is noise in the data or an inaccurate seismic interpretation.

In the northern part of segment C, the AVO algorithm locates a few anomalies in a small structure, but they are further south than the amplitude hits. There are a few amplitude hits in the structure north of the E-W trending fault, but not in the structure with the AVO hits. Further south, the AVO hits are consistent in TWT and line up along the original OWC (only slightly deeper). In this part, the amplitude hits and AVO hits are consistent with each other. One of the hits in the segment can be seen in detail on the section in figure 5.13. In the southernmost part of segment C, some AVO hits are located along the original OWC. The amplitude hits in this area are much deeper and likely not reliable.

In segment D, to the far north, the AVO hits are in the same area as the amplitude hits. These hits are related to a small gas-filled structure. The AVO hits are less consistent, and the deepest hits are about 100 ms deeper than the shallowest hits. By inspecting the fluid factor sections in the area, it appears that there are large local variations in the fluid factor.

In the structure further south in segment D, there are many AVO hits, and in the same way as in segment B, some lines have hits at different depths. In figure 5.13, an example of two hits in the same structure is shown. In this section, the fluid factor is quite strong in the shallowest part of the reservoir, and two separate contrasts are within the expected window. It could be that the first contrast is related to a change from oil saturation to residual oil saturation and the deeper one is related to the change from residual oil to brine. In the area around the location of well 34/10-3, the AVO hits convey the same message as the amplitude hits, that the contact is shallower in this part.

In the southernmost part of segment D, there are a few hits, and they are related to a local brightening of the fluid factor, but the hits are located significantly shallower than the amplitude hits in the area. In this part the data quality is low, and this is probably the reason for the inconsistency between the amplitude and AVO hits.

In segment E, the AVO hits are in the vicinity of the amplitude hits, but again, they have a larger spread in TWT than the amplitude hits. There are some areas with several hits at different TWT in this area as well, and one of them can be seen in figure 5.13. The fluid factor variation here is similar to that in segment D, but it appears that the top reservoir interpretation is too shallow and the extraction does not capture the correct fluid factor.

In segment F, the AVO hits are spread around in the entire segment. The amplitude hits are spread similarly but to a lesser extent. As mentioned in the analysis of the amplitude hits, this is an area with significant erosion and faulting. It looks like the fluid factor is more sensitive to these amplitude variations and this leads to unreliable and inconsistent hits.

6 Discussion

This chapter aims to discuss how the experience gained from testing the algorithms at Luva and Gullfaks can benefit regarding further development and future use of the algorithms. Since the testing have been performed at datasets where the position of the fluid contact is known, the direct results from these tests are not of much value. The real value lies in the knowledge and experience we have gained, and based on the tests, the algorithms will be evaluated in terms of their accuracy and limitations. Finally, an analysis regarding if it is worthwhile completing the full workflow that was proposed in chapter 3 will be provided.

6.1 How well does the amplitude algorithm work?

From the results presented in the previous chapter, it is reasonable to claim that the amplitude search algorithm works, at least in the sense that it does what it is supposed to do. The algorithm extracts the amplitudes from the seismic and searches for the inputted contrast. Any inaccuracies or poor results are, therefore, likely due to other factors than the algorithm itself.

At Luva, the results from the amplitude search are for the most part accurate. Most hits are located at, or near, the GWC. At Gullfaks, the accuracy is harder to assess due to the uncertainties regarding the position of the fluid contact. However, the results are reasonably consistent, but it is likely that a combination of several factors affects the accuracy of the results. To be able to say something definite about the validity and accuracy of the results, these factors need to be addressed.

6.1.1 Accuracy of the interpretation

As mentioned in the previous chapter, the extracted amplitudes along the top reservoir reflector are dependent on the accuracy of the seismic interpretation of the top reservoir. If the interpretation is completed using auto-tracking or the resulting surface is heavily smoothed, the interpretation is likely to deviate from the top reservoir reflector in some areas. At Gullfaks, this was a significant issue. The interpretation was in many areas not

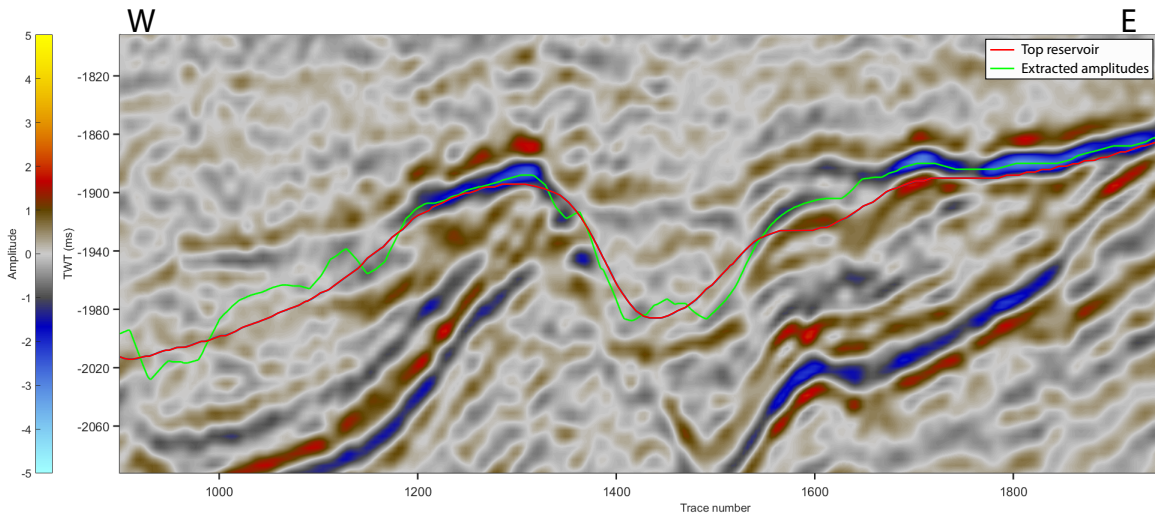

Figure 6.1: A seismic section from Gullfaks with the top reservoir interpretation and the line of amplitude extraction, which indicate where the extraction algorithm picks the amplitudes.

accurate enough for the extraction algorithm to extract the correct amplitudes. Since the brightest amplitude in a window around the exact interpretation is extracted, the interpretation can deviate slightly, and the correct amplitude will still be picked. However, the algorithm will struggle in areas where the reflector is weak, or the signal-to-noise ratio is low.

In figure 6.1, the difference between the interpretation and the location of the extracted amplitudes is displayed for a seismic section at Gullfaks. In the eastern part, the correct amplitudes are extracted despite the interpretation being inaccurate. At the apex of the structure in the western part, around trace 1300, the interpretation is not accurate, but the correct amplitudes are still extracted. However, further downflank, where the reflector is less clear and appears to change polarity, the algorithm struggles. In this area, the extracted amplitudes will not represent the amplitudes along the top reservoir. Therefore, the optimal solution is to be very precise when interpreting the top reservoir, instead of relying on the extraction algorithm.

At Luva, the interpretation is accurate, and the top reservoir reflector is bright and continuous, so this issue is non-existent.

Another aspect is the quality of the interpretation in fault zones. As mentioned, a script was developed to remove hits that are caused by amplitude discontinuities related to fault zones. This method is based on calculating the dip of the reservoir, and if the interpretation of the top reservoir through the fault zones is inaccurate or if the surface is

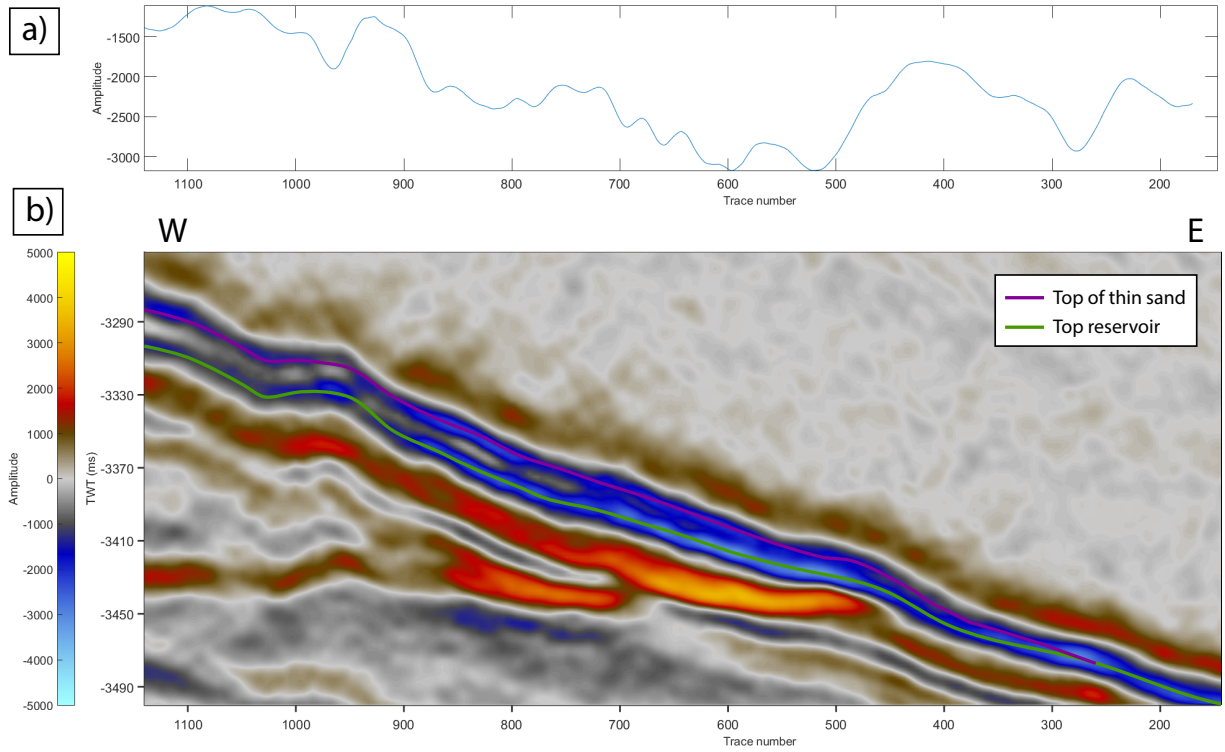

Figure 6.2: (b) A seismic section at Luva, with the top reservoir and the overlying reflector interpreted. (a) The extracted amplitudes along the top reservoir from the seismic section in (b).

too heavily smoothed, the actual dip of the faults will not be captured. Therefore, it is important to be accurate when interpreting the fault zones as well.

6.1.2 Geological variability

One of the major problems with the methods in this study is the fact that local variations in geology can be quite significant. At Luva and Gullfaks there are several factors, which are not related to the pore-fluid, that affects the amplitude along the top reservoir.

The first factor to discuss is the amplitude variation along the top reservoir at Luva. As highlighted in figure 6.2 (b), there is a thin sand layer just above the top reservoir. Both reflectors have the same polarity, and the amplitude strength is similar. At the top of the structure, the difference in TWT between the two reflectors is about 20 ms. For a 20 Hz Ricker wavelet, the maximum destructive interference between two reflectors of the same polarity will occur when the difference in TWT between the layers is 20 ms. So we can expect that the two reflectors are close to the maximum destructive interference, and since

the two layers converge, there will be an increasing amount of constructive interference at depths below the maximum destructive thickness. This interference could explain why there is a relatively constant increase in amplitude as we move down dip from the top of the structure. It could also explain why there is a continuing decrease in amplitude after the shut-off. The maximum tuning between two reflectors of the same polarity occurs when they meet, and it is suggested that the bright amplitudes around trace 300 could be the area of maximum tuning.

The variation in the amplitude at the top reservoir reflector due to the mentioned tuning effect is much less abrupt than the change related to the fluid contact. Therefore, the tuning between the top reservoir and the overlying layer does not affect the size of the shut-off in a significant way, and it does not lead to any problems regarding the results of the algorithms.

At Gullfaks, a significant challenge is the complex geological situation. There are faults of different size in all the segments, there is a variable amount of erosion of the top reservoir surface in the different segments, and in many places, there is an onlapping layer at the top reservoir. All these factors will have an impact on the amplitude strength. The question is if they will have a significant effect on the accuracy of the results.

An important distinction is between geological variations that are expected to be consistent in depth and those that are not. Faults can lead to discontinuities in the amplitude, but it is unlikely that faults will conform to structures in the same ways fluids do and are therefore less likely to lead to hits that could be misinterpreted as a fluid contact. The main problem with faults is that they disrupt the amplitudes along the top reservoir, and the consequence is that the discontinuities lead to parts of the fluid contact not being located. Erosion and onlapping layers, on the other hand, can in many cases be consistent in depth. Since onlapping layers and erosion both can lead to amplitude changes similar to those caused by a change of pore-fluid, they are more likely to lead to hits that could be misinterpreted as a fluid contact.

At the seismic section in figure 6.3, many of the complicating geological variabilities are present. The onlapping layer is present in segment C, D and E, and it pinches out close to the brine points in all the segments. The onlapping layer leads to a change in caprock, and this will affect the contrast in acoustic impedance between the top reservoir reflector and the caprock. It is possible that this is the reason why the amplitudes are weaker in the brine zone than what is expected from the modelling. The modelled brine zone value

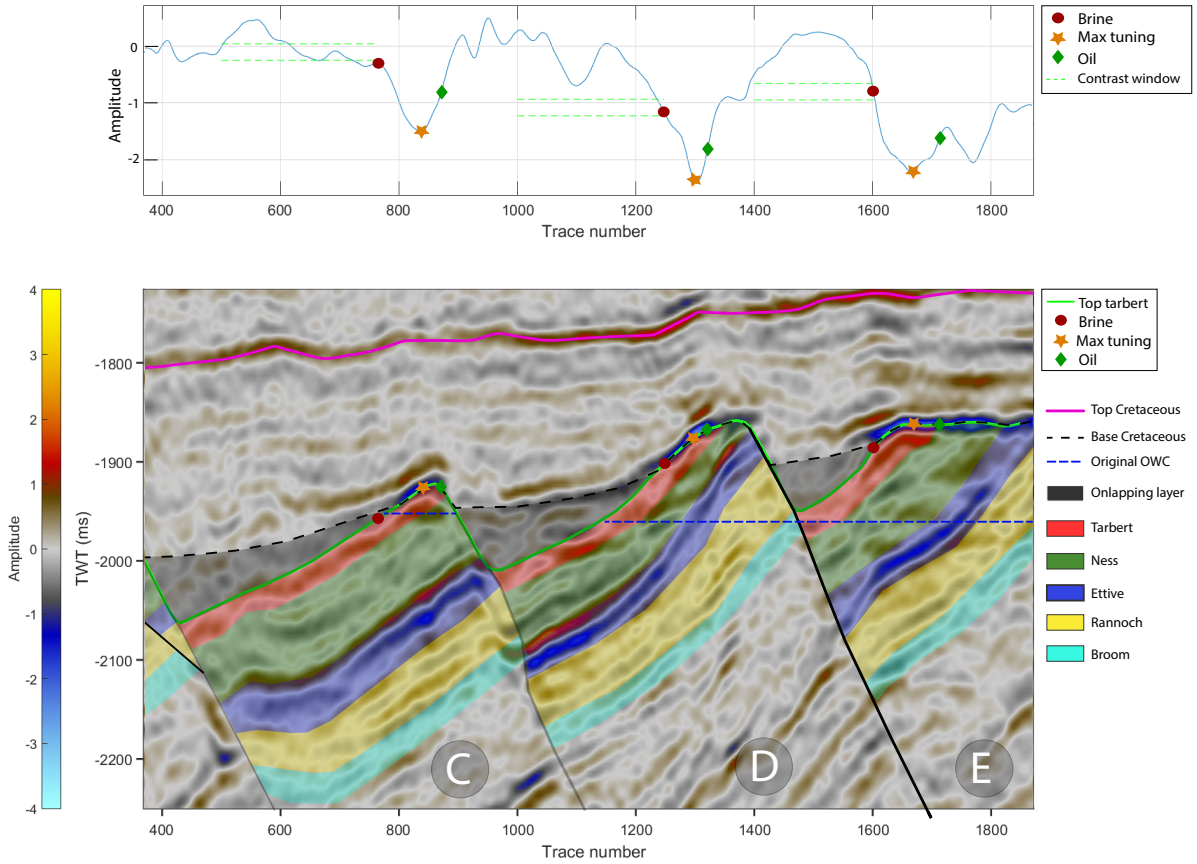

Figure 6.3: A zoomed version of figure 5.9. (a) The curve of the extracted amplitude along the top reservoir from the seismic section in (b). (b) A seismic section from Gullfaks with the interpreted layers and the result from the amplitude search algorithm. The onlapping layer is the Heather formation of upper Jurassic age. The segments are the same as in figure 5.8.

at Gullfaks is -1.27, but from the curve in figure 6.3 (a) it is close to zero.

It is possible that there is a tuning effect between the onlapping layer and the top reservoir. However, no visible tuning effects can be seen from the extracted amplitudes, and this is probably because the reflector at the top of the onlapping layer is relatively weak.

A difference between the hits in segment C, D and E is that the hits in segment D and E are located in the middle of a large contrast. That is, the amplitude continues to increase after the brine point, which is not the case for the hit in segment C, where it flattens out down dip from the brine point. A possible cause for this is the fact that segment C was undrained in 1996, but in segment D and E, there has been significant water flooding. This is backed up by the position of the hits relative to the original OWC. Therefore, there is likely residual oil in the reservoir between the original OWC and the OWC in 1996, and waterflooding could explain the difference in amplitude variations in segment

C compared to D and E. The effect of erosion is also notable in segment D, where the amplitudes are less bright above the Ness formation than above the Tarbert formation.

The experience from the testing at Gullfaks is that only a few areas have amplitude variations close to what we expect. This is likely due to one or several of the factors already discussed. Residual saturation, erosion or onlapping layers could all lead to amplitude variations that deviate from the ideal case. Ideally, all these complicating factors should be accounted for, either by including them in the modelling or by somehow removing the effects from the data.

We claimed that searching for the contrast in value, instead of the actual values in each zone, would reduce or remove these issue with variable geological factors. If this claim holds will be discussed further in section 6.3.

6.1.3 Direction of search

In the current form, the algorithm is only able to search in the direction determined by the inlines and crosslines. In some cases, it is likely that the results would improve by searching in directions that have a different orientation than those set by the crosslines and inlines. At Luva, in the northern segments, the crosslines are oriented in the ideal direction that for the algorithm, because the lines are oriented in the same direction as the dip of the reservoir and do not cross any large faults in the vicinity of the GWC. In the other segments, the faults are an issue since most crosslines cut across at least one fault. The orientation of the crosslines relative to the faults is probably a contributing factor to the fact that the results are more accurate in the northernmost segment than in the southern parts. By searching in different directions, it would be possible to avoid searching across the major faults, and this would improve the accuracy of the algorithm.

6.1.4 Scoring system

An essential part of the amplitude search algorithm is the scoring system. Every time the algorithm locates the correct contrast, the scoring system determines the exact position of the brine point. This part is therefore of significant importance for the accuracy of the algorithm's prediction.

At Luva a significant amount of the hits receive the maximum amount of five points. Most of these are in the northernmost segment, and as discussed above, this is likely due to fewer faults and a more optimal searching direction. Most of the hits in the other segments receive four points, and since Luva is very close to an ideal setting to test the amplitude search algorithm in, anything else would be a discredit to the method.

At Gullfaks, the situation is different where few hits receive more than three points. It is evident that removing all points that do not receive four or five points is too strict. Generally, the experience is that hits with three points could very well be caused by hydrocarbons, but in these cases, one can expect that some other factors affect the amplitudes as well. It is likely that the accuracy of the hits with three points is less than the accuracy of hits with five points.

There is, of course, a trade-off here. By accepting points that are not exactly as expected, the algorithm might be more successful in some areas, but there is also a chance that it will accept contrasts that are not related to a fluid contact. Therefore, it would be a good idea to analyse some of the hits that receive three points before completely relying on them to be caused by a fluid contact.

6.2 How well does the AVO algorithm work?

Similarly to the amplitude algorithm, the AVO algorithm does what it is supposed to. The procedure to invert for intercept and gradient using the partial stacks works, and so does the search for contrast in fluid factor. Still, the results from running the AVO search algorithm at Luva and Gullfaks are inconsistent.

6.2.1 Mismatch at Luva

At Luva, as illustrated in the previous chapter, there is a discrepancy between the expected AVO response and the response observed in the data. The result is that the expected contrast in fluid factor is not present in the data, and the AVO algorithm is therefore unsuccessful in predicting a fluid contact. Since the model and the actual data does not match, we need to address possible reasons for this.

As mentioned in section 3, there are several factors, other than those caused by hydro-

carbons, that could affect the AVO response. In the gas zone, the gradient and intercept values are close to what was modelled. In the brine zone, the intercept is value is close to the expected value, but the gradient is not. The gradient in the brine zone is similar to the gradient in the gas zone, which disagrees with the results from the modelling.

Two uncertainties regarding the AVO modelling was mentioned in chapter 3, namely anisotropy and tuning effects. The modelling performed in this study does not include any of these effects, so it could be that any these two factors cause the disagreement between the model and the real values.

According to Thomsen (1986), most rocks have a weak anisotropy and Kim et al. (1993) report that anisotropy can have a significant impact on the AVO response for a gas-sand encased in shale. In some cases, the gradient could be reversed compared to the isotropic case. These results are also reported by Chopra and Castagna (2014), who also found that similar effects could apply for water-filled sandstones. And since the calculated gradient at Luva is more significant in the brine zone than what we expect from the model, this could be explained by anisotropy.

Chopra and Castagna (2014) state that if tuning effects are suspected, offset-dependent tuning should also be considered while performing AVO analysis. Since travel times differ with offset, the tuning effect is dependent on offset as well. The simple modelling performed by Hamlyn (2014) indicates that both intercept and gradient could be affected by tuning effects. Again, this begs the question if tuning effects would affect the gas zone and brine zone differently? The tuning effect between the flat spot and the top reservoir will only be present in the gas zone, and the tuning effect between the top reservoir and the overlying reflector will either be present in the gas zone or both. Exactly how these tuning effects will affect the AVO response would require a more thorough investigation.

6.2.2 Partial stack interpretation

At Gullfaks, there is, for the most part, correlation between the modelled values and the actual values. Still, the results from AVO search algorithm are not consistent. There are clear anomalies in the fluid factor in many of the areas we expect, but the fluid factor is discontinuous in many areas. These discontinuities lead to several hits along the same lines and a large spread in TWT between the different hits.

The importance of an accurate interpretation has already been discussed. At Gullfaks, the problem was not only an inaccurate interpretation, but the fact that top reservoir reflector was significantly different in the near compared to the far stack, both in terms of position, dip and characteristics. This leads to inaccuracies in the AVO inversion. If the reflectors are positioned at a slightly different location in the partially stacked cubes, the amplitudes at the top reservoir in the near stack will not be compared with the associated top reservoir amplitudes in the far stack. This will lead to inaccurate gradient and intercept values.

A solution is to interpret the near and far stack separately and then use the interpretation to extract the correct amplitudes in each cube. This would result in gradient and intercept values that are accurate. Therefore, if the top reservoir reflector is positioned differently in the partial stacks, it is highly recommended to do a thorough interpretation in both near and far stacked cubes. It is likely that some of the inaccuracies in the AVO results at Gullfaks are related to this issue. At Luva, however, this is not an issue.

6.2.3 Partial saturation

According to the AVO modelling at Gullfaks, the fluid factor for the brine zone is close to that of 20% residual oil saturation. It is therefore likely that the algorithm will struggle to separate between fully water saturated rocks, and partially oil saturated rocks.

It could be that some of the AVO hits at Gullfaks are caused by a change from 100% oil saturation to 20% oil saturation. Since the contrast in fluid factor from 20% oil saturation to 0% oil saturation is much less than that of fully oil saturation to 20% oil saturation, it is unlikely that the algorithm will locate the contrast from 20% to 0% oil saturation. Therefore, in structures where there are two or three hits at different depths, these are likely not caused by the effect of residual saturation.

6.3 Searching for contrasts

An important aspect regarding the algorithms is the choice to search for the contrast instead of the exact values in each zone. We claimed that this would reduce the uncertainties relating to variable rock parameters and lateral changes in geology. Since the

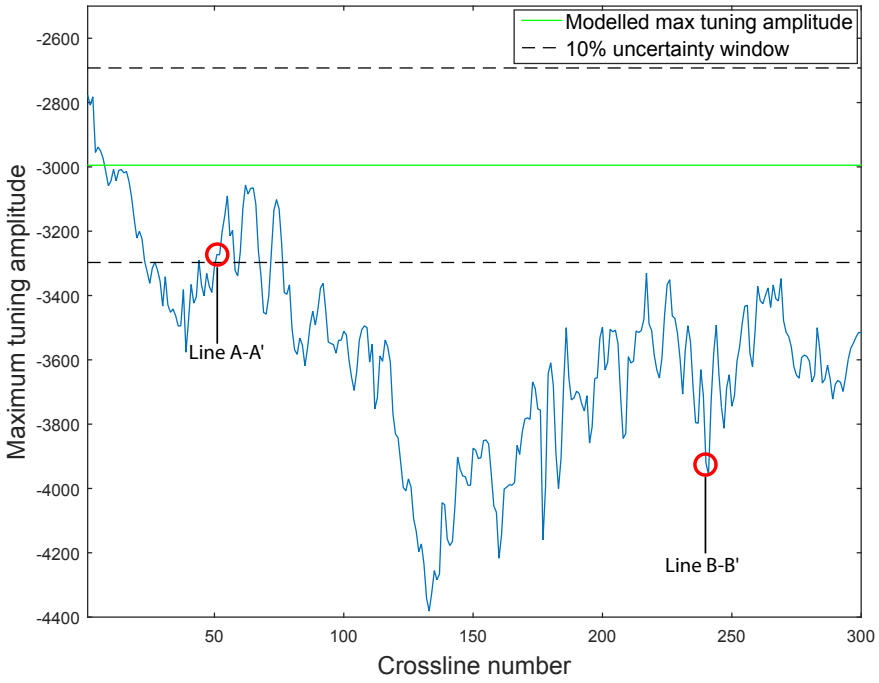

Figure 6.4: The max tuning amplitude at different crosslines at Luva, with the modelled maximum tuning amplitude at Luva (-2097) with a 10% uncertainty window plotted. The location of the lines A-A' and B-B' are marked, and their location can be seen in fig 5.1 and fig. 5.4.

modelled values are based on data from a single well, the modelled values might not be representative of the areas far away from the well location. The assumption was that the contrast between the different zones would be less affected by lateral changes than the exact values. It is necessary to analyse if this is a valid claim.

In figure 6.4, the maximum tuning amplitudes at different crosslines at Luva are plotted. From this plot, it is obvious that by using the exact modelled amplitudes in the search, instead of the contrast, the algorithm would, at most, locate a few hits. The vast majority of lines have max tuning amplitudes that are outside the 10% window of the modelled value. None of these lines would be accepted if the algorithm was searching for the exact values.

Since the modelled value of the max tuning amplitude is quite far from the actual values, the question should be raised why this is the case. The modelled amplitude values are based on and scaled to match the amplitude at the well location. The well penetrates the top reservoir near the apex of the structure, and the difference in TWT between the top reservoir reflector and the overlying reflector is about 20 ms at the well location. This difference in TWT is likely to be within the zone of destructive interference. Therefore,

the amplitudes are scaled to a value that does not reflect the actual amplitude at the top reservoir in the gas zone. This scaling could explain why the modelled maximum tuning amplitude is lower than the actual max tuning amplitudes in the seismic data.

Another point regarding the plot in figure 6.4 is that the max tuning amplitude has significant local variations. In the previous chapter, this was mentioned as a reason for why some of the parts at Luva were missing hits. In areas where the max tuning amplitude is relatively weak, the following shut-off is in some areas lower than the expected contrast. This indicates that the contrast, to some degree, is affected by local variations in amplitude as well.

Still, in most areas, the actual contrast between the amplitudes at max tuning and the brine zone is within the modelled window. This is a testament to the method and proves that, at least in the Luva case, it is better to search for the contrast than for the actual values. It does not remove the entire problem with lateral changes, but it significantly reduces it and is far superior to the alternative.

6.4 Detection limits

Both Luva and Gullfaks have a significant change in amplitude related to the fluid contact. At Luva the modelled shut-off from the max tuning amplitude to the brine amplitude is a 55% decrease, while at Gullfaks the same number is 53%. By inspecting the amplitude variation along the top reservoir at Luva, it seems that local variations (seemingly random) rarely exceeds a change in amplitude of more than 15%. Since the local variations are well below the expected change at the shut-off, there should not be any problem in locating the shut-off. It would require large amounts of noise in the data, much more than what is the case at Luva, for such a large change in amplitude to be disguised in noise.

One of the most important aspects to discuss regarding future use is how the algorithms will be able to locate contrasts and anomalies that are less obvious than at Luva and Gullfaks. For a stiff, low-porosity sandstone, a change of pore-fluid will likely have a small effect on the elastic properties of the rock, and the associated change in amplitude across the fluid contact will be less significant than at Luva and Gullfaks.

However, it is hard to say anything definite about the how well the algorithm would be able to locate subtle contrasts. It will depend on local factors, for instance, the noise in

the data. As observed at Gullfaks, a complicated geological setting is likely to result in a less accurate prediction of the fluid contact. So the more subtle the contrast related to the fluid contact it, the more important it is to deal with the local geological variations. The effect of optical stacking has proved to increase the accuracy of the algorithm, and this is an option to deal with random noise and geological variations that are not consistent in depth, and would be more important when searching for subtle changes.

6.5 Future use

After finishing the first version of the amplitude algorithm at Luva, it was tested at Gullfaks without any modifications. These results were inconsistent and far from useful. But analysing these results and identifying which factors were likely to cause the inaccuracies were useful as a learning process, and this lead to further development of the algorithms to make them more suitable in a more complex geological setting. The result was an algorithm that performs better, not only at Gullfaks but Luva as well.

The point is that by running the algorithms at new datasets with new geological settings, it is likely that new issues that have not been considered will be encountered. The algorithms would then need to be modified and further developed to deal with the new complexities. Ideally, the algorithms should have been tested at more than two datasets to provide a better outlook of the full potential. However, the results from Luva and Gullfaks leads us to believe that there is potential in the methods.

Only parts of the workflow presented in chapter 3 are completed in this study, and one of the main objectives was to determine if it is worth the time and effort to complete the full workflow. Based on the results and experiences that have been presented in this study, the lesson is that there are some uncertainties related to it. And since only two datasets have been investigated, no guarantees can be made regarding future success of the methods. However, it is still believed that it would be worth the time and effort to develop the algorithms further.

7 Conclusion

The primary objective of this study has been to investigate the potential of a new quantitative method for direct hydrocarbon prediction. By creating algorithms and testing them at Luva and Gullfaks, it was concluded:

- The fluid contacts at Gullfaks and Luva were in most places correctly identified by the algorithm that searched for seismic amplitude differences along the top reservoir reflector. Increasing geological variability leads to a decrease in accuracy of the algorithm. At Luva, the geological setting is uncomplicated, and the results are, for the most part, accurate. At Gullfaks, the geological setting is more complex, which leads to less accurate results in the areas that have the most significant geological variability.
- By calculating the fluid factor along the top reservoir reflector, it has been demonstrated that the AVO search algorithm can, to some extent, locate the fluid contact in many areas. At Gullfaks, the result from the AVO search was promising, but it is concluded that the quality of the interpretation and the complicated geological setting resulted in a predicted fluid contact from the AVO algorithm that was less consistent than the one predicted by the amplitude algorithm. At Luva, there was a disagreement between the modelled and observed values, likely because of anisotropy and tuning effects. Because of this, the AVO search was inconclusive at Luva.
- The importance of local geological variability is significant. Changes in lithology of the reservoir, e.g. due to erosion, changes in lithology of the caprock, e.g. due to onlapping layers, tuning effects from closely spaced reflectors and the presence of faults are some of the most important geological variabilities that affect the results. Ideally, such local effects should be accounted for in the modelling. Also, being accurate while interpreting the reflectors is of considerable importance to the accuracy of the results.
- By analysing the results at Luva and Gullfaks, it has been demonstrated that the contrast in amplitude across the fluid contact is less sensitive to lateral variations in geology than the actual amplitude values in the gas and brine zone. Therefore, searching for the contrast across a contact, instead of the actual values, is the superior method.

- The experiences gained from developing these algorithms and testing them at Luva and Gullfaks have been valuable and leads us to believe that the potential of the methods are promising and would be worthwhile further development. Possible future development includes making the algorithms work in an exploration setting and without a top reservoir interpretation.

8 Future work

The algorithms have been tested at two datasets where the position of the fluid contact is known. The results and experiences gained from performing these tests demonstrated that there is potential value in the methods. Therefore, it was concluded that the workflow described in chapter 3 (see fig. 3.2), would be worthwhile to attempt. The most significant challenge is to make the algorithms work in an exploration setting, that is, without any well data. Another possible application is determining the exact position of a fluid contact in a well where there is hydrocarbons, but the fluid contact is not encountered.

This chapter will discuss some of the challenges related to future development and some potential DHI methods and attributes that could be included in the future. This includes a DHI method that has not, at least to the best of my knowledge, previously been used.

8.1 Use in an exploration setting

In an early exploration setting, one cannot expect to have well data at the prospect. At best, there is a nearby well available. A crucial part of the current method is to quantify the expected values of different attributes. If no well data is available, the current modelling workflow will not be useful.

To be able to predict the amplitude response at a potential prospect, the key parameters to estimate are the elastic properties of the reservoir rock and the caprock. The dry rock bulk modulus (K_{dry}) of the reservoir rock is also crucial to be able to utilise Gassmann's equation and predict the elastic properties of the different fluid cases. There exist some rock physics models that could aid in such estimations.

A standard model used to estimate the dry rock modulus is Hertz-Mindlin theory (Mindlin, 1949). Necessary inputs are the differential pressure, the coordination number and the Poisson's ratio and shear modulus of the solid part of the rock. Next, by calculating the Hashin–Shtrikman bounds, the dry rock moduli can be estimated for any porosity. The Hertz-Mindlin model is useful in unconsolidated sands, but the input parameters need to be estimated, and ideally, to do that with some confidence, both well logs and cores should be used.

There are many similar models, each covering a different scenario. Avseth et al. (2005) mention the contact-cement model, the constant-cement model, the constant-clay model and several others. The main message is that before choosing which model to use, knowledge about the geological setting and the depositional environment is needed. This could stem from knowledge of the regional geology, data from nearby fields and wells, empirical models, expected depth to the prospect and so on. It is impossible to pick one model that will be valid in every case, and a possible approach is to cover several "what if" scenarios (Avseth et al., 2005).

If we assume that the reservoir consists of sandstones and that the caprock consists of shales, we could use models or empirical relations to estimate the properties of sandstones and shales versus depth and temperature. The more the local geology can be constrained, the better the accuracy of the prediction will be. Further steps could be to model the expected response for different reservoir properties, e.g. porosity, depositional environment, net-to-gross value and cementation. Then, by performing fluid substitution, the elastic properties can be estimated for the different fluid cases. The result is a model of the expected response at different depths, for different reservoir properties and different fluids.

As discussed in chapter 6, there is clear evidence that the amplitude contrast across a fluid contact is less sensitive to changes in geological parameters than the amplitude values in each zone. Therefore, even if the estimation of the amplitudes is uncertain, it is likely that the uncertainty in the contrast will be lower than the uncertainty in the other properties.

8.1.1 Statistical rock physics

The likelihood of being able to accurately estimate the elastic properties of reservoir rocks and caprocks without any well data is low. Incorporating statistics into the modelling workflow could help reduce the uncertainties. Mukerji et al. (2001) provide a good overview of a statistical rock physics method. By estimating probability density functions, the uncertainty can be quantified and incorporated into the modelling. This can be done using available well data or training data.

By performing Monte Carlo simulations, the expected variability in the different parameters is included in the modelling. The uncertainties in the input variables will then transfer through the simulations and lead to an estimation of the probability of each output

value. This is a useful way of dealing with uncertainties in the modelling, and according to Avseth et al. (2005), it is superior to using average values as input.

The AVO attributes can be modelled using a workflow proposed by Avseth et al. (2005), which is based on rock physics depth trends. By using nearby or regional wells to establish an expected compaction trend, that is, how the porosity is expected to vary with depth, the seismic properties can then be estimated using theoretical rock physics models. Which model to use depends on if the area of interest is expected to be unconsolidated or cemented. By defining likely facies, based on knowledge of the sedimentological system in the area, a Monte Carlo simulation could then be performed to estimate the probability functions of the different AVO parameters. Then, by extracting intercept and gradient from the seismic data and calibrating these to match the values from the models, an estimation of the expected contrast for different facies and fluid cases can be made.

Incorporating statistical rock physics in the modelling is a possible way of dealing with the increasing uncertainties that come from not having any direct measurements of the seismic properties at the prospect.

8.2 Use without a top reservoir interpretation

In its current form, the algorithm relies on a seismic interpretation of the top reservoir as input. A valuable development would be to make it possible to search without a top reservoir interpretation as input. A possible way to do this is to look for consistent reflectors of a given polarity. A solution for what to do when encountering discontinuities in the amplitude, for example in fault zones, would be needed. However, without trying in practice, no guarantees can be made of how well this would work.

8.3 Include more attributes and DHI's

Many attributes have the potential to be included in a DHI method. A useful development of the method is to include other attributes than amplitude shut-offs and AVO response.

8.3.1 Intra-reservoir reflection strength

In a setting with a hydrocarbon-filled sandstone reservoir with thin internal layers, it is likely that the intra-reservoir layers have brighter amplitudes in the gas zone than in the brine zone. These bright reflections are equivalent to the way the top reservoir reflector is brighter above the gas zone than in the brine zone; this is assuming that the reservoir is in a bright spot regime. A completely homogeneous reservoir would have no internal reflections, but once one or several internal layers are present, it is expected that the fluid content of the reservoir will affect the contrast in acoustic impedance between the reservoir and the internal layers. Since lithologies like shale and coal have low porosity and permeability, their elastic properties will likely be largely unaffected by the pore-filling fluid. And since a porous sandstone is affected by the pore-filling fluid, the contrast in acoustic impedance between the sandstone layers and the internal layers are expected to be larger in the hydrocarbon zone than in the brine zone. Based on this reasoning, a new DHI method utilising the internal reflectivity in the reservoir is suggested. By calculating the average amplitude in time slices through the reservoir and below the fluid contact, we expect the average amplitudes in the hydrocarbon zone to be larger than in the brine zone.

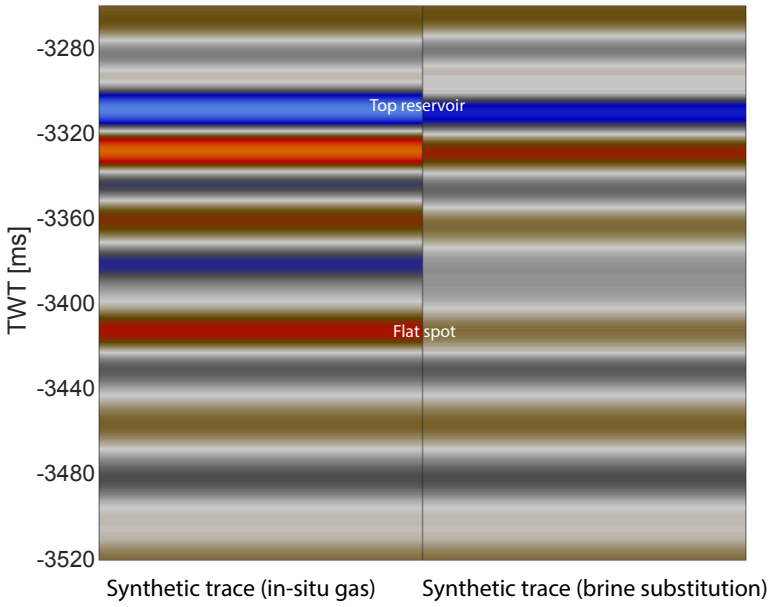

Figure 8.1: Synthetic traces created using the well logs from Luva. The trace at the right is after brine substitution. Notice the relatively dimmer amplitudes between the top reservoir and the flat spot on the brine trace.

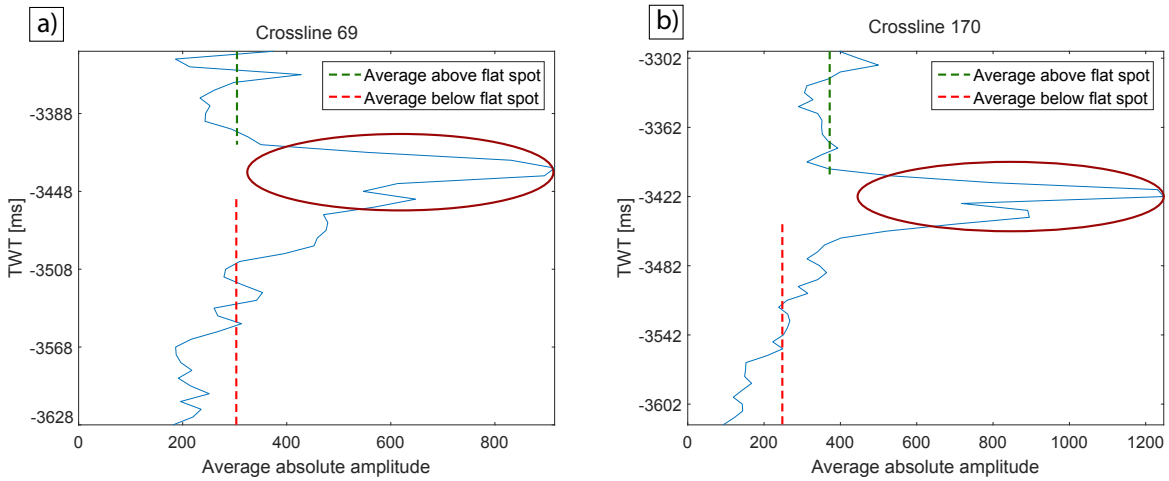

Figure 8.2: The average internal amplitude at crosslines 69 and 170 at Luva. The location of the two lines is marked in figure 8.3. The effect of the flat spot is indicated with the red circle. The flat spot related amplitudes are not included in the calculations of the average amplitudes, whose values are indicated by the green and red lines, respectively.

Further evidence of the potential of this method is displayed in figure 8.1. The synthetic trace created from the well logs at Luva is displayed to the left, and the trace created after substituting the gas with brine to the right. As expected, the reflectivity of the internal layers is lower in the brine case than in the gas case. The calculated average amplitude in the gas case, below the first sidelobe of the top reservoir reflector and above the flat spot, is 35% higher in the gas zone than the same amplitudes in the brine case.

A simple algorithm was created to test the potential of this method using the Luva data. By calculating the average amplitudes in the reservoir for 10 ms time windows, and progressively moving deeper and eventually below the flat spot. The top reservoir reflector and the side lobe below were removed prior to the calculation, as this is not the information we want to evaluate.

In figure 8.2, the calculated average amplitudes in 10 ms windows for two lines, that is, crossline 69 and 170 at Luva are plotted. In (a), the difference between the amplitude above and below the flat spot is 1% while in b) it is 32%. By inspecting the two seismic lines, it does not appear to be much difference between them, although, the reflectors in the brine zone appears to be slightly brighter at crossline 69 than 170. Also, the flat spot differs somewhat in TWT, which might lead to parts of it being included in the amplitudes below the flat spot. The location of the two crosslines is marked in figure 8.3.

In figure 8.4 the same value for the crosslines covering the Luva structure are plotted.

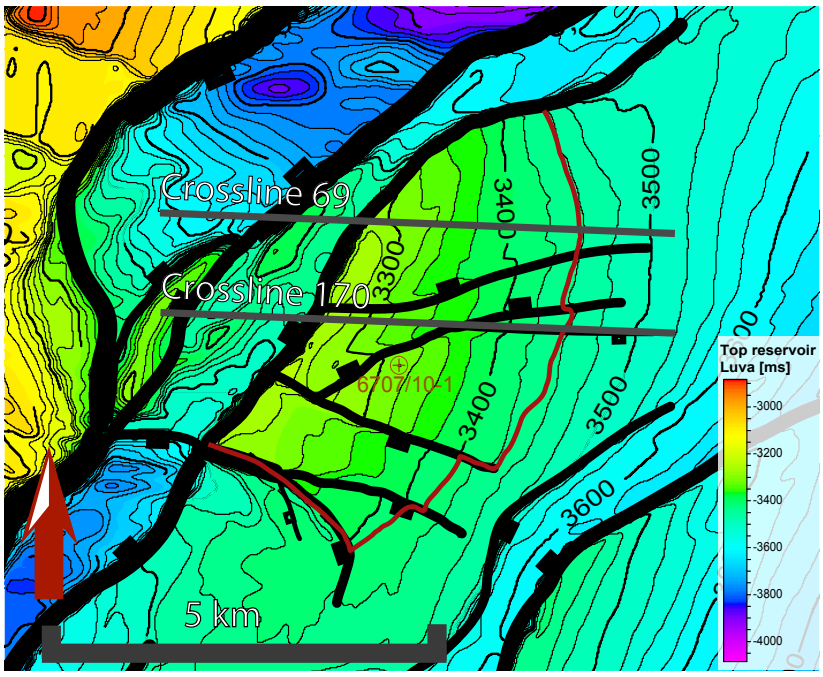

Figure 8.3: Top reservoir map at Luva. The internal reflectivity of crossline 69 and 170 is displayed in figure 8.2 (a) and (b), respectively.

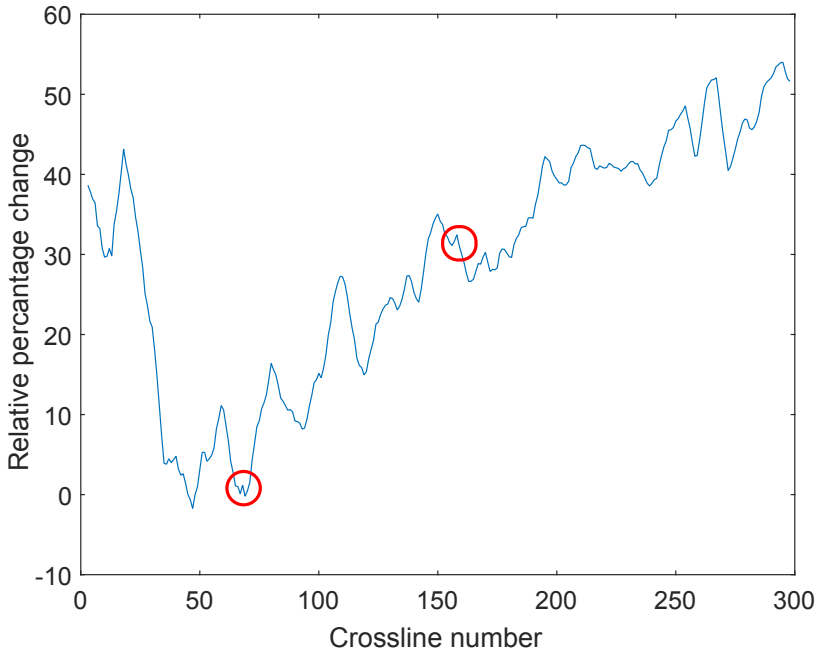

Figure 8.4: The relative percantage change between the average amplitudes above and below the GWC for crosslines covering the Luva structure. Crosslines 69 and 170 are marked with the red circles.

At most lines, there are higher amplitudes above than below the GWC, but the relative difference is variable. At a few lines there is a negative difference, that is, the average amplitude is larger below than above the GWC. However, most lines have at least 20% higher amplitudes above the GWC than below. This is somewhat below the estimate from the synthetic traces, but still significant. At most, the difference is above 50%.

The algorithm behind these calculations is only a simple version created to test the potential of the method at Luva and is not made to work in the general case. Before applying it at Gullfaks or other datasets, it will require further work.

8.3.2 Flat spots

Flat spots have been described earlier in this thesis, and the question is if it is possible to create an algorithm to look for flat spots in the data. One possibility is to use the hits from the amplitude and AVO search and search for flat reflectors in the nearby area. Since flat spots will always represent a positive contrast in impedance, all negative reflectors could be disregarded. Optical stacking could help make flat spots stand out and make it easier for an algorithm to locate them as well.

Since the flat spot at Luva is as clear as it gets, this would be a good starting point for developing a flat spot algorithm. In areas where the geology is complicated, and the fluid contact is not possible to locate visually in the seismic, it would be a challenge to locate flat spots using quantitative methods.

8.3.3 Frequency

Tai et al. (2009) demonstrated, both using synthetic models and real data, that gas reservoirs, due to low velocities, can lead to a low-frequency shadow below the reservoir. Castagna et al. (2003) presented a method to analyse the energy contained for the different frequencies in the signal and how it can be used to analyse the frequencies below a reservoir. It is not clear if high attenuation in gas reservoirs is the only contributing factor, and Ebrom (2004) proposes ten possible mechanisms that could explain these frequently observed shadows.

The question is if frequency is a DHI that could be utilised in a quantitative algorithm.

Given that it is possible to extract the energy at different frequencies from the seismic data, using the method of Castagna et al. (2003) or some similar method, it seems plausible that it would be possible to create an algorithm to evaluate if any areas have anomalously high energy at low frequencies. It is hard to say anything definite without testing, but based on the theory and the experiences from this study, it does seem plausible.

8.3.4 Amplitude shut-off at the bottom seal

In some geological settings, the reservoir is bounded below by an impermeable layer. In many stratigraphic traps, such bottom seals are necessary for the hydrocarbons to be retained, but a bottom seal can be present in other settings as well. It is possible that the amplitude along the bottom seal is brighter and more continuous than at the top reservoir, and in such cases, it could be an option to look for an amplitude shut-off at the bottom seal instead of, or in addition to, at the top reservoir reflector. It does require that the hydrocarbon column reaches the bottom seal, but by modelling the expected shut-off at the bottom seal, a search for an amplitude search along the bottom seal is just as likely to work as at the top reservoir.

References

Adam, L., Batzle, M., and Brevik, I. (2006). Gassmann's fluid substitution and shear modulus variability in carbonates at laboratory seismic and ultrasonic frequencies. *Geophysics*, 71(6):173–183.

Aki, K. and Richards, P. (1980). *Quantitative seismology: Theory and methods: Volume I*. W.H. Freeman & Co, San Francisco.

Ashcroft, W. (2011). *A Petroleum Geologist's Guide to Seismic Reflection*. John Wiley & Sons.

Avseth, P., Mukerji, T., and Mavko, G. (2005). *Quantitative Seismic Interpretation: Applying Rock Physics Tools to Reduce Interpretation Risk*. Cambridge University Press, Cambridge.

Ba, J., Cao, H., Carcione, J. M., Tang, G., Yan, X.-F., Sun, W.-t., and Nie, J.-x. (2013). Multiscale rock-physics templates for gas detection in carbonate reservoirs. *Journal of Applied Geophysics*, 93:77–82.

Backus, M. M. and Chen, R. L. (1975). Flat spot exploration. *Geophysical Prospecting*, 23(3):533–577.

Bacon, M., Redshaw, T., and Simm, R. (2012). *3-D Seismic Interpretation*. Cambridge University Press, Cambridge.

Bakke, N. E. and Ursin, B. (1998). Thin-bed AVO effects. *Geophysical Prospecting*, 46(6):571–587.

Batzle, M. and Wang, Z. (1992). Seismic properties of pore fluids. *Geophysics*, 57(11):1396–1408.

Biot, M. A. (1956a). Theory of Propagation of Elastic Waves in a Fluid-Saturated Porous Solid. I. Low-Frequency Range. *The Journal of the Acoustical Society of America*, 28(2):168–178.

Biot, M. A. (1956b). Theory of Propagation of Elastic Waves in a Fluid-Saturated Porous Solid. II. Higher Frequency Range. *The Journal of the Acoustical Society of America*, 28(2):179–191.

Bortfeld, R. (1961). Approximations to the reflection and transmission coefficients of plane longitudinal and transverse waves. *Geophysical Prospecting*, 9(4):485–502.

Brown, A. (2004). Flat Spots Are Not Always Flat. *Search and Discovery*.

Brown, A. and Abriel, W. (2014). Detection of hydrocarbons using non-bright-spot seismic techniques. *Interpretation : a journal of subsurface characterization*, 2(4):SP1–SP4.

Brown, A. R. (2011). *Interpretation of Three-Dimensional Seismic Data*. Society of Exploration Geophysicists and American Association of Petroleum Geologists, Tulsa, Oklahoma, 6th ed. edition.

Brown, R. and Korringa, J. (1975). On the dependence of the elastic properties of a porous rock on the compressibility of the pore fluid. *Geophysics*, 40(4):608–616.

Carstens, H. (2007). The Luva Gas Field: Detailed Analyses Reveal Subtle Anomaly. *GEO ExPro*, 4(4).

Castagna, J., Batzle, M., and Eastwood, R. (1985). Relationships between compressional-wave and shear-wave velocities in clastic silicate rocks. *Geophysics*, 50(4):571–581.

Castagna, J. and Smith, S. (1994). Comparison of AVO indicators: A modeling study. *Geophysics*, 59(12):1849–1855.

Castagna, J., Sun, S., and Siegfried, R. (2003). Instantaneous spectral analysis: Detection of low-frequency shadows associated with hydrocarbons. *The Leading Edge*, 22(2):120–127.

Castagna, J. P. (1993). AVO analysis - tutorial and review. In *Offset-dependent reflectivity - Theory and practice of AVO analysis*, pages 3–37. Society of Exploration Geophysicists, Tulsa, Oklahoma.

Castagna, J. P. and Swan, H. W. (1997). Principles of AVO crossplotting. *The Leading Edge*, 16(4):337–344.

Castagna, J. P., Swan, H. W., and Foster, D. J. (1998). Framework for AVO gradient and intercept interpretation. *Geophysics*, 63(3):948–956.

Chopra, S. and Castagna, J. P. (2014). *AVO*. Soc. of Exploration Geophysicists, Tulsa, Oklahoma.

Churlin, V. V. and Sergeyev, L. A. (1963). Application of Seismic Surveying to Recognition of Productive Part of Gas-Oil Strata. *Geolog. Nefti i Gaza*, 7(11):636.

Dvorkin, J., Gutiérrez, M. A., and Grana, D. (2014). *Seismic reflections of rock properties*. Cambridge University Press, Cambridge.

Dvorkin, J. and Nur, A. (1993). Dynamic poroelasticity: A unified model with the squirt and the Biot mechanisms. *Geophysics*, 58(4):524–533.

Dvorkin, J. and Nur, A. (1996). Elasticity of high-porosity sandstones: Theory for two North Sea data sets. *Geophysics*, 61(5):1363–1370.

Dvorkin, J. and Nur, A. (1998). Acoustic signatures of patchy saturation. *International Journal of Solids and Structures*, 35(34):4803–4810.

Ebrom, D. (2004). The low-frequency gas shadow on seismic sections. *The Leading Edge*, 23(8):772–772.

Fossen, H. and Hesthammer, J. (1998). Structural geology of the Gullfaks Field, northern North Sea. *Geological Society, London*, 127(1):231–261.

Gardner, G. H. F., Gardner, L. W., and Gregory, A. R. (1974). Formation velocity and density - the diagnostic basics for stratigraphic traps. *Geophysics*, 39(6):770–780.

Gassmann, F. (1951). Elastic waves through a packing of spheres. *Geophysics*, 16(4):673–685.

Gelfand, V., Ng, P., Nguyen, H., and Larner, K. (1986). Seismic lithologic modeling of amplitude versus offset data. In *SEG Technical Program Expanded Abstracts 1986*, SEG Technical Program Expanded Abstracts, pages 334–337. Society of Exploration Geophysicists.

Gelius, L.-J. and Johansen, T. A. (2012). *Petroleum Geophysics*. UniGEO, Bergen, 2 edition.

Hamlyn, W. (2014). Thin beds, tuning, and AVO. *Leading Edge Leading Edge*, 33(12):1394–1396.

Hashin, Z. and Shtrikman, S. (1963). A variational approach to the theory of the elastic behaviour of multiphase materials. *Journal of the Mechanics and Physics of Solids*, 11(2):127–140.

Henry, S. (2004). Understanding Seismic Amplitudes. *AAPG Explorer*.

Kearey, P., Brooks, M., and Hill, I. (2002). *An Introduction to Geophysical Exploration*. Blackwell Publishing, Malden, Massachusetts, 3 edition.

Kim, K., Wrolstad, K., and Aminzadeh, F. (1993). Effects of transverse isotropy on P-wave AVO for gas sands. *Geophysics*, 58(6):883–888.

Knight, R., Dvorkin, J., and Nur, A. (1998). Acoustic signatures of partial saturation. *Geophysics*, 63(1):132–138.

Mavko, G., Chan, C., and Mukerji, T. (1995). Fluid substitution: Estimating changes in Vp without knowing Vs. *Geophysics*, 60(6):1750–1755.

Mavko, G., Dvorkin, J., and Mukerji, T. (2009). *The rock physics handbook*. Cambridge University Press, Cambridge, UK.

Mindlin, R. D. (1949). Compliance of Elastic Bodies in Contact. *J. Appl. Mech*, 16:259–268.

Mukerji, T., Avseth, P., Mavko, G., Takahashi, I., and González, E. (2001). Statistical rock physics: Combining rock physics, information theory, and geostatistics to reduce uncertainty in seismic reservoir characterization. *The Leading Edge*, 20(3):313–319.

Norris, A. N., Callegari, A. J., and Sheng, P. (1985). A generalized differential effective medium theory. *Journal of the Mechanics and Physics of Solids*, 33(6):525–543.

Ødegaard, E. and Avseth, P. (2003). Interpretation of elastic inversion results using rock physics template.

Ostrander, W. (1984). Plane-wave reflection coefficients for gas sands at nonnormal angles of incidence. *Geophysics*, 49(10):1637–1648.

Reuss, A. (1929). Berechnung der Fließgrenze von Mischkristallen auf Grund der Plastizitätsbedingung für Einkristalle. *Zeitschrift für Angewandte Mathematik und Mechanik*, 9(1):49–58.

Richards, P. and Frasier, C. (1976). Scattering of elastic waves from depth-dependent inhomogeneities. *Geophysics*, 41(3):441–458.

Rutherford, S. R. and Williams, R. H. (1989). Amplitude-versus-offset variations in gas sands. *Geophysics*, 54(6):680–688.

Sheriff, R. E. (1975). Factors Affecting Seismic Amplitudes. *GPR Geophysical Prospecting*, 23(1):125–138.

Sheriff, R. E. (1977). Limitations on Resolution of Seismic Reflections and Geologic Detail Derivable from Them. In Payton, C. E., editor, *Seismic stratigraphy - applications to hydrocarbon exploration*, pages 3–14. The American Association of Petroleum Geologists, Tulsa, Oklahoma.

Shuey, R. T. (1985). A simplification of the Zoeppritz equations. *Geophysics*, 50(4):609–614.

Simm, R. and Bacon, M. (2014). *Seismic Amplitude: an Interpreter's Handbook*. Cambridge University Press, Cambridge.

Smith, G. and Gidlow, P. (1987). Weighted stacking for rock property estimation and detection of gas. *GPR Geophysical Prospecting*, 35(9):993–1014.

Smith, G. and Sutherland, R. (1996). The fluid factor as an AVO indicator. *Geophysics*, 61(5):1425–1428.

Smith, T. M., Sondergeld, C. H., and Rai, C. S. (2003). Gassmann fluid substitutions: A tutorial. *Geophysics*, 68(2):430–440.

Tai, S., Puryear, C., and Castagna, J. (2009). Local frequency as a direct hydrocarbon indicator. In *SEG Technical Program Expanded Abstracts 2009*, SEG Technical Program Expanded Abstracts, pages 2160–2164. Society of Exploration Geophysicists.

Taner, M., Koehler, F., and Sheriff, R. (1979). Complex seismic trace analysis. *Geophysics*, 44(6):1041–1063.

Thomsen, L. (1986). Weak elastic anisotropy. *Geophysics*, 51(10):1954–1966.

Voigt, W. (1910). *Lehrbuch der kristallphysik (mit ausschluss der kristalloptik)*. B.G. Teubner, Leipzig.

Wiggins, R., S. Kenny, G., and D. McClure, C. (1986). A method for determining and displaying the shear-wave reflectivities of a geologic formation. *Journal of The Acoustical Society of America*, 79:589–590.

Wright, J. (1984). The Effects of Anisotropy On Reflectivity- Offset. In *SEG-1984-0670*, SEG. Society of Exploration Geophysicists.

Wrobel, K., Imhof, M., Terrell, M. J., and Hussenoeder, S. (2012). Method for quantitative definition of direct hydrocarbon indicators.

Zoeppritz, K. (1919). *VII b. Über Reflexion und Durchgang seismischer Wellen durch Unstetigkeitsflächen*. Nachrichten von der Gesellschaft der Wissenschaften zu Göttingen. Mathematisch-physikalische Klasse, Göttingen.